Preliminary Cruise Report: Hahnaro 5

Dynamics, Biology, Optics, and Meteorology of the Subpolar Front in the Japan/East Sea

19 May – 3 June 1999, R/V *Revelle*

Craig M. Lee
Applied Physics Laboratory
University of Washington

Clive E. Dorman
Center for Coastal Studies
Scripps Institution of Oceanography

Richard W. Gould
Remote Sensing Applications Branch
Naval Research Laboratory

Burton H. Jones
Department of Biological Sciences
University of Southern California

Technical Memorandum
APL-UW TM 3-99
July 1993

Applied Physics Laboratory **University of Washington**
1013 NE 40th Street Seattle, Washington 98105-6698

Office of Naval Research Grants N00014-98-1-0370, N00014-98-1-0345,
N00014-99-WX30303, and N00014-98-1-0344

Acknowledgments

A program such as this succeeds only because of the hard work of many individuals. We extend out thanks to Captain Desjardins and the crew of the R/V *Roger Revelle*, whose friendly, professional help made our operations possible. Marc Silver and Eugene Pillard provided invaluable assistance throughout the cruise. Captain Thomas Althouse, Rose Dufour, and Elizabeth Rios of Scripps Ship Operations expended enormous effort on our behalf, working through the long, involved process of securing the necessary operating clearances. The various members of the science party (listed in the appendix), with the additions of Robert Arnone (NRL), Dr. Kenneth H. Brink (WHOI), Dr. Moon-Sik Suk (KORDI), and Dr. Sung Ryull Yang (University of Kwangju)) deserve many thanks for their hard work, enthusiasm, and humor over the course of the cruise. We gratefully acknowledge the support of the Office of Naval Research under grants N00014-98-1-0370 (CML), N00014-98-1-0345 (CED), N00014-99-WX30303 (RWG), N00014-98-1-0344 (BHJ), and N00014-98-1-0369 (KHB).

Preface

In the descriptions that follow, please note that only minimal calibration and quality control have been applied to the measurements. This quick-look report focuses on general observations based on preliminary data. In particular, the oxygen sensor underwent a clear change in calibration after the collision on 26 May. As the dissolved oxygen estimates shown here are based on the pre-cruise sensor calibration, all oxygen estimates after 26 May are suspect. Only profiles from the cross-basin section and the first occupation of the intensive frontal survey bear consideration at this time.

ABSTRACT

This report presents preliminary physical, biological, and bio-optical observations from towed profiler (SeaSoar) surveys, hydrographic profiles, and meteorological measurements undertaken from the R/V *Roger Revelle* between 19 May and 3 June 1999 in the Japan/East Sea. This study focuses on understanding the processes that control upper-ocean physical and bio-optical variability in the region surrounding the subpolar front, with particular emphasis on frontal dynamics, water mass formation, and response to strong wintertime forcing. The observations include a long zonal section which sampled eddy variability in the mid-basin Japan/East Sea, repeated, intensive, three-dimensional surveys of the subpolar front, and a section extending across the Korean shelf. Sections across the subpolar front reveal subsurface variability in dissolved oxygen, chlorophyll fluorescence, light transmission, and salinity suggestive of waters that have recently been near the surface. These results are consistent with ideas of wintertime water mass formation, subduction, and southward spreading at the subpolar front. A second cruise, which will take place in January and February 2000, will make observations of the upper ocean's response to strong wintertime forcing and water mass formation in the vicinity of the front. This work is part of a broader scientific effort sponsored by the Office of Naval Research which includes studies of eddy variability, meteorological variability, and basin-scale circulation in the Japan/East Sea.

TABLE OF CONTENTS

LIST OF FIGURES

INTRODUCTION

Program Summary

The subpolar front at approximately 40˚N in the Japan/East Sea forms an important physical and biological boundary, separating seasonally stratified southern waters from northern waters which exhibit deep wintertime mixed layers and only weak summertime stratification. Energetic meanders and active eddy generation mark the frontal region. Remotely sensed sea surface temperature and ocean color reveal strong temperature and chlorophyll contrasts associated with these features. The front may also be a region of water mass formation and subduction, influencing stratification beneath the seasonal pycnocline and thus the general circulation within the basin. Wintertime outbreaks of cold, dry Siberian air extending offshore from the continent provide strong atmospheric forcing over the subpolar front and are likely to exert a strong influence on water mass formation and southward spreading.

This report describes preliminary results of measurements conducted in the area of the subpolar front during May 1999 to sample the upper ocean and atmospheric boundary layer. Another, similar cruise is planned for January 2000.

Scientific Goals

This program involves the efforts of several principal investigators with diverse, but interrelated, interests. The primary focus of the various groups can be summarized as follows:

SeaSoar Surveys and Hydrographic/Bio-Optical Profiling

This study seeks to understand the processes that control physical and bio-optical variability in the upper ocean of the Japan/East Sea. Specifically, we are interested in

- The upper ocean's response to strong wintertime forcing at the subpolar front
- The resulting formation, subduction, and spreading of intermediate waters
- The dynamics of the subpolar front
- Contrasting seasonal and coastal/central basin bio-optical variability.

These question fit within our broader long-term efforts to understand

- Physical and biological responses of the upper ocean to atmospheric forcing and how these responses penetrate to the interior
- The dynamics and biological influences of instabilities, secondary circulations, and vertical motions associated with upper ocean fronts
- Physical and bio-optical transitions between coastal and central basin waters.

Atmospheric Observations

The atmospheric measurement program seeks to

- Characterize the lower atmosphere over the Japan/East Sea
- Examine the role played by the marine boundary layer in determining air–sea heat fluxes in the Japan/East Sea.

Satellite Characterization of Bio-Optical and Thermal Variability in the Japan/East Sea

The primary remote sensing objectives during the May 1999 cruise were to

- Examine the relationships between thermal and ocean color (bio-optical) features in the Japan/East Sea, focusing on the region of the subpolar front
- Examine the spatial and temporal variability of the spring bloom in the Japan/East Sea, during both the formation and dissipation phases
- Collect ground truth reflectance, absorption, and scattering measurements to calibrate/validate the SeaWiFS sensor and optical algorithms.

The combination of upper ocean physics, marine boundary layer physics, bio-optics, biological oceanography, and remote sensing represented by the various principal investigators involved in these cruises provides a unique opportunity to gain a depth of understanding which would be difficult to achieve by any one of the components alone. There are obvious connections between the dynamics of the atmospheric boundary layer and that of the underlying ocean mixed layer. Proper interpretation of bio-optical observations requires an understanding of the biological variability in the upper ocean. Upper ocean dynamics are likely to exert strong controls on biological, and thus bio-optical, variability. Real-time remote sensing allows us to better focus our observational efforts and optimize the use of our ship time. These images also help us place our observations in a larger context. We intend to work together, exploiting the diverse nature of these observations to advance our understanding along both disciplinary and interdisciplinary lines.

Observational Program

Two cruises, the first in May 1999 and the second in January 2000, focus on sampling the variability of the upper ocean and atmospheric boundary layer in the Japan/East Sea. The spring cruise, discussed here, focused on frontal dynamics, characterizing bio-optical variability associated with the spring phytoplankton bloom and documenting the location, range, and properties of water masses formed at the subpolar front during the preceding winter. The wintertime cruise will document the upper ocean's response to cold air outbreaks, with particular attention to processes associated with water mass formation and subduction at the subpo-

lar front. Both cruises employ a towed, undulating profiler (SeaSoar) to make highly resolved observations of the upper ocean. Shipboard meteorological sensors and GPS sondes sample the lower atmosphere. We use real-time, remotely sensed images of sea surface temperature and ocean color to determine the location of the subpolar front and to select intensive survey locations. Real-time access to remotely sensed imagery allows us to modify our sampling in response to changes in the front. Repeated intensive grid surveys provide approximately synoptic, three-dimensional coverage, while a sequence of longer sections documents oceanic and atmospheric boundary layer variability away from the front. In addition to the suite of physical and bio-optical sensors carried by SeaSoar, we use a shipboard acoustic Doppler current profiler (ADCP) and GPS navigation to measure upper ocean currents. Sampling also includes a limited number of hydrographic and optical stations off the Korean coast and across the subpolar front.

METHODS

SeaSoar Surveys and Hydrographic/Bio-Optical Profiling

SeaSoar surveys produced highly resolved, three-dimensional snapshots of physical and bio-optical variability in the upper ocean. At typical tow speeds of 8 knots, SeaSoar profiles between the surface and 300–350 m, with an effective horizontal resolution of approximately 3 km. Sensor payload included dual Sea-Bird conductivity cells and temperature probes, a Langdon fast-response dissolved oxygen sensor, and sensors to measure chlorophyll fluorescence, light transmission, photosynthetically available radiation (PAR), and bioluminescence. Two high-bandwidth bio-optical sensors, a Wetlabs HiStar spectral absorption and attenuation instrument (100 wavelength bands at 3.3 nm resolution), and a Hobilabs Hydroscat-6 six-wavelength backscatter sensor provide the focus of our bio-optical measurements. A 150-kHz narrowband ADCP combined with P-code GPS navigation and GPS heading information provided continuous profiles of upper ocean velocity. Surface nutrient and fluorescence measurements were also taken while the ship was under way.

A limited number of hydrographic stations provided water samples for measuring nutrients, dissolved oxygen, and pigment concentrations. The majority of the hydrographic stations form a single section across the subpolar front, with a smaller number placed in a section across the Korean shelf at 36˚10’N. Immediately following each hydrographic section, we surveyed the line with SeaSoar. Thus high-resolution SeaSoar sections complement more coarsely spaced measurements of properties such as nutrient concentrations, which SeaSoar does not provide. Primary productivity measurements (N^{15} method) were also made at selected stations. Separate optical casts, using the HiStar, Satlantic upwelling and downwelling irradiance sensors, and a Biospherical PAR sensor, were made at selected daytime stations.

Atmospheric Observations

Atmospheric observations employed both ship-based sensors and automated surface stations. Most of the sensors in the improved meteorological (IMET) system on board *Revelle* are on a mast in the bow 15 m above the sea surface. Variables measured are wind speed, wind direction, air temperature, humidity, air pressure, rainfall, and short- and long-wave radiation. The ship’s direction and position are obtained from the ship's GPS and gyro data, which are logged on the shipboard computer system along with the IMET data.

An attempt was made to measure the vertical gradient directly to examine assumptions about the bulk heat flux method. To this end, the Center for Coastal Studies (CCS) mounted two additional automated meteorological stations on the bow mast, one 4.2 m below and the other 6.6 m below the IMET station. CCS replaced the ship's two anemometers on either side of the top of the main mast, added temperature, humidity, and pressure sensors,

and directed the output to the on-board CCS data-logging computer. The main mast sensors are 22.7 m above sea level. Thus there are four levels of meteorological sensors on the *Revelle* recording data at 1-minute intervals or faster.

Atmospheric soundings were made from the ship to obtain vertical profiles of temperature, humidity, pressure, and winds. A free balloon was used to carry a Vaisala GPS sonde once a day to above 300 hPa (10 km). The surface observations will be used as a context for the soundings to characterize the lower atmosphere.

The surface stations were operational for the entire cruise with minor exceptions. The ship's data-logging computer for the IMET system hung up a number of times, but was quickly restarted, resulting in minor data gaps. The CCS system operated continuously for the period. Data from both systems were displayed in real time so they could be easily followed. At times, there were systematic vertical gradients, both positive and negative, in the air temperature and humidity.

The balloon sounding system was set up in the after part of the ship. Balloons were inflated in a large "preparation" hanger and, when sonde was attached, walked out to the stern for release. A technique was developed for successful launches that should work in the high wind, winter cases.

The twelve soundings were made at 0000 UTC with the exception of the sounding on 28 May, which was made at 0600 (see Table 1). The latter delay was to wait until the ship was in Japanese waters as there was a prohibition against sounding in Russian waters. Not counted in the 12 soundings is a sonde that failed after launch. The temperature, humidity, and pressure portions of the sondes generally functioned properly. The wind portion was a disappointment, failing or missing substantial parts of the profile on half of the 12 soundings. The manufacturer will be consulted about how to improve this.

Table 1. R/V *Revele* Japan Sea atmospheric soundings.

Date	Time (UTC)	Latitude	Longitude	Comments
21/05/99	0010	37.57 N	131.36 E	No Winds
22/05/99	0011	38.60 N	134.00 E	Good
23/05/99	0002	39.07 N	134.31 E	Good
24/05/99	0001	40.04 N	135.17 E	No winds above 1255 m
25/05/99	0010	38.31 N	134.47 E	Good
26/05/99	0000	39.70 N	134.00 E	No winds, No humidity > 982 m
27/05/99	0008	38.22 N	134.00 E	Good
28/05/99	0616	39.40 N	134.23 E	Good
29/05/99	0009	39.23 N	134.79 E	No winds
30/05/99	0000	38.71 N	134.70 E	No winds below 5300 m
31/05/99	0004	35.12 N	129.07 E	No winds below 1387 m
01/06/99	0008	35.12 N	129.07 E	Good

Satellite Characterization of Bio-Optical and Thermal Variability in the Japan/East Sea

Our main focus during this cruise was to collect real-time, satellite thermal and ocean color imagery. After overcoming a variety of software and hardware problems with the satellite receiving system, we successfully captured over 200 AVHRR (advanced very high resolution radiometer) images and 20 SeaWiFS (sea-viewing wide-field-of-view sensor) images over the course of the 16-day cruise. We received direct HRPT broadcast of AVHRR data from three polar-orbiting sensors: NOAA-12, NOAA-14, and NOAA-15. We typically received 9–12 AVHRR passes per day (3–4 passes from each sensor), although some of the passes did not cover our area of interest. We also received 1–2 SeaWiFS passes per day. We produced geo-located sea surface temperature (SST) products from the AVHRR thermal imagery and bio-optical products (chlorophyll, absorption, scattering coefficients) from the SeaWiFS ocean color imagery. Also, Korean and Japanese colleagues at shore-based receiving stations provided additional AVHRR and SeaWiFS imagery (via e-mail transmission of processed scenes to the ship from the Naval Research Laboratory (NRL) at the Stennis Space Center).

The real-time satellite imagery provided synoptic views of the basin and enabled us to optimize the cruise track, place stations in regions of maximum gradients, and chase features of interest (such as the large eddy we sampled south of the front following the second radiator pattern with the SeaSoar). The Japan/East Sea frequently experiences cloudy and/or hazy conditions over much of the basin, although April and May are two of the clearest months, and weather conditions change rapidly. The frequent reception of each direct broadcast during a satellite overpass on the shipboard system enabled us to collect a large number of excellent images. Forty-two of the best images were incorporated into a time-sequential "movie loop" to provide a visualization of the spatial and temporal variability of the subpolar front and eddy field.

In addition to the real-time satellite reception on board ship, NRL has constructed data bases of AVHRR and SeaWiFS imagery covering the Japan/East Sea. The data bases currently cover 15 months, from March 1998 through the present, and the program reported here should provide data for approximately another year. These data bases provide a climatology for the region and enable us to place the features and patterns observed during the two cruises into a broader spatial and temporal context. The data bases are accessible with browse capabilities through our web site (www7240.nrlssc.navy.mil/ocolor), although SeaWiFS products are password protected and restricted to NASA-approved investigators.

During this cruise our secondary efforts involved the collection of underway absorption, scattering, and attenuation measurements (using an AC9 instrument in flow-through mode coupled with the ship's system for sampling surface seawater while under way). We will couple these measurements, collected every 10 s along track, with the satellite imagery to better understand the linkages between the thermal and optical fields. These data will also provide ground truth values to validate and improve the SeaWiFS optical algorithms. We also collected remote sensing reflectance (R_{rs}) measurements at 40 stations during the cruise, using an ASD field spectroradiometer; we can compare these measurements with the satellite-derived values to assess sensor calibration and the accuracy of the atmospheric correction routines. We collected 79 atmospheric scans using a sun photometer to provide validation data for the SeaWiFS atmospheric correction algorithms (ozone thickness and aerosol optical depth). The white squares in Figure 1 represent the locations of the reflectance stations, the magenta triangles are the CTD stations, and the black diamonds are atmospheric soundings (radiosondes - Clive Dorman, Scripps). The cruise track (red) and station locations are overlaid on an AVHRR SST image from 21 May. Note the strong thermal gradient of the subpolar front along 40°N across the entire basin.

CRUISE NARRATIVE

The following are notes from the daily cruise log, intended to track major events and record general observations.

19 May

All aboard by 1430. *Revelle* sails at 1600 (all times are local).

20 May

Deploy SeaSoar at approximately 0700. The vehicle initially has a bad roll at 50 m (shallower and more severe than in previous deployments) which limits its dive range. Primary temperature sensor appears to be malfunctioning. Secondary temperature sensor has incorrect calibration coefficients in real-time display software. This has no effect on baseline data acquisition, but needs to be corrected for display purposes. Recover SeaSoar to reballast (add weight on the side opposite the HiStar to stabilize the roll) and to test and replace faulty sensor. Tests (intercomparison with fresh sensors in an icewater bath on deck) show that the primary temperature sensor has failed. Replace primary sensor and alter calibration file for secondary. Added weight stabilizes the roll and allows the vehicle to dive. Steam back to the start of the west–east line (200 m isobath) prior to redeployment. Secondary conductivity cell now exhibits a slight hysteresis, but the effect is minor and at this time we believe it is a thermal lag effect induced by the wide temperature swings between the surface and waters at depth. Tow a line directly east from the Korean coast at 134˚45’N.

21 May

Lag effects in the secondary conductivity cell amplify through the morning and afternoon. Very clear lag in the signal. Primaries look OK, but also show more pronounced lag than expected. We elect to recover the SeaSoar to troubleshoot the sensor problem. Recover SeaSoar at the end point of the eastward line, just prior to the turn north. Inspection reveals that the hosing on the secondary sensor is badly kinked (a tie wrap broke. allowing the hose to double back on itself), and that the hose on the primaries is just starting to kink. We replace both hoses, armoring the new plumbing with a flexible, accordion-like plastic sheath and tie-wrapping it securely to the frame. While repairs are taking place, we execute a 500 m CTD cast. The profile exhibits a large subsurface fluorescence maximum. HiStar is water calibrated on deck, and both Histar and Hydroscat are cleaned.

Shortly after redeployment, Histar a-channel quits. We recover SeaSoar again at around midnight. The a-channel flow tube has broken loose and is hanging by its pump tube. Reinsert and secure both tubes to the sensor. We backtrack south along the line, redeploy, and steam north.

22 May

First section across the front completed, extending from 37˚45’N to 40˚25’N along 134˚E. The section captures both the subpolar front, which has a clear surface expression in the AVHRR images, and a subsurface front-like feature farther to the south. Both features have optical signals extending in a finger downward along the frontal interface.

23 May

Continue first intensive frontal survey. Set 100 km north–south legs centered on the northern (surface) front, with 20 km cross-track separation. Images suggest that the front curves northward at the eastern end. Shorten the southward reach of legs 3 and 4 and extend legs 5 and 6 farther northward.

24 May

SeaSoar shows signs of trouble starting in the morning. Wings flutter and sometimes come into the up-wing position, even though there is clearly a command for down-wing current. After sporadic episodes like this, flight degrades to an unacceptable level around 1700. Possible mechanisms include hydraulic unit failure (unlikely, as the signature is unlike any other such failure we've seen) or a leaking bring-it-home bottle (BIHB, an emergency component designed to force the SeaSoar to the surface in the event of telemetry loss). Recover SeaSoar around 1900 at 38˚50’N, 135˚10’E and execute a 500 m CTD cast while SeaSoar is on deck for repairs. Inspection finds a miniature meca-type connector on the BIHB has either loosened or broken at the endcap. No water found inside the BIHB. BIHB removed from the system and SeaSoar recabled and tested for operation without it. No further problems seen on redeployment. CTD cast shows a slight subsurface chlorophyll fluorescence maximum, transmissivity minimum and elevated salinities at approximately 200 m, near the 5˚C isotherm. This is similar to the signal seen by SeaSoar at the frontal interface in the previous section.

25–26 May

Complete the first intensive survey and execute another long north–south SeaSoar tow from 40˚10’N to 38˚00’N along 135˚10’E (southbound) and 134˚42’E (northbound). The strong subsurface feature seen in the southern half of the western section was not present in the eastern section. Following this, we begin the second pass over the survey pattern. Near the end of the first leg, SeaSoar collides with something large and rigid. Fishing gear had been extremely light (we've seen very little gear since we left the Korean coast—even the front is uncluttered), but is still the most likely suspect. No surface expression of the obstacle was seen. SeaSoar’s stainless steel nose cone has a deep horizontal crease across the brow, both sides of the upper tail fin have been sheared off, and a couple of the impeller blades are bent. One of Hydroscat’s bulkhead connectors was sheared off by the impact, allowing water into the pressure case. Paul Fucile (our electrical engineer) cracked the case, broke down the com-

ponents, and cleaned and packed them for shipment back to the US. We cannot effect repairs here.

While repairs are being made to SeaSoar, we execute a cross-front hydrographic survey originally planned for later in the cruise. This is an all-hands drill due to the tight station spacing and the intensive nature of the water sampling, and everyone responds wonderfully. The section will provide valuable *in situ* data to help us interpret the SeaSoar observations. Both CTD casts and optical profiles are collected. SeaSoar requires approximately 12 hours to repair, including a change of nose cone to compensate for the loss of Hydroscat. Using the SeaSoar deck period to execute an already planned hydrographic section should minimize the amount of time lost to this incident.

Weather-wise we have been very fortunate. We've had mostly clear skies (and thus good remote sensing) for most of the cruise. A low pressure system passed over us yesterday, bringing about 12 hours of bumpy riding. Seas picked up quickly but calmed within hours of the time the winds relaxed. Just a taste of the fun to come in January.

27 May

Redeploy SeaSoar after completing the cross-front hydrographic section, repairing fairing as we go. SeaSoar tows off to starboard (even more than usual), with the largest wire angles coincident with the bottom of the dive cycle. Roll remains fairly small, though. The starboard angle prevents SeaSoar from profiling below 330 m. As only a limited amount of sampling time remains and the problem is not critical, we elect to leave the system as is and continue sampling. Jerry Dean believes that SeaSoar is too heavily weighted to port (opposite the HiStart mount). This would cause the vehicle to list to port and could induce a starboard slew in the flight path.

28 May

Executing the second pass of the intensive survey.

29 May

Complete second pass of the intensive survey. In the easternmost section. the front appears either to have weakened or to have shifted north since the initial pass. A time budget indicates that the final days of the cruise will be tight. A third intensive frontal survey is possible, but this would require all of the remaining sampling time and thus prevent us from making a cross-shelf section. Alternatively, we can survey the meander-like feature observed in the southwest corner of the radiator survey. This appears to be topographically steered and may influence the fate of water subducted at the subpolar front. Waters beneath the seasonal pycnocline in this feature carry slightly elevated dissolved oxygen concentrations, suggesting that they have recently seen the surface. We opt for the meander. Although they dominate

many of the SST images, we really don't have much data on the structure of these features. This will allow us to do a coarsely resolved meander survey and a cross-shelf section at the end of the cruise.

Secondary temperature sensor failed late in the evening. It looks healthy over part of each profile, but is clearly malfunctioning (large amplitude, high-frequency noise) over the rest. Will need to keep a close watch on data quality from the primary sensor pair.

30 May

"Meander" survey. On east–west crossings of the meander, we see a homogeneous lens of water between approximately 50 and 175 m. A relatively narrow band of warmer, saltier water runs along the edges, extending from the surface to 100 m. The central water seems to have higher subsurface oxygen concentrations than the water along the edges. Fishing gear, which has been absent in most of our surveys, is much heavier near the Yamato Tablemount. Rather than being directly over the mount, the highest concentrations are on the slopes and over the deep water on the sides. We find a combination of high-flyers with radio gear, simple glass and styrofoam floats, and general debris which look like gear that has been adrift for some time. There are often fields of floats, which are probably connected and support some sort of long net or line. SeaSoar's depth range decreases over time. We started with 330–350 m, but by the end of the day, 320 m is more typical. The ship must slow to between 7.0 and 7.4 knots to achieve this range.

31 May

Depth range and speed are still restricted. After doing a time budget, we decide to pull SeaSoar so that we can repair the faulty temperature sensor and try to correct its flight problems. Predict a 2-hour turn-around. As SeaSoar is reeled in, it becomes obvious that the fairing has suffered extensive damage. Approximately 20% of the fairing is either badly damaged or missing altogether. Repair/replacement on recovery is difficult, as the low wire angle required to permit access to the cable makes level winding and laying down the fairing on the drum difficult. We thus defer fairing repair to the next deployment. Inspection reveals that the cable for the secondary (tail fin) temperature sensor has abraded through. It appears that it cut against the edge of its pass-through hole in the SeaSoar body. The cable was tie-wrapped to the pass-through using a nearby drill-hole made especially for the purpose. We replace the cable and add anti-chaffing gear (plastic tubing and a build-up of self-vulcanizing tape) to protect potential wear points. Check all other cables. Shift one lead bar from the port side to the starboard side of the instrument cage in an attempt to correct a suspected ballasting problem. Redeploy SeaSoar and, with the help of many members of the science party as well as Gene (resident technician) and Steve (bosun), repair and replace a large amount of fairing. The turn-around ends up taking over 6 hours, but the fairing is once again in good shape. Rethink plans for using the final hours of sampling. We may not have time to tow all the way

into the Korean coast. Instead, we could recover SeaSoar on the west side of the “meander” feature and steam full speed to the start of the cross-shelf hydro section.

1 June

Continue survey. Time constraints force us to recover SeaSoar around 2300 to conserve time for the cross-shelf section.

2 June

Arrive at 2000 m isobath around 1200 local time for a noontime optics cast, but overcast weather makes this timing less critical. We thus decide to steam inshore to the 1000 m isobath before beginning the hydro section. Unfortunately, timing is very tight. We plan four cross-shelf hydrographic casts, but have time to execute only three. The shallowest cast is in 200 m of water. We also use this traverse of the hydrographic section to scout the potential SeaSoar tow path for obstacles. Following the hydrographic work, secondary temperature and conductivity sensors and the HiStar are moved from the bio-optical profiling package (BOP) to SeaSoar. We also shift an additional weight from the side opposite the HiStar in an attempt to balance the load and damp the SeaSoar's roll. Following this, we steam inshore to the 100 m isobath, to a point approximately 2 nmi north of the survey line. This is meant to give us room to deploy SeaSoar and stabilize its flight before we turn onto the survey line. In the nearshore region, the bathymetry rolls off quickly enough that if we deployed directly at the inshore end of the hydro line, we could easily find ourselves in 500+ m of water before we got our first good profile. Initial deployment is in 100 m of water with 150 m of cable out. The ship steams at 4–5 knots during deployment to keep SeaSoar off the bottom. Initial deployment goes well, and by the time we turn onto the line, SeaSoar is executing reliable profiles between the surface and 15 m off the bottom. We pay out additional cable as we move into deeper waters, but SeaSoar refuses to dive below 250 m. We tow until 2300, when the bridge requests that we begin recovery. We need to have operations wrapped up by 0000 to enable *Revelle* to make port at 0900 on 3 June. SeaSoar returns with a large mass of medium-weight nylon line tangled in around the section of cable closest to the fish and an even larger mass caught in the bridle, wings, and tail fin of the vehicle itself. Some of this we bring on deck. We cut the remainder loose once the vehicle is safely on board. Other than some minor fairing loss, there is no damage to the system. This helps explain the poor dive performance in deep water. It is not clear when in the tow we picked up the line. Note that earlier in the day, we steamed the entire line while executing the hydrographic section. During this scouting session, we saw moderate concentrations of fishing gear but nothing obviously in the tow path.

3 June

Arrive in Pusan at 0800. Offloading goes smoothly. All gear packed and ready for transport off the pier by the end of the day.

PRELIMINARY RESULTS

SeaSoar Surveys and Hydrographic/Bio-Optical Profiling

The SeaSoar surveys examine the region surrounding the subpolar front, a warm streamer or meander just to the south of the front, mid-basin eddy variability, and cross-shelf variability off the Korean coast (Figure 1). The outbound transit to the subpolar front samples an east–west oriented section along 37˚45'N, passing through a prominent eddy located between 25 and 175 km (Figures 3a and 4). Although the eddy appears as a cold feature in the SST imagery (Figure 1), beneath the surface layer the lens is warmer and saltier than surrounding waters. Farther to the east (Figure 4, centered near 350 km), the section reveals a 40-km-wide band of warm, salty water extending from the surface to 100 m. In the AVHRR imagery (Figures 1 and 2) this appears as a streamer or loop of warm water originating near the Japanese coast and extending northward to 39˚N between 134˚E and 134˚30'E. Note the elevated dissolved oxygen concentrations beneath the seasonal pycnocline in the eastern two-thirds of the section.

Intensive surveys of the subpolar front were designed to sample the southward bow in the front seen in the AVHRR imagery between 134˚E and 135˚E near 39˚30'N (Figures 1, 2, and 3a,b). Each survey consists of six meridionally oriented sections, each approximately 100 km long with 20 km cross-track separation. Selected sections extend farther to the south in an attempt to map the possible spreading of waters subducted at the front. In the text and figures, section numbers 1–6 (Figure 3a,b) refer to these meridionally oriented survey lines, labeled sequentially from west to east. We occupied this pattern twice, performing a hydrographic survey (Figures 7–13) along section 1 between the two passes.

Cross-front sections from surveys 1 and 2 (Figures 5 and 14b–14e) reveal a strong front in the upper 200 m, with surface temperature contrasts as strong as 5˚C over 10 km. The front is sharpest in the western half of the survey, becoming more diffuse to the east. Upper ocean stratification varies markedly across the front. South of the interface, a 30-m-deep, weakly stratified surface layer rests on top of a sharp seasonal pycnocline. Beneath the seasonal pycnocline, a more weakly stratified permanent pycnocline extends to 250 m. Stratified waters extend to near the surface on the northern side of the front, with a weaker, shallower seasonal pycnocline and only weak stratification below. Southern waters are warmer and more saline than those to the north. South of the front, a chlorophyll fluorescence maximum hugs the top of the seasonal pycnocline, while elevated levels of chlorophyll fluorescence extend closer to the surface to the north. Dissolved oxygen concentrations are highest beneath the seasonal pycnocline north of the front. Elevated levels of dissolved oxygen follow the region near the 27 $kg\,m^{-3}$ isopycnal as it slips beneath the seasonal pycnocline south of the front. A weak signal of elevated chlorophyll fluorescence and low transmissivity extends downward in a finger along the frontal interface. Careful inspection reveals that these waters are also slightly fresher than their surroundings, with salinities similar to those found in sur-

face waters to the north of the front. The combination of oxygen, fluorescence, light transmission, and salinity signals suggests that these waters have recently been near the surface, perhaps forming in winter or spring and spreading southward along isopycnals. ADCP current profiles show a jet-like flow associated with the front (Figures 6 and 15). The currents follow the southward bowing of the front, with the flow broadening to the east.

Survey 3 consists of a coarsely spaced set of sections (Figures 3c and 16) through the warm streamer passing southwest of where we sampled the front (Figures 1 and 2). The feature flows northward from near the Japanese coast and around the Yamato Tablemount, but turns southward where it encounters the Yamato Rise. Zonal sections extending across both north- and south-flowing branches reveal narrow, 25-km-wide streamers of warm, salty water confined to the upper 100 m. The streamer encircles a homogeneous lens extending from 50–200 m. An earlier section (Figure 4), taken before the collision altered the calibration of the dissolved oxygen sensor, sampled the western edge of this lens (350–400 km) and suggests that its waters have higher dissolved oxygen concentrations than surrounding waters.

Atmospheric Observations

The big story is the shifting structure of the boundary layer. The sea temperature differs from the air temperature by only a few degrees, so the difference readily changes sign owing to changes in the wind and low level air mass.

An example of the marine boundary layer structure in the case of a colder sea surface and a surface-based inversion is shown in Figure 23 for 23 May 0000 UTC (0900 LST). There is a 7°C difference between the base and top of the air temperature inversion. The winds in the lower 3 km were at a maximum speed and from the south at sea level (Figure 19). The surface IMET sea–air temperature difference persisted for most of the day (not shown).

The 24 May sounding revealed a complex structure in which the sea surface was warmer than the air and the base of the air temperature inversion shifted to 300 m capped by an overcast stratus layer (Figure 20). The surface IMET station time series for the day revealed a slightly warmer sea surface with increasing wind speeds, rain, and falling pressure marking the passage of a weak disturbance over the Sea of Japan (not shown)

After the center of the disturbance passed, the weak inversion was replaced with humid, less stable air. The sea surface was slightly warmer than the air. The sounding profile on 25 May was uniform and without structure in the lower levels (Figure 21).

Satellite Characterization of Bio-Optical and Thermal Variability in the Japan/East Sea

Preliminary examination of the SeaWiFS chlorophyll imagery suggests that the spring bloom started around late March or early April in the southern East Sea, and gradually migrated north. By late April, the bloom covered the entire central and southern regions of the basin, including the area of the subpolar front and even coastal areas along the Russian coast in the north. By the time we departed Pusan at the start of the cruise, the bloom extended over the northern reaches of the basin, with values remaining high along the eastern margin of the front and decreasing in the southern region (Figure 22). By the end of May, chlorophyll values had decreased to 0.2–0.4 µg/l in the south but remained as high as 3–4 µg/l north of the front. By early June, values in the south/central basin had decreased even further, with relatively higher values localized in the Korean and Japanese coastal currents from the south. Values north of the front were starting to decline as well by this time.

Reflectance spectra derived from the field spectroradiometer measurements are shown in Figure 23 for selected stations representing a variety of water masses. The imagery downloaded directly from the satellite was utilized to place stations in features of interest and to ensure sampling a wide range of water types. The lower reflectances in the blue region of the spectrum (400–450 nm) at the stations north of the front are indicative of higher absorption due to chlorophyll pigments. Warm waters south of the front and in the warm filament (edge of the large southern eddy) had higher reflectances and lower chlorophyll concentrations. Spectral scattering coefficients derived from the R_{rs} spectra using a recently developed optical algorithm are shown in Figure 24 for the same stations. Note the consistency in samples from the same water type. The Korean coastal waters and waters south of the front and in the warm filament exhibited higher scattering levels, possibly because of senescent and declining phytoplankton cells that remained in the surface waters following the spring bloom. Absorption-to-scattering ratios from the flow-through AC9 data may help elucidate patterns and bio-optical provinces.

Variability of the flow-through absorption coefficient at 412 nm (a412) for surface waters is shown in Figure 25. The area covered extends from Pusan northward along the Korean coast, offshore along the east/west section, and northward to the first meridional section of survey 1. Note the higher values near the coast relative to offshore waters. Also, the peaks and valleys in the magnitude of the a(412) values correspond to features in the SST imagery. For instance, absorption values decrease sharply around 36˚48’°N, 129˚48’°E as the ship passed out of the slightly cooler water hugging the Korean coast (blue pixels in Figure 1) and cut across a section of the East Korean Warm Current (yellow pixels in Figure 1). In Figure 26, showing absorption (a) and beam attenuation (c) at 412 nm along the east–west section at 37˚45’ N, both a and c decrease at ASD station 8, located in the warm filament flowing northward along 133˚20’°E (Figure 1).

Figure 27 shows the absorption coefficient at 440 nm (a440) along sections 1–3 of survey 1 at the subpolar front. Note the relatively higher values north of the front along the sections 1 and 3. Recall that the surface expression of the front cuts across the figure from the southwest to the northeast (see Figures 1 and 2).

Figure 28 is a zoomed subsection of the SST image from 26 May corresponding in time to the cross-front CTD hydrosection, which is depicted as the red line in the figure. In Figure 29 we show the surface a(440) and c(440) values from the flow-through system corresponding to the red hydrosection line in Figure 28. Note the decrease in a and c at 39.7°N as the section passes out of the cooler waters north of the front (bluish-white pixels in Figure 28) and the increase at 39˚30'°N at the front. At 38˚54'°N, a and c decrease again as the section passes into the warm waters of a branch of the filament to the south (yellow pixels in Figure 28). Note that clouds (darker blue pixels) obscure a portion of the warm filament along the southern portion of the section in Figure 28.

By 31 May, chlorophyll concentrations in the northern region of the East Sea remained high, while concentrations at the front diminished (compare Figure 30 with Figure 22). Note the two loops of relatively enhanced chlorophyll concentrations covering section 1 and the northern part of section 3 (bluish-white pixels in Figure 30). These areas of higher chlorophyll correspond to the areas of high a(440) in Figure 27. Figure 31 is the SST image from 31 May, collected about 4 hours after the SeaWiFS pass of Figure 30. Whereas the SeaWiFS image showed a spatially variable chlorophyll distribution across the northern portion of the survey (and slightly northward), the temperature pattern over the same area is essentially homogeneous, indicating that the thermal and optical fields do not necessarily coincide.

As analyses proceed, we will use the SeaWiFS and AVHRR data bases to describe the spatial and temporal variability of thermal and optical fields in the East Sea. In addition, we will relate the shipboard *in situ* measurements with features in the satellite imagery, and we will collaborate with US, Korean, Japanese, and Russian investigators to better understand the evolution of the surface/subsurface linkages along the subpolar front.

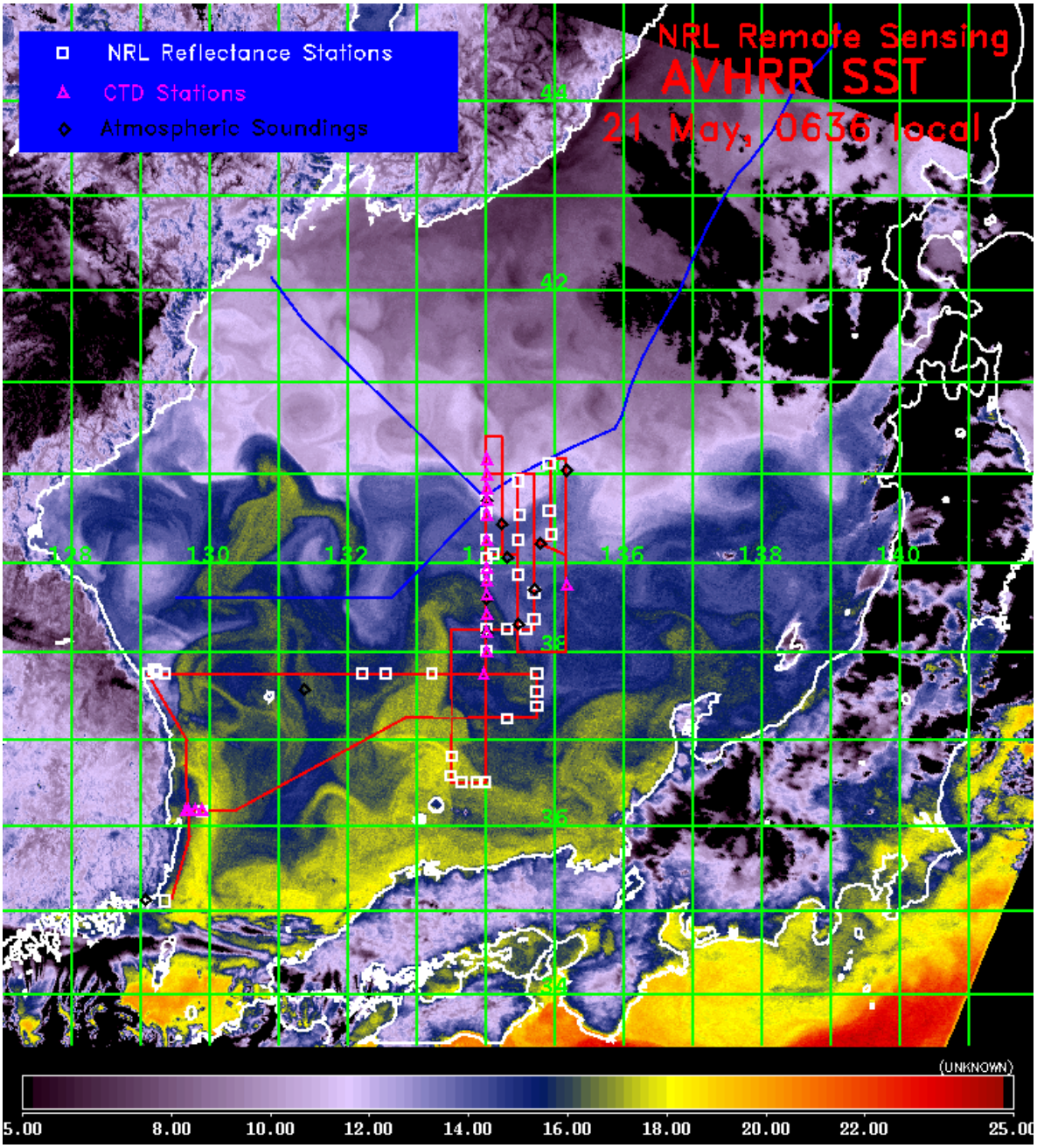

Figure 1. Cruise track and station locations (NRL reflectance stations, CTD stations, and atmospheric soundings) superimposed on AVHRR SST image from 21 May 1999. Imagery collected with shipboard receiving system. Blue lines on image represent exclusive economic zone boundaries.

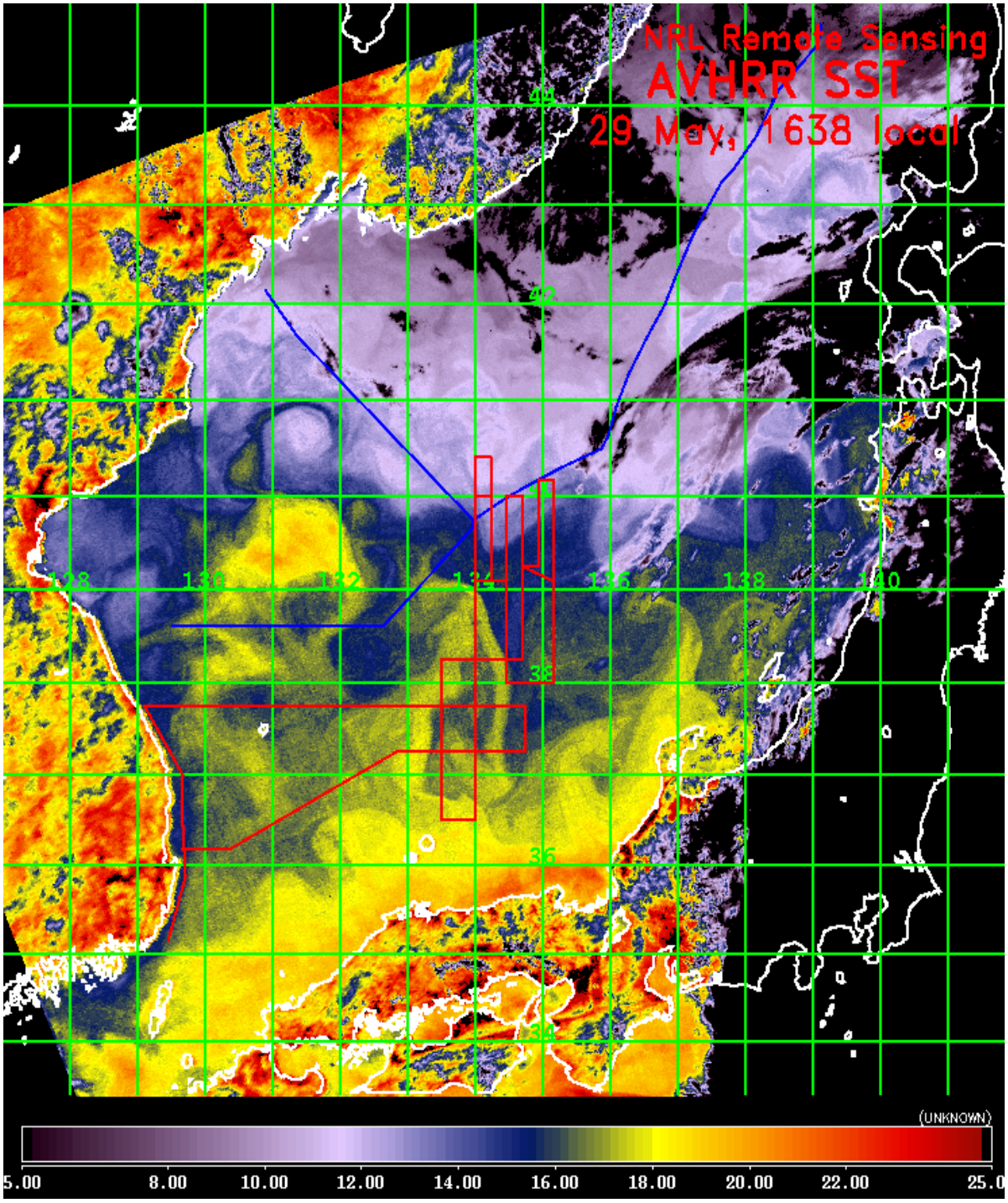

Figure 2.AVHRR SST image from 29 May 1999.

(a) JES2 Cross-basin and Survey 1

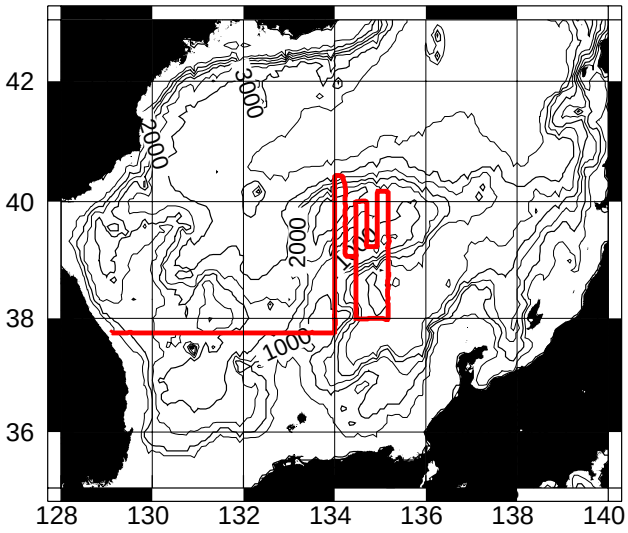

(b) JES2 Survey 2

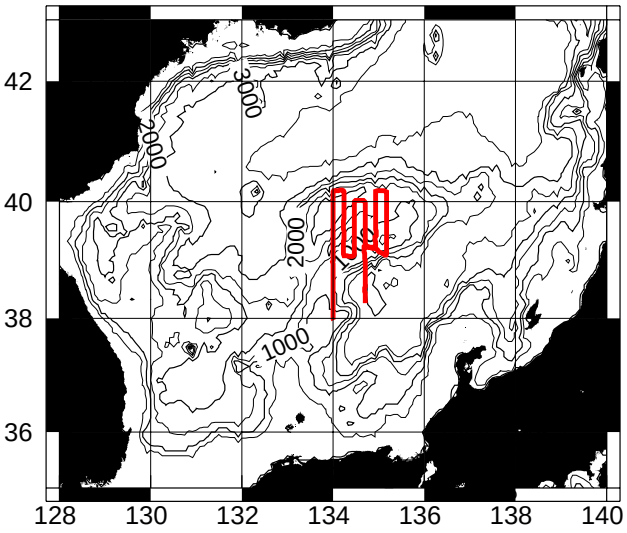

(c) JES2 Survey 3 and Cross-shelf

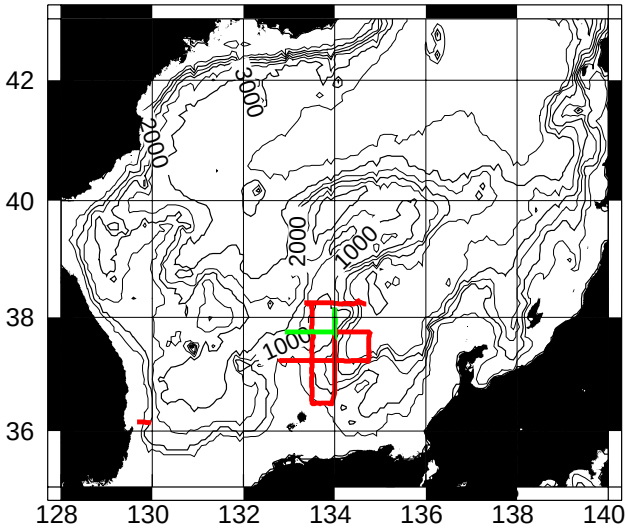

Figure 3. Charts showing SeaSoar survey tracks for (a) zonal cross-basin section and subpolar front survey 1, (b) subpolar front survey 2, and (c) survey of a warm meander current (survey 3) and a section across the Korean shelf. In surveys 1 and 2, we number the meridional sections 1–6 working from left to right. In survey 3, meridional sections are referred to as west and east, and the three zonal sections are referred to as south, central, and north. The green line marks parts of survey 1 that are included in subsequent section plots from survey 3.

JES2: Outbound, East from Coast along 37^{o} 45 N

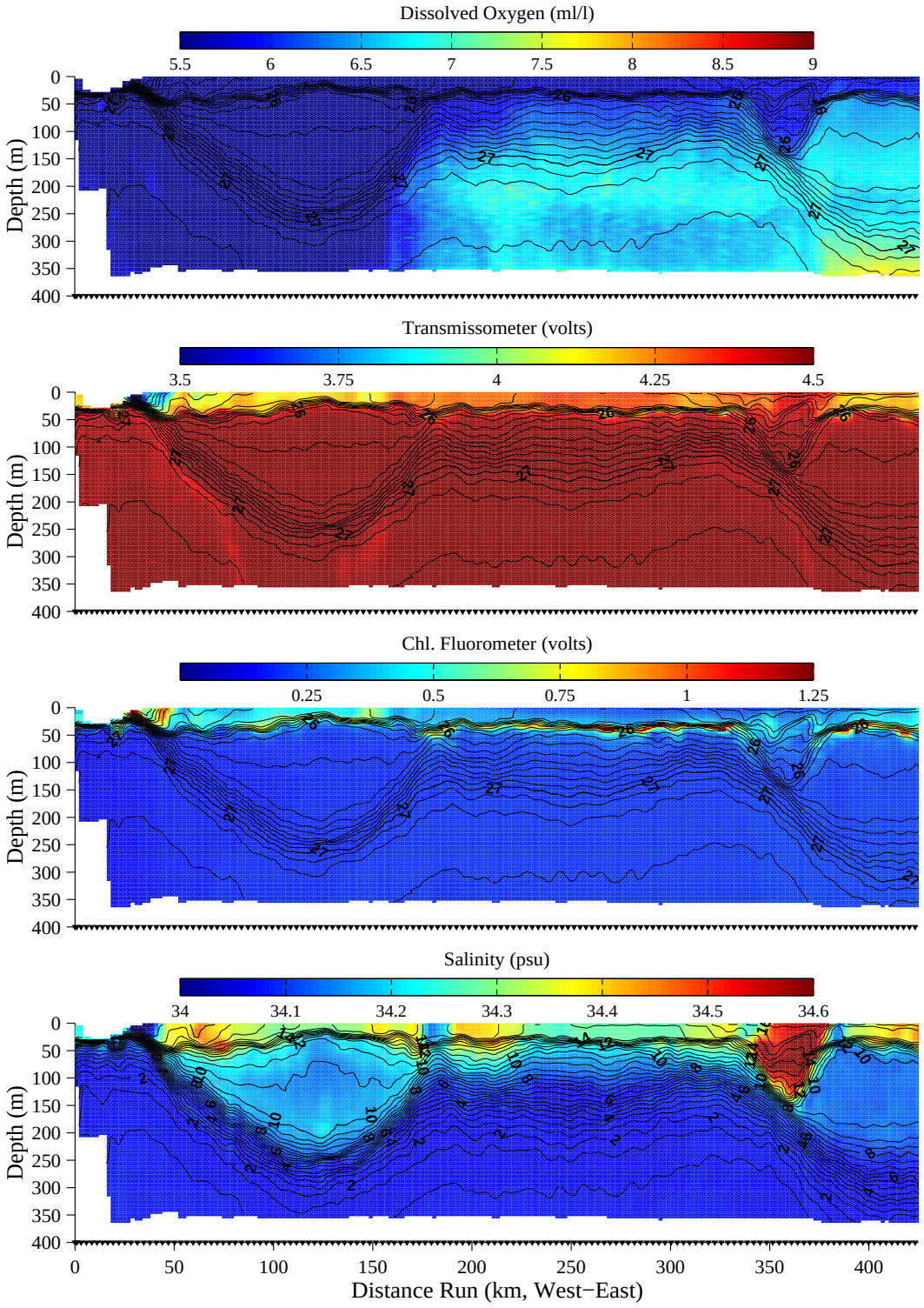

Figure 4. SeaSoar section extending eastward from the Korean coast along 37˚45'N. From top to bottom, the panels display (contours/colors) temperature/dissolved oxygen, temperature/light transmission, temperature/ chlorophyll fluorescence, and potential density/salinity. All calibrations are preliminary, and fluorescence and transmission are shown in volts. High values indicate high chlorophyll content or low light transmission. Small triangles running across the bottom of each panel mark profile locations.

JES2: Survey 1, Section 1

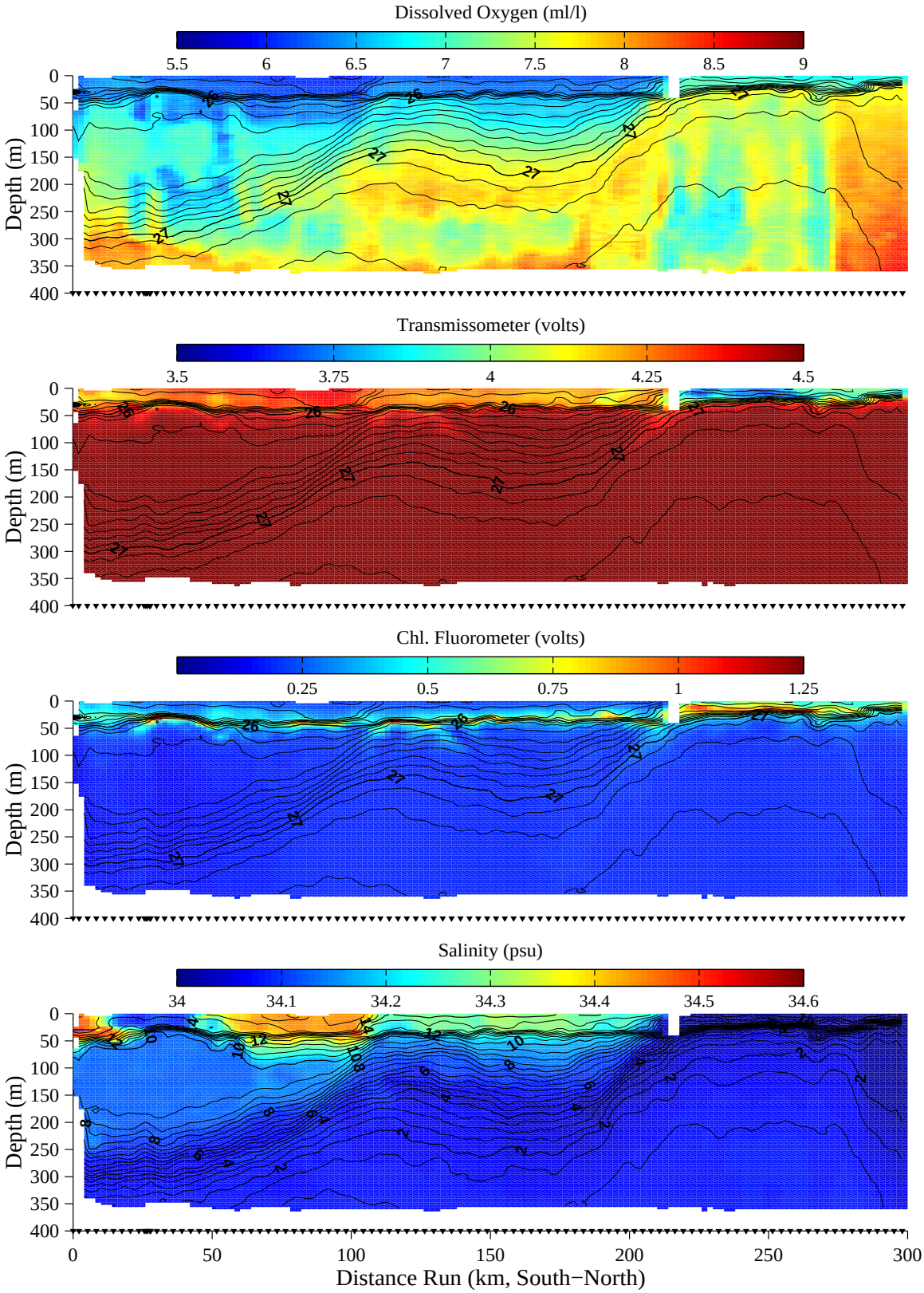

Figure 5a. Meridional section 1 across the subpolar front in survey 1 (see also Figures 1 and 3), plotted as in Figure 4. Sections in Figuires 5a–5b are presented sequentially (1–6) from west to east.

JES2: Survey 1, Section 2

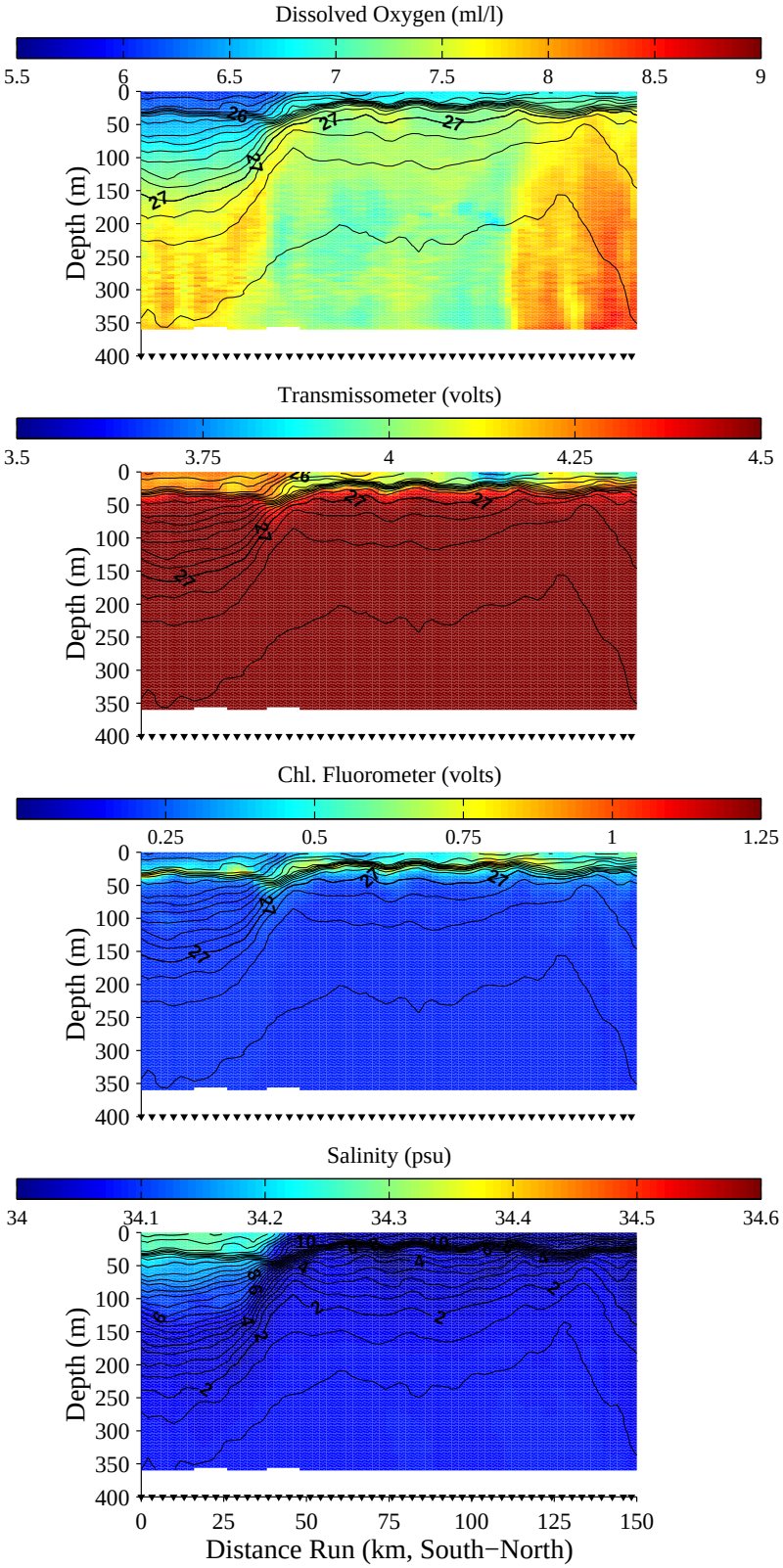

Figure 5b. Meridional section 2 across the subpolar front in survey 1, plotted as in Figure 4. .

JES2: Survey 1, Section 3

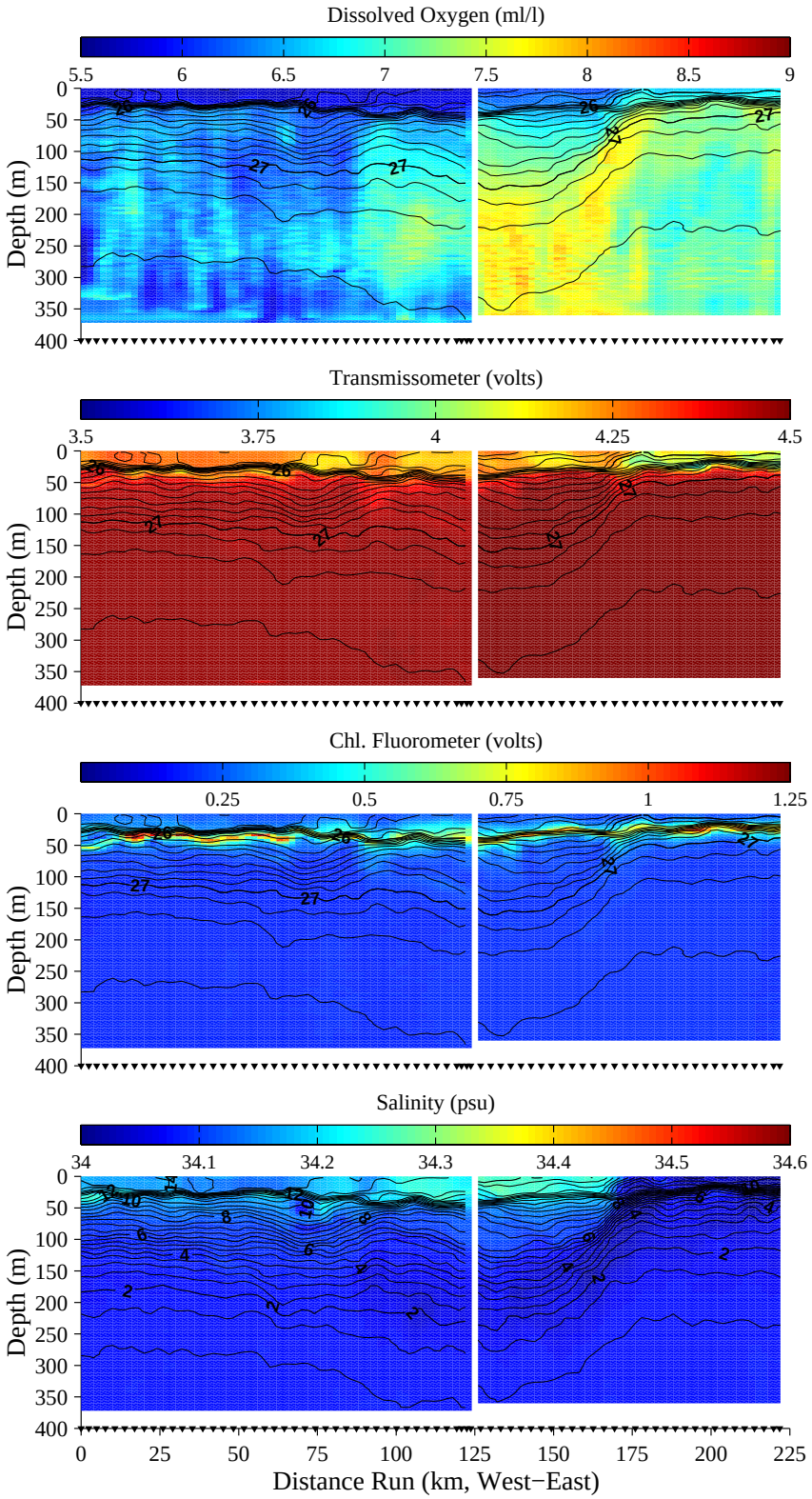

Figure 5c. Meridional section 3 across the subpolar front in survey 1), plotted as in Figure 4. The gap separates regions that were sampled approximately one and a half days apart.

JES2: Survey 1, Section 4

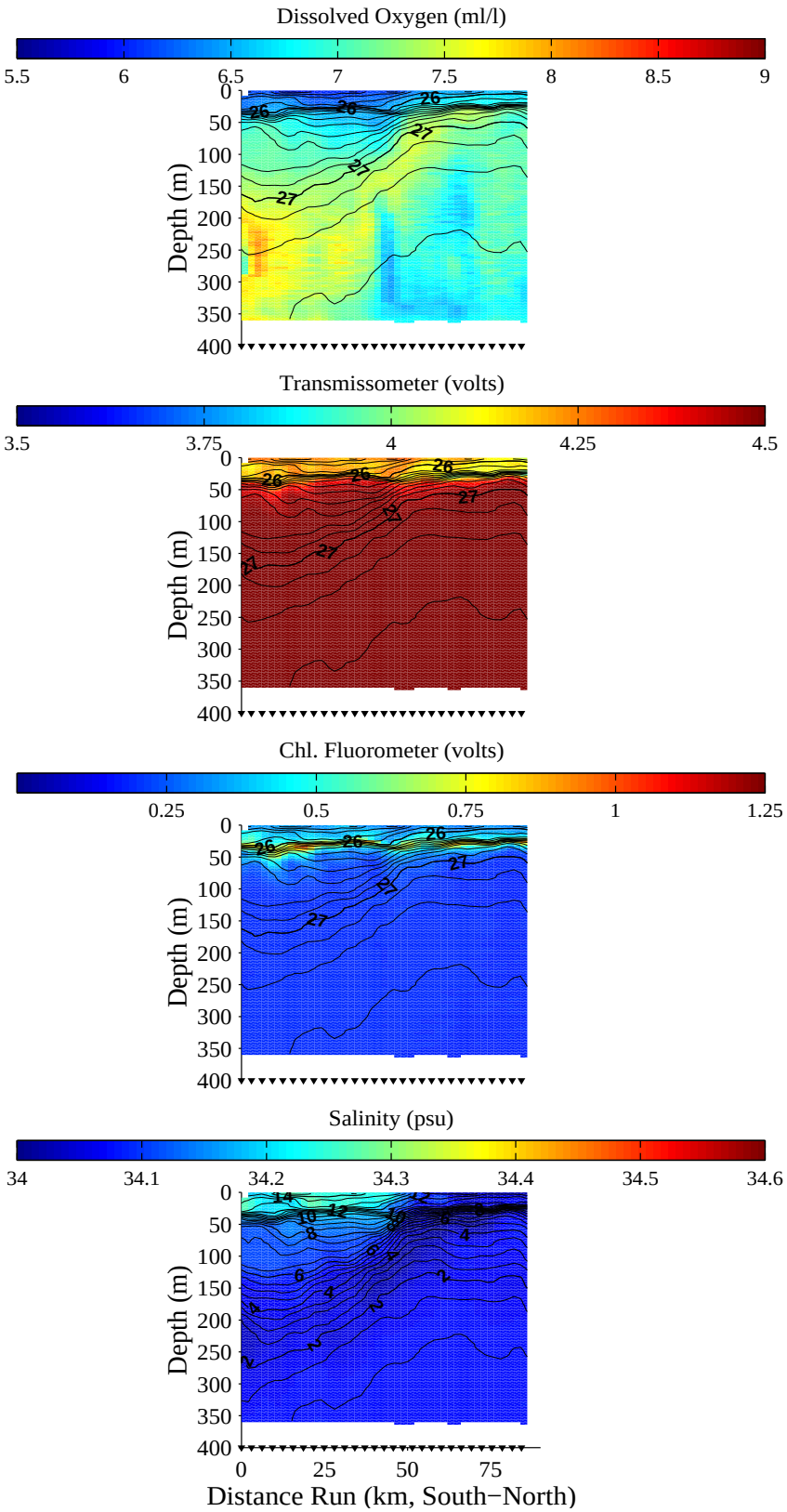

Figure 5d. Mmeridional section 4 across the subpolar front in survey 1, plotted as in Figure 4.

JES2: Survey 1, Section 5

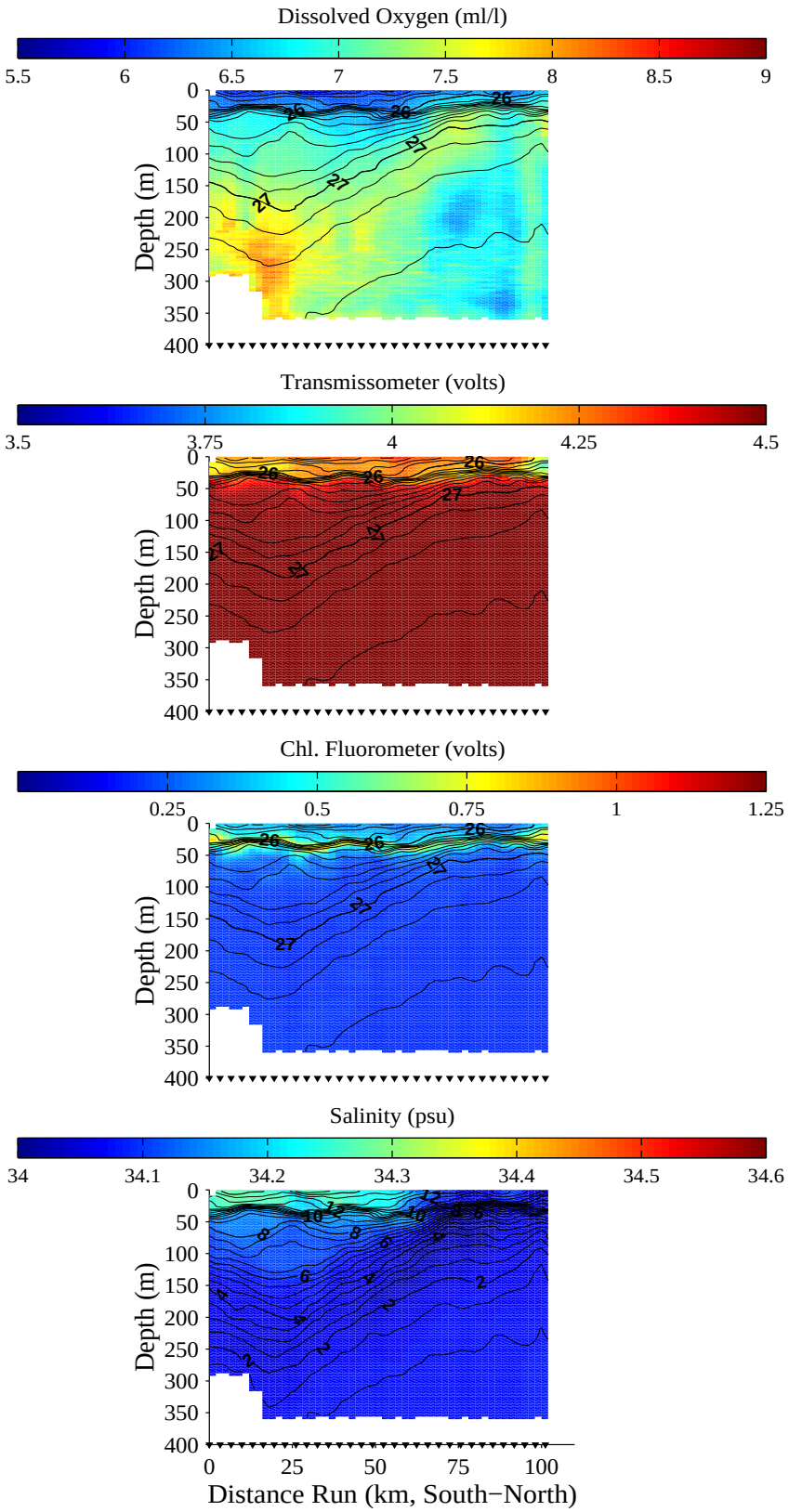

Figure 5e. Meridional section 5 across the subpolar front in survey 1), plotted as in Figure 4.

JES2: Survey 1, Section 6

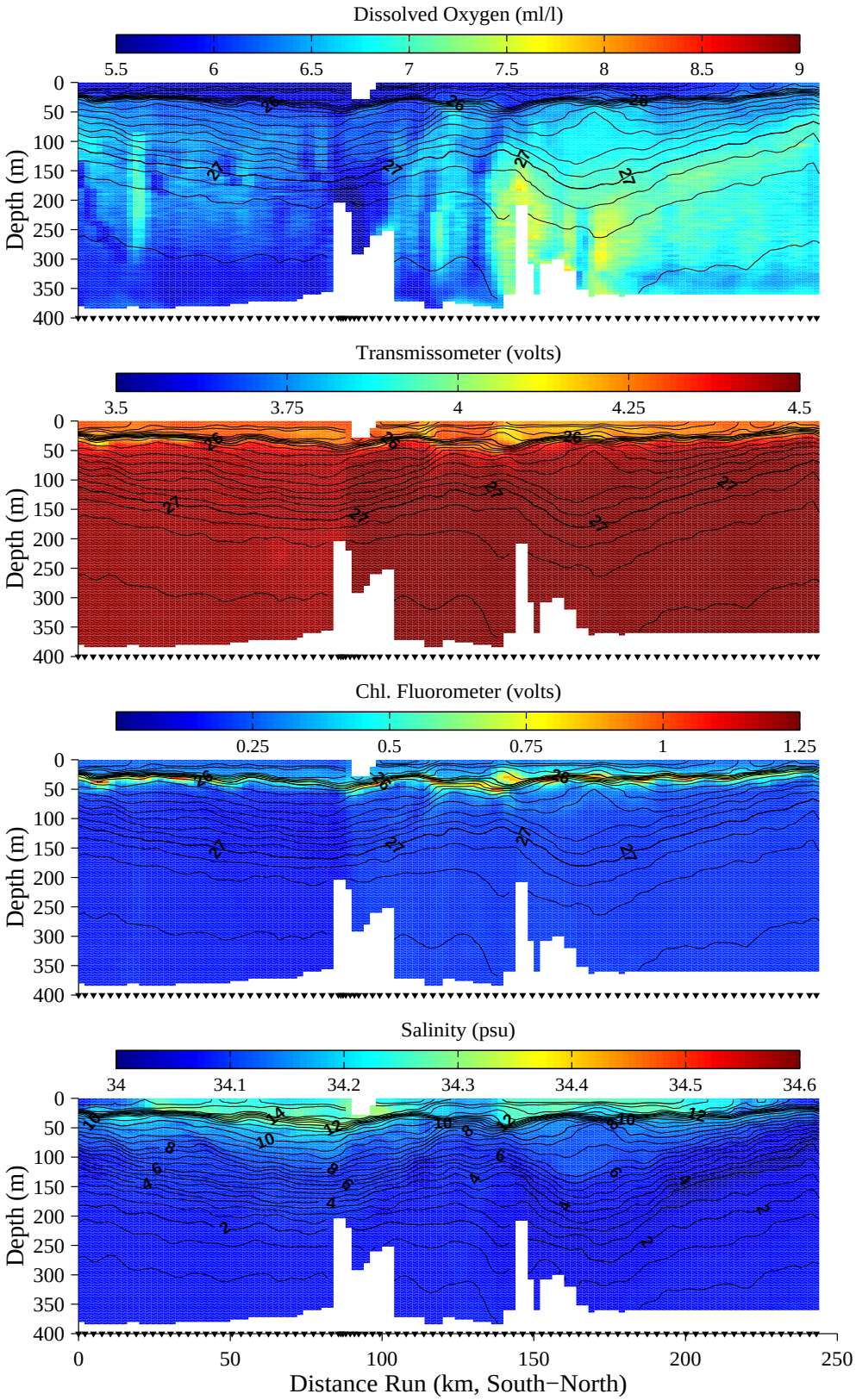

Figure 5f. Meridional section 6 across the subpolar front in survey 1, plotted as in Figure 4.

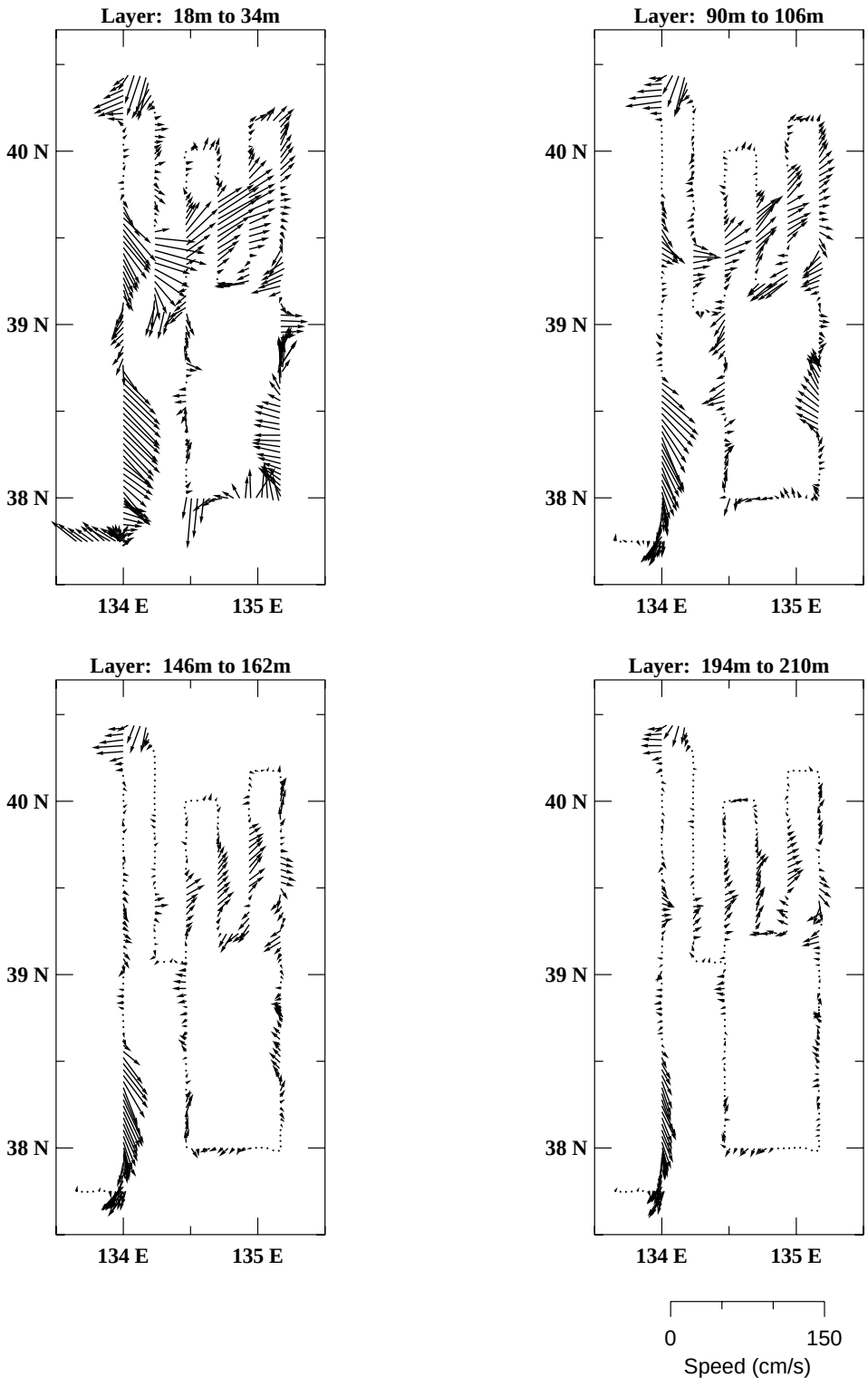

Figure 6. Upper ocean velocities measured by the shipboard acoustic Doppler current profiler (ADCP). The panels show velocity vectors for survey 1, averaged over selected depth ranges. The scale bar in the lower left corner indicates the speeds represented by the vector lengths.

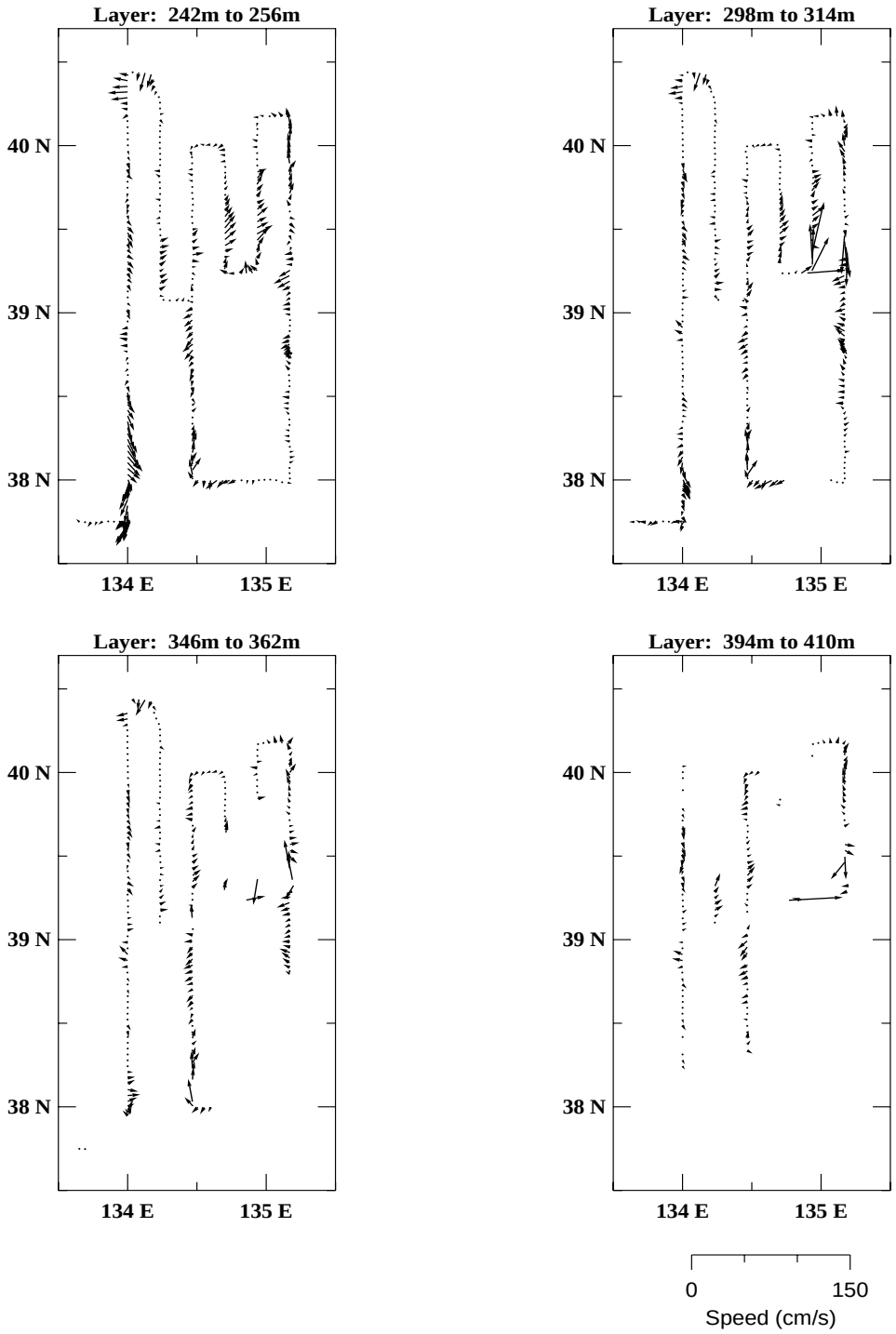

Figure 6, cont.

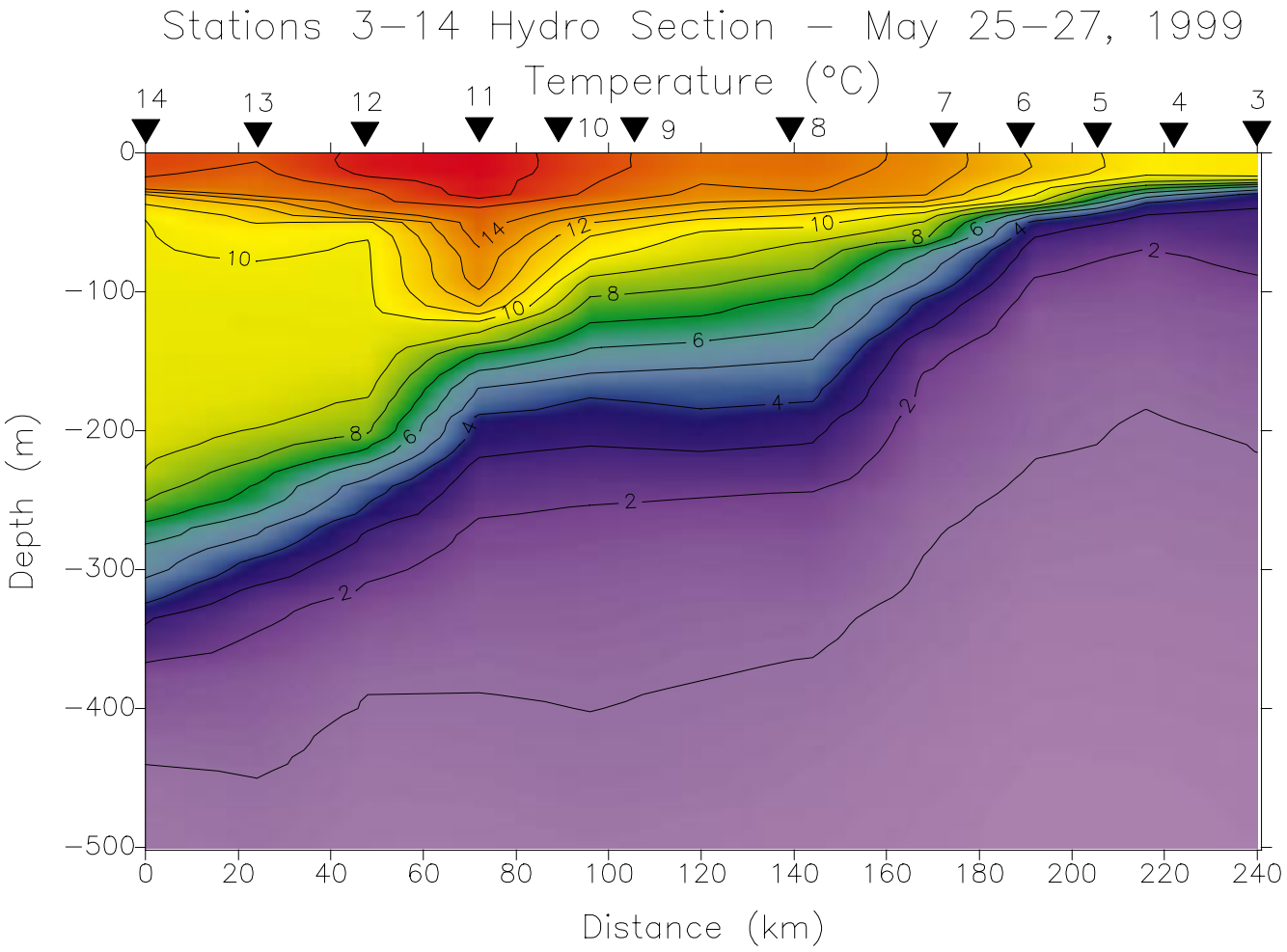

Figure 7. Temperature data from the cross-front hydrographic section occupied along survey 1, section 1 (see Figures 1, 3, and 5). The large triangles along the top of the frame indicate station locations.

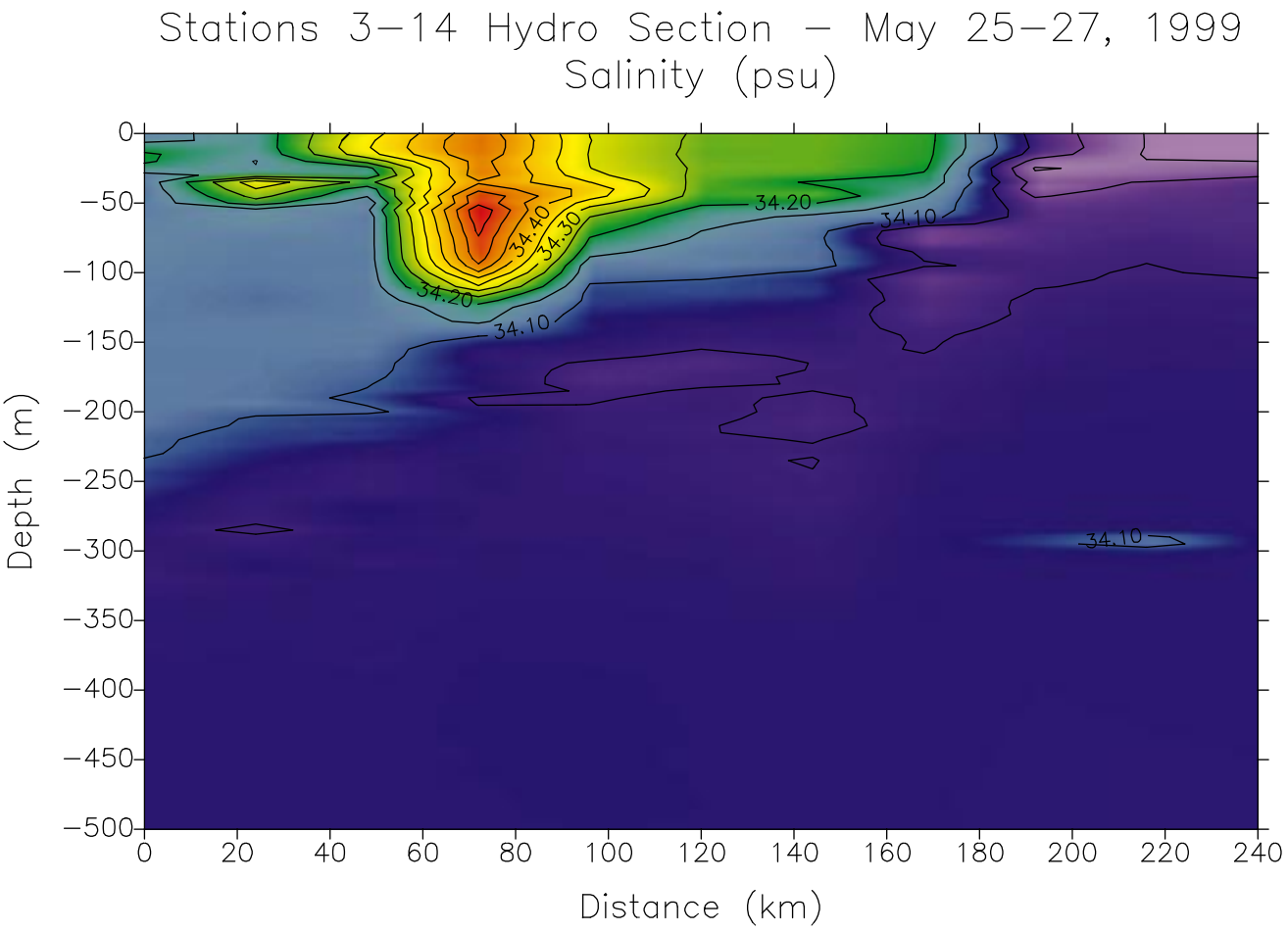

Figure 8. Salinity data from the cross-front hydrographic section, plotted as in Figure 7.

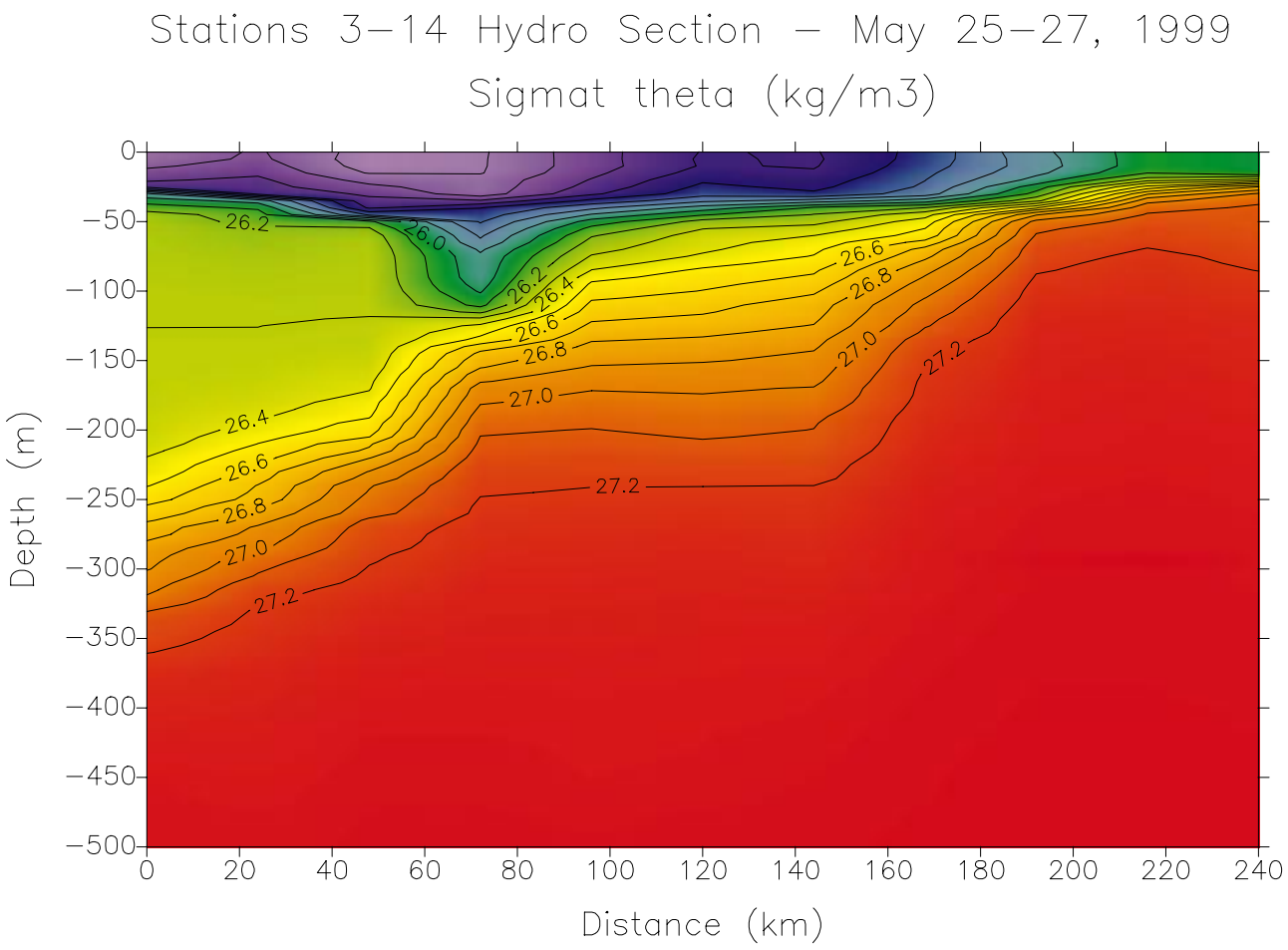

Figure 9. Potential density from the cross-front hydrographic section, plotted as in Figure 7.

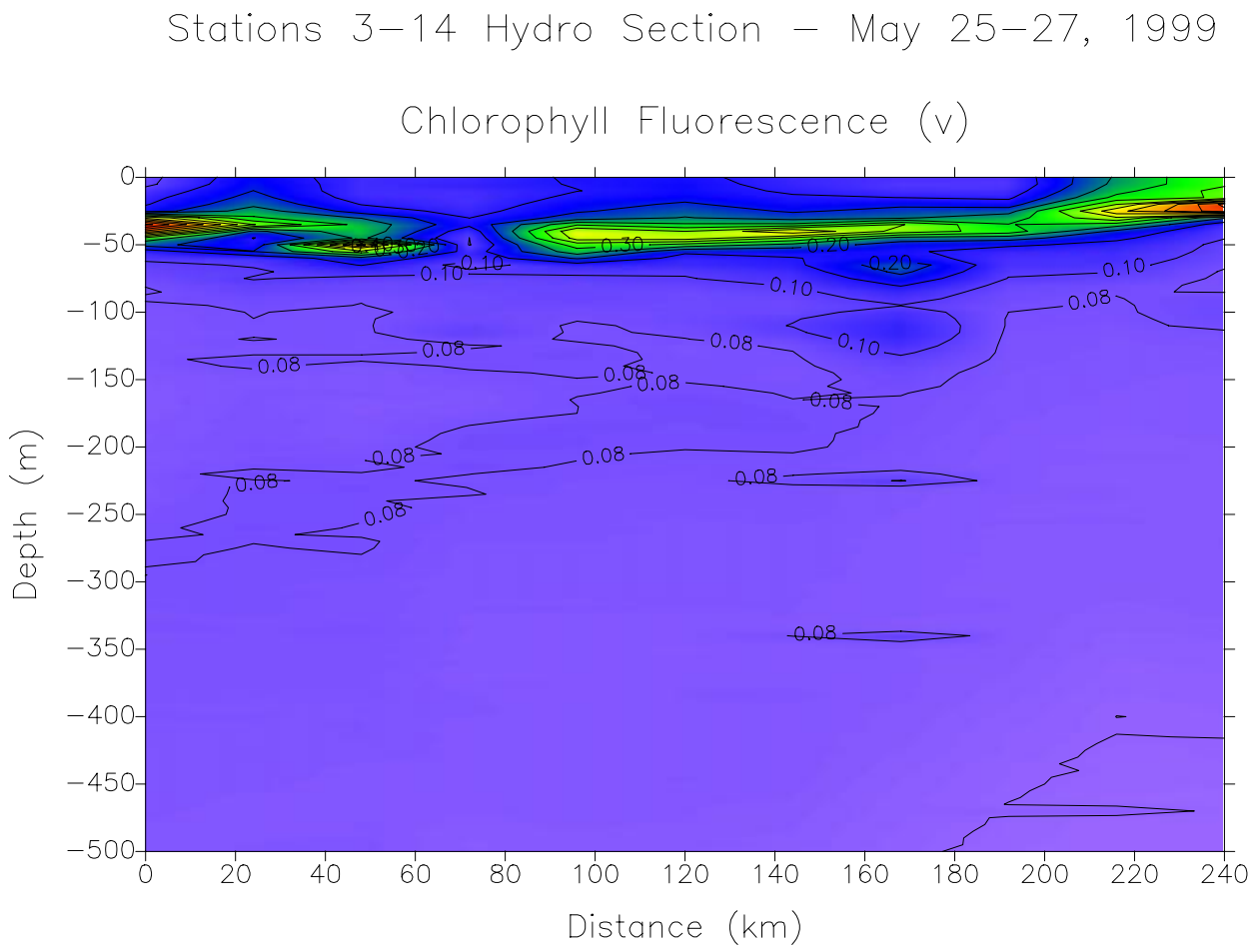

Figure 10. Chlorophyll fluorescence (shown in volts; large values suggest high chlorophyll content) from the cross-front hydrographic section, plotted as in Figure 7.

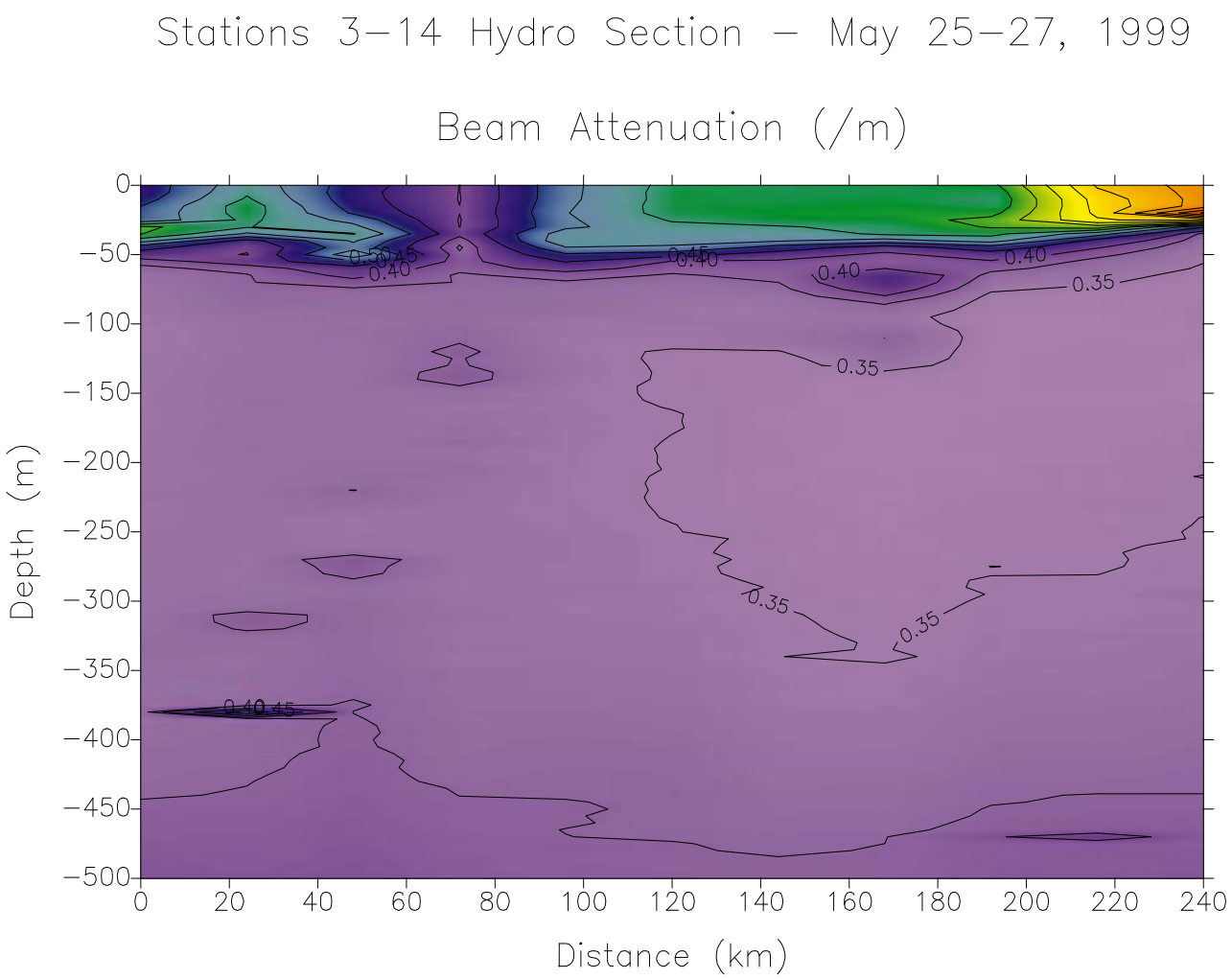

Figure 11. Light transmission (shown in volts; large values indicate low light transmission) from the cross-front hydrographic section, plotted as in Figure 7.

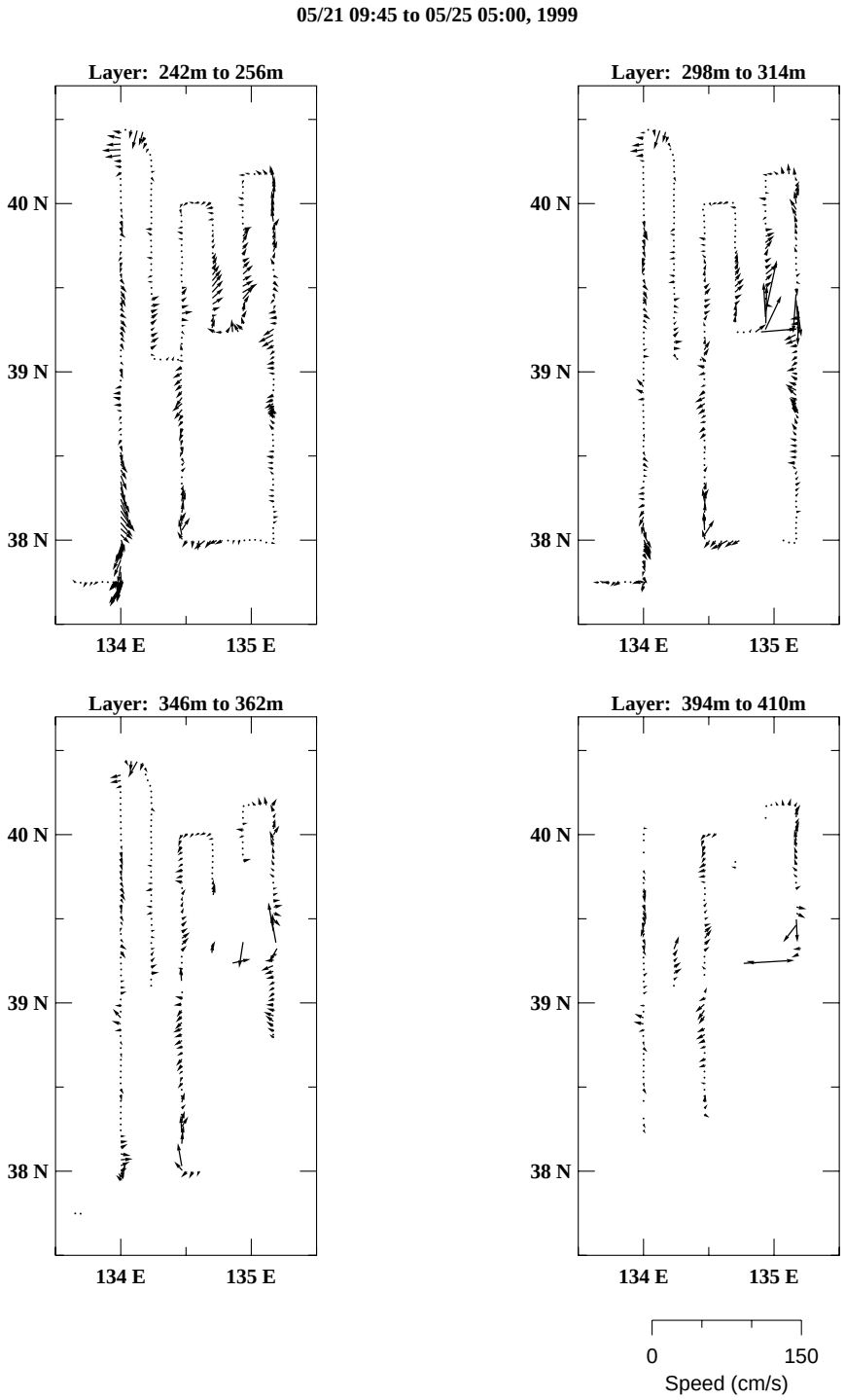

Figure 12. Dissolved oxygen concentration and percent saturation from the cross-front hydrographic section, plotted as in Figure 7. These values were obtained from the analysis of discrete water samples.

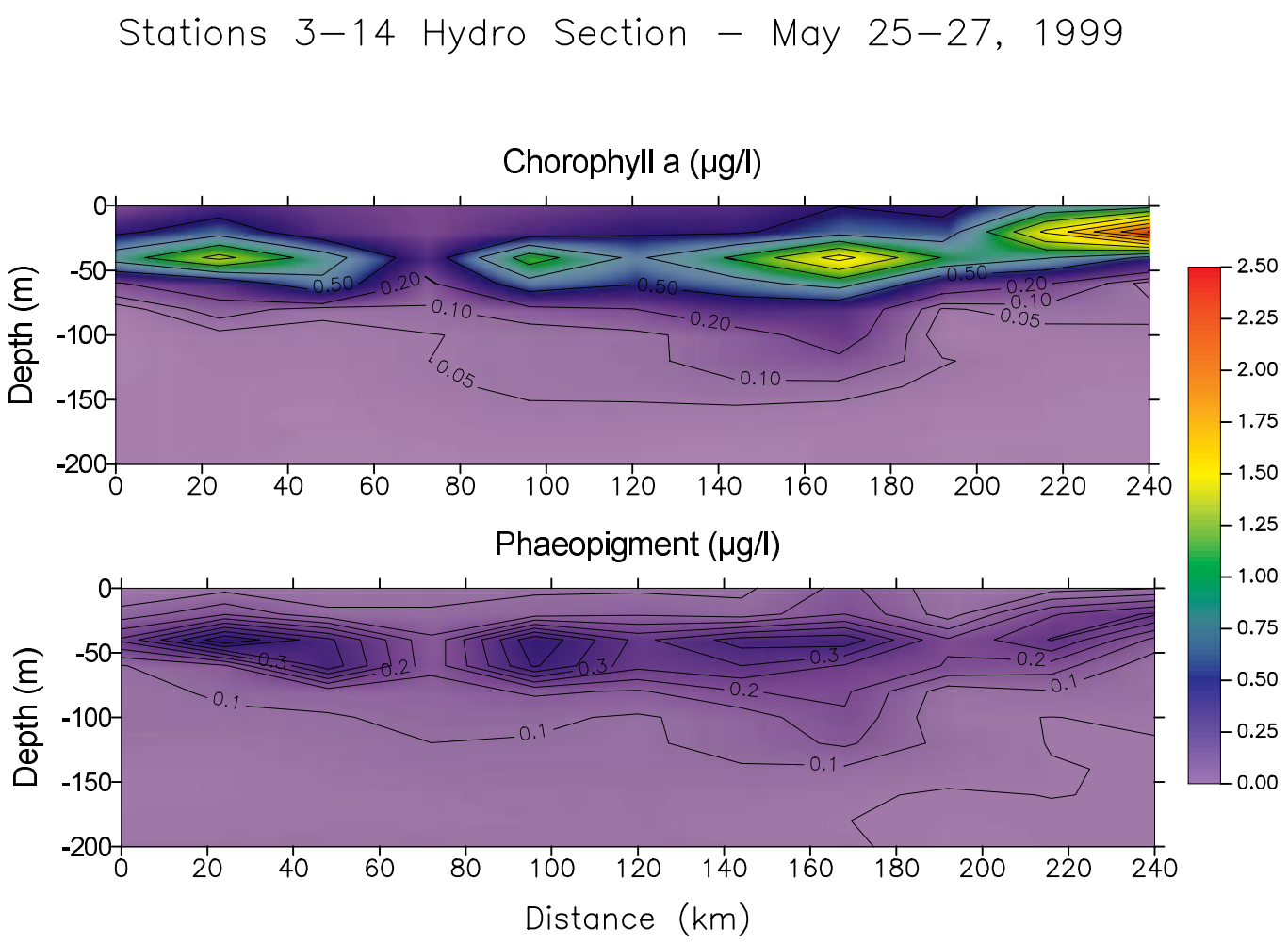

Figure 13. Chlorophyll a and phaeopigment concentrations from the cross-front hydrographic section, plotted as in Figure 7. These values were obtained from the analysis of discrete water samples and are displayed only for the upper 200 m.

JES2: Survey 2, Section 1 Pass 2

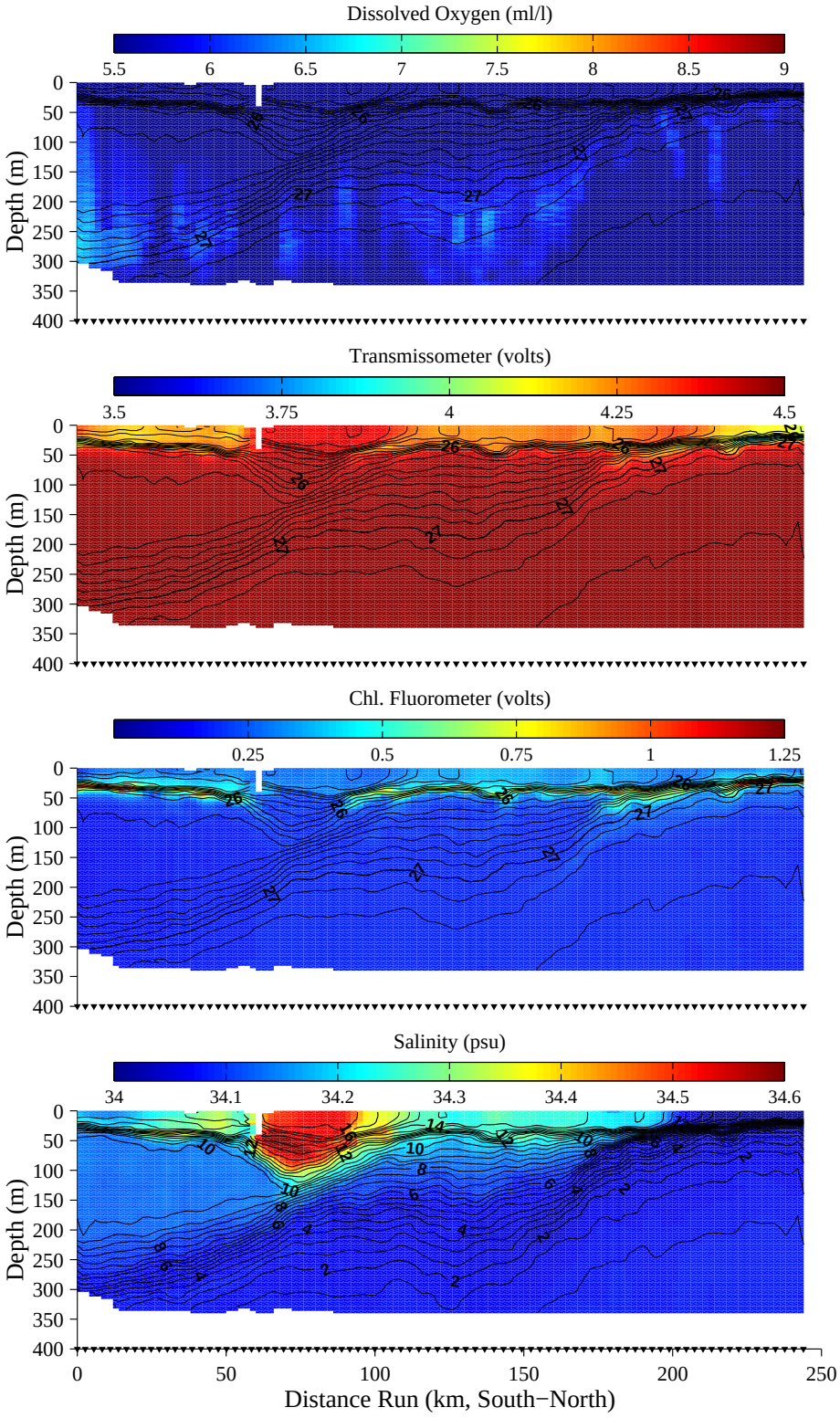

Figure 14a. Meridional section 1 across the subpolar front on survey 2 (see also Figures 1 and 3), plotted as in Figure 4. Sections are presented sequentially (1–6) from west to east.

JES2: Survey 2, Section 2

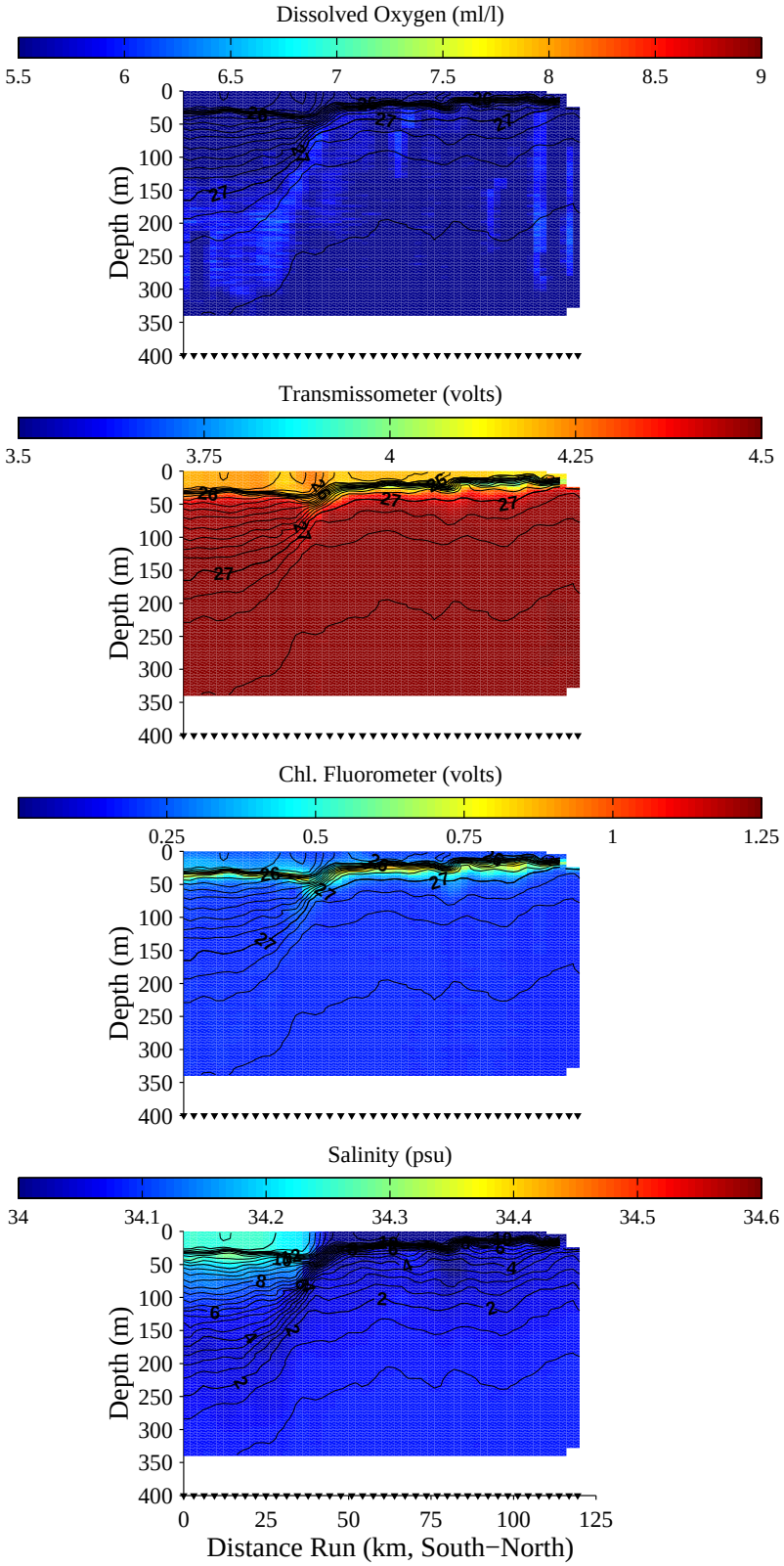

Figure 14b. Meridional section 2 across the subpolar front on survey 2 , plotted as in Figure 4.

JES2: Survey 2, Section 3

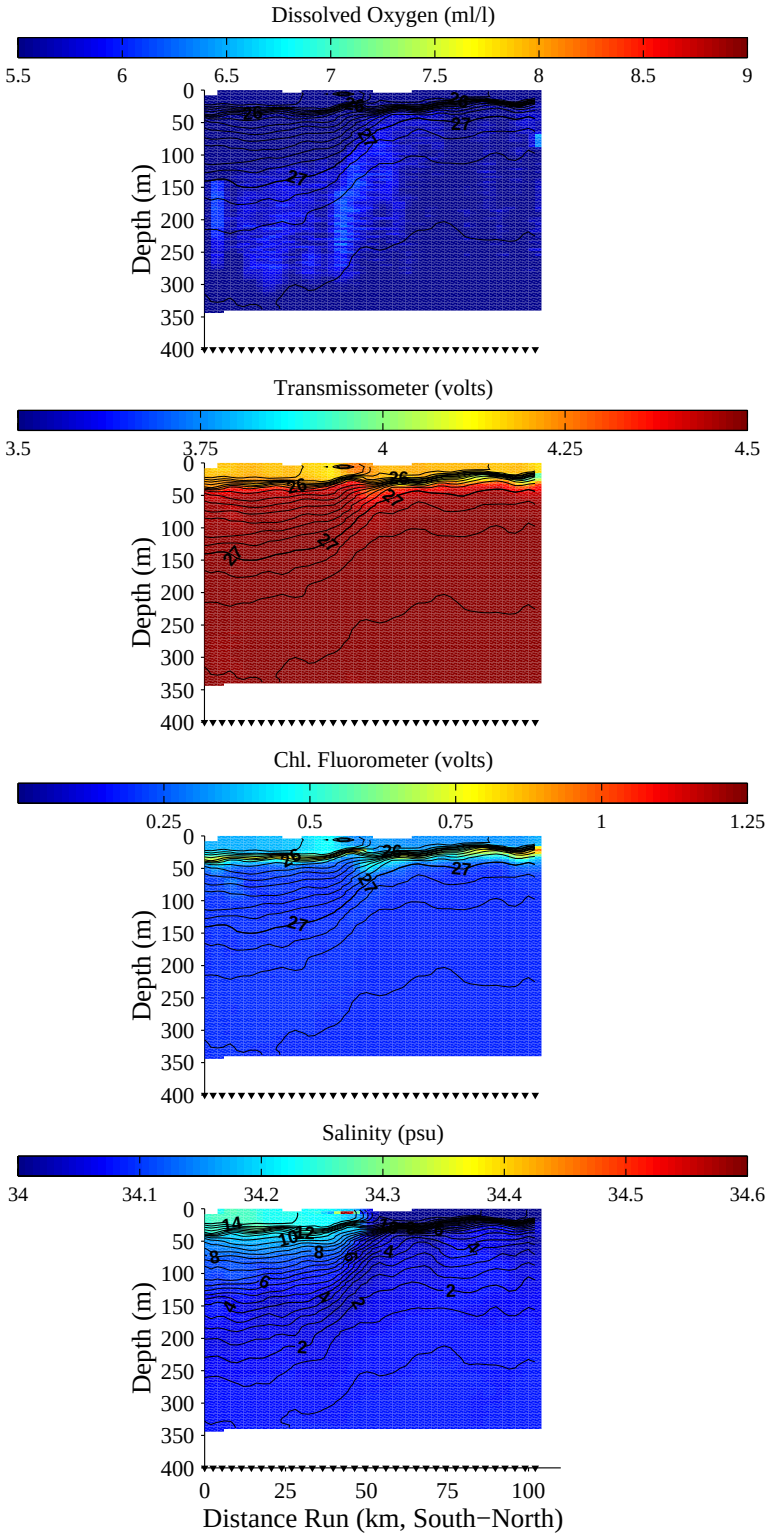

Figure 14c. Meridional section 3 across the subpolar front on survey 2 , plotted as in Figure 4.

JES2: Survey 2, Section 4

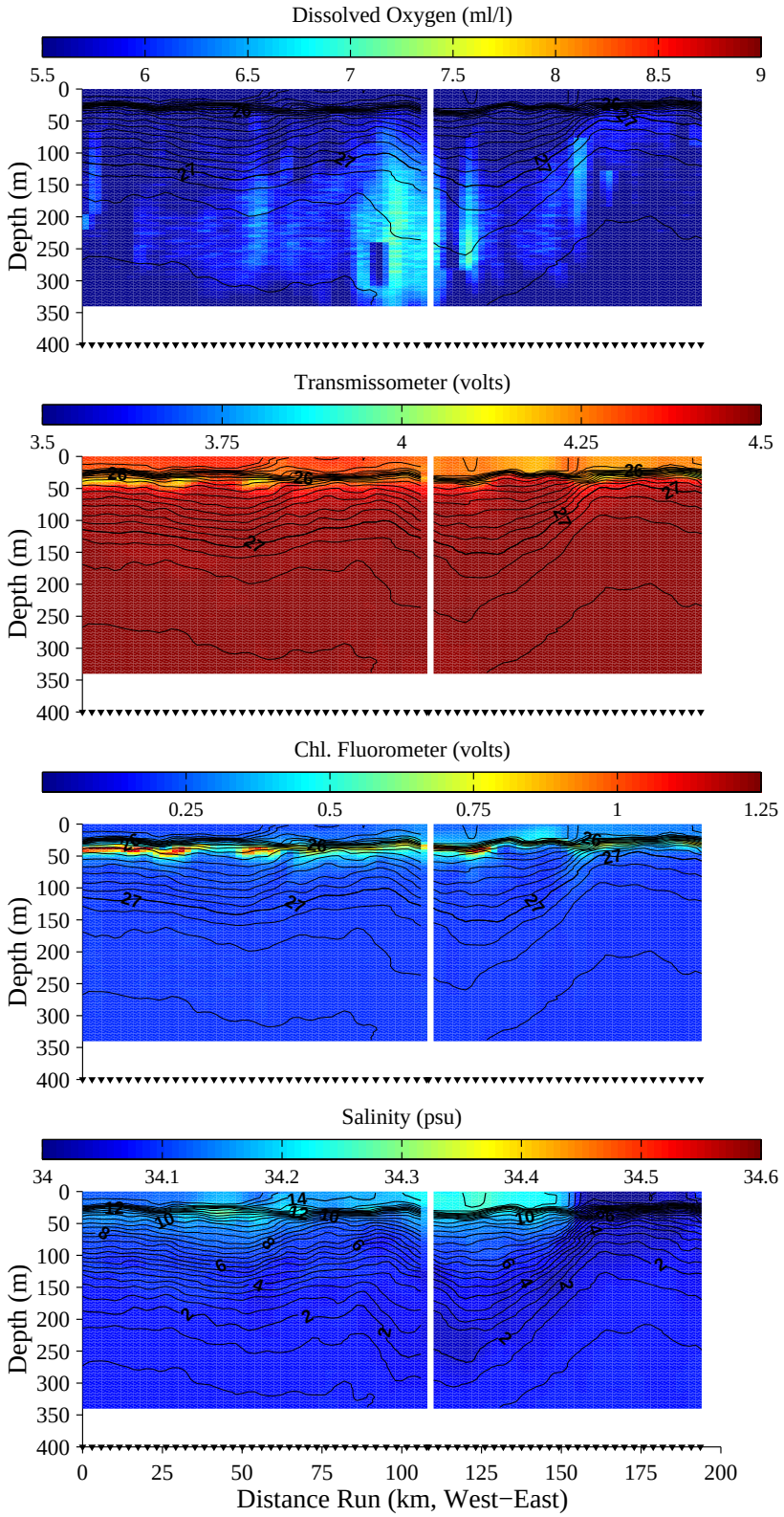

Figure 14d. Meridional section 4 across the subpolar front on survey 2 , plotted as in Figure 4. The gap separates regions that were sampled approximately 1 day apart.

JES2: Survey 2, Section 5

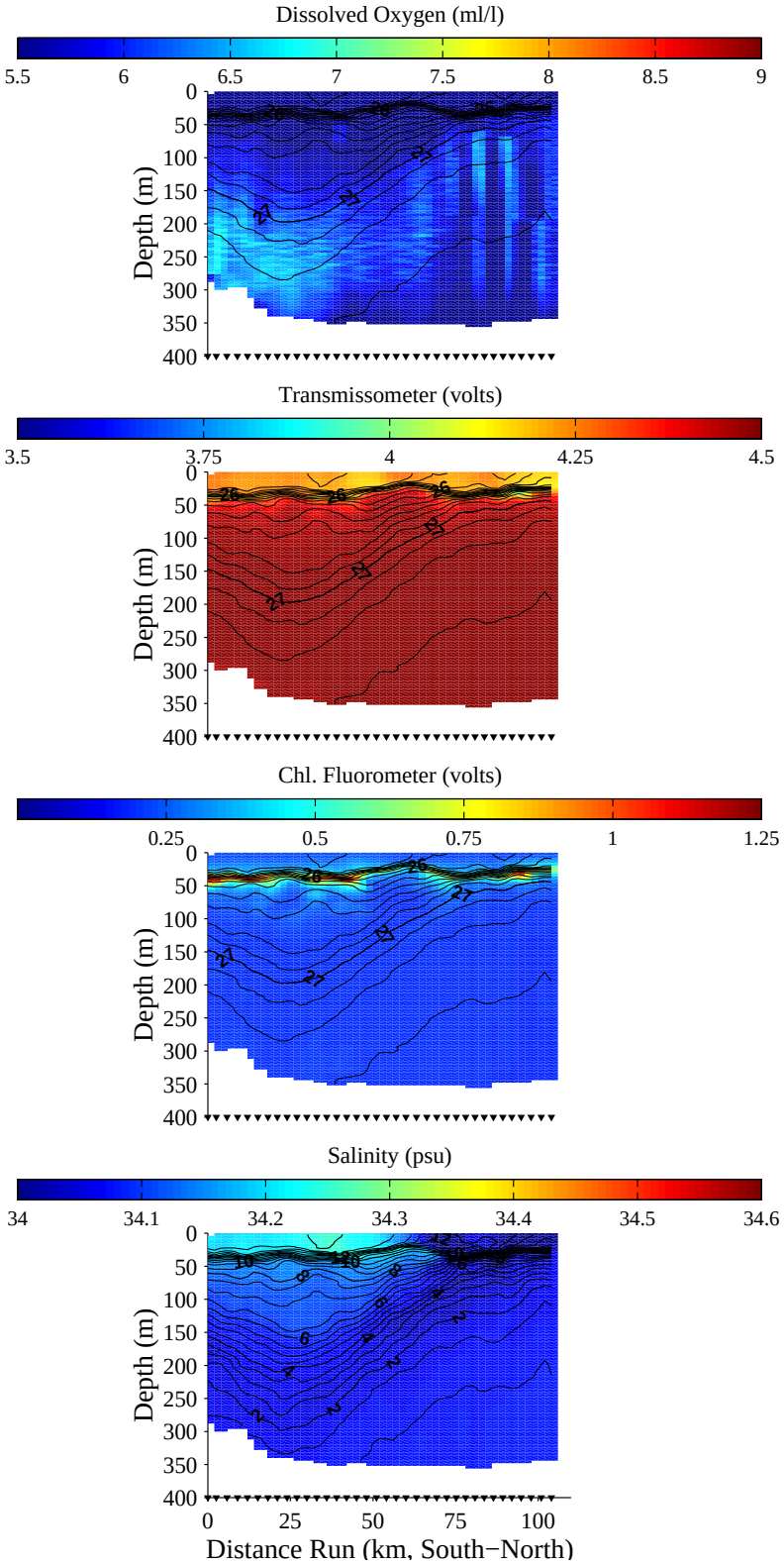

Figure 14e. Meridional section 5 across the subpolar front on survey 2 , plotted as in Figure 4.

JES2: Survey 2, Section 6

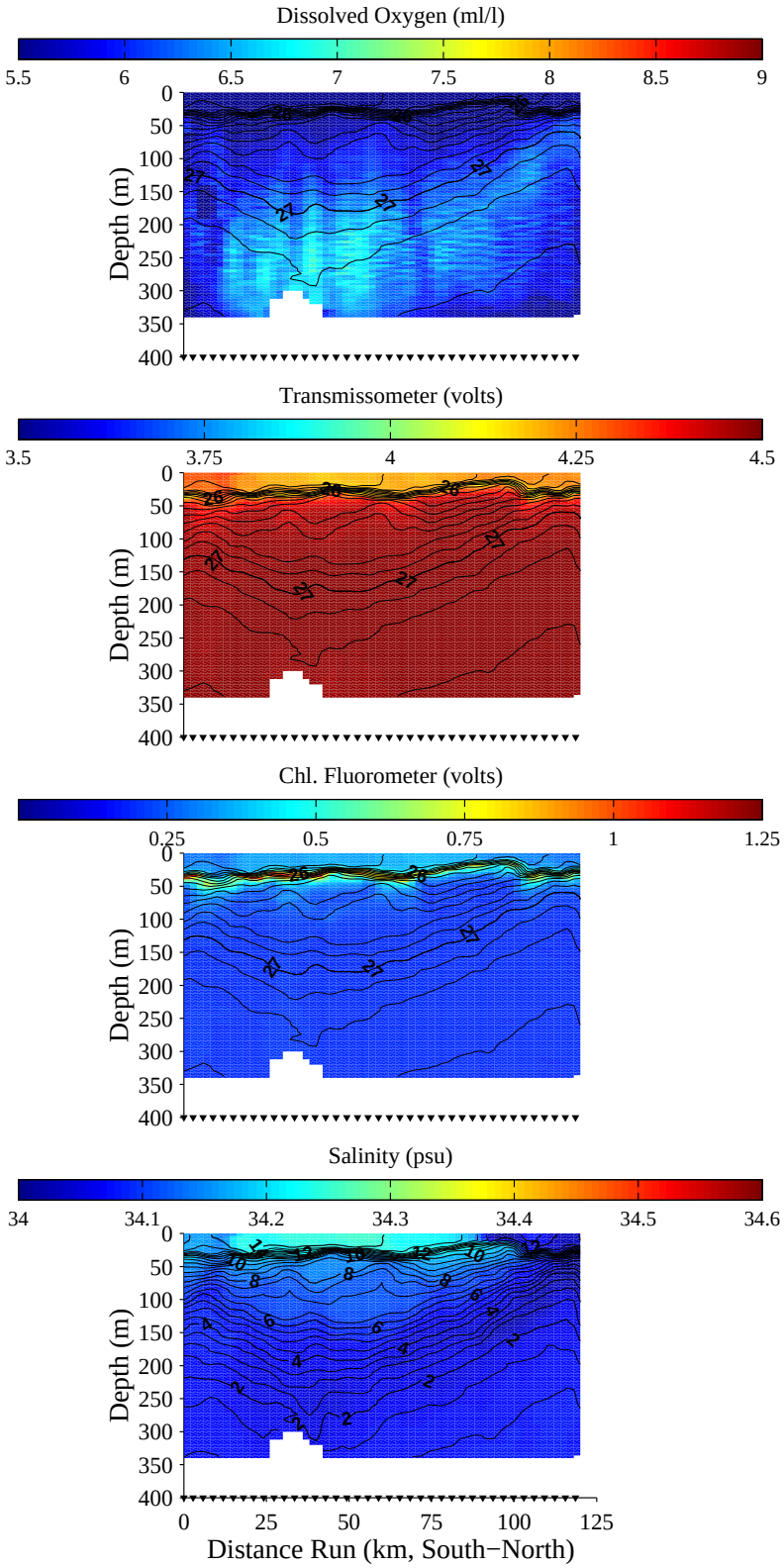

Figure 14f. Meridional section 6 across the subpolar front on survey 2, plotted as in Figure 4.

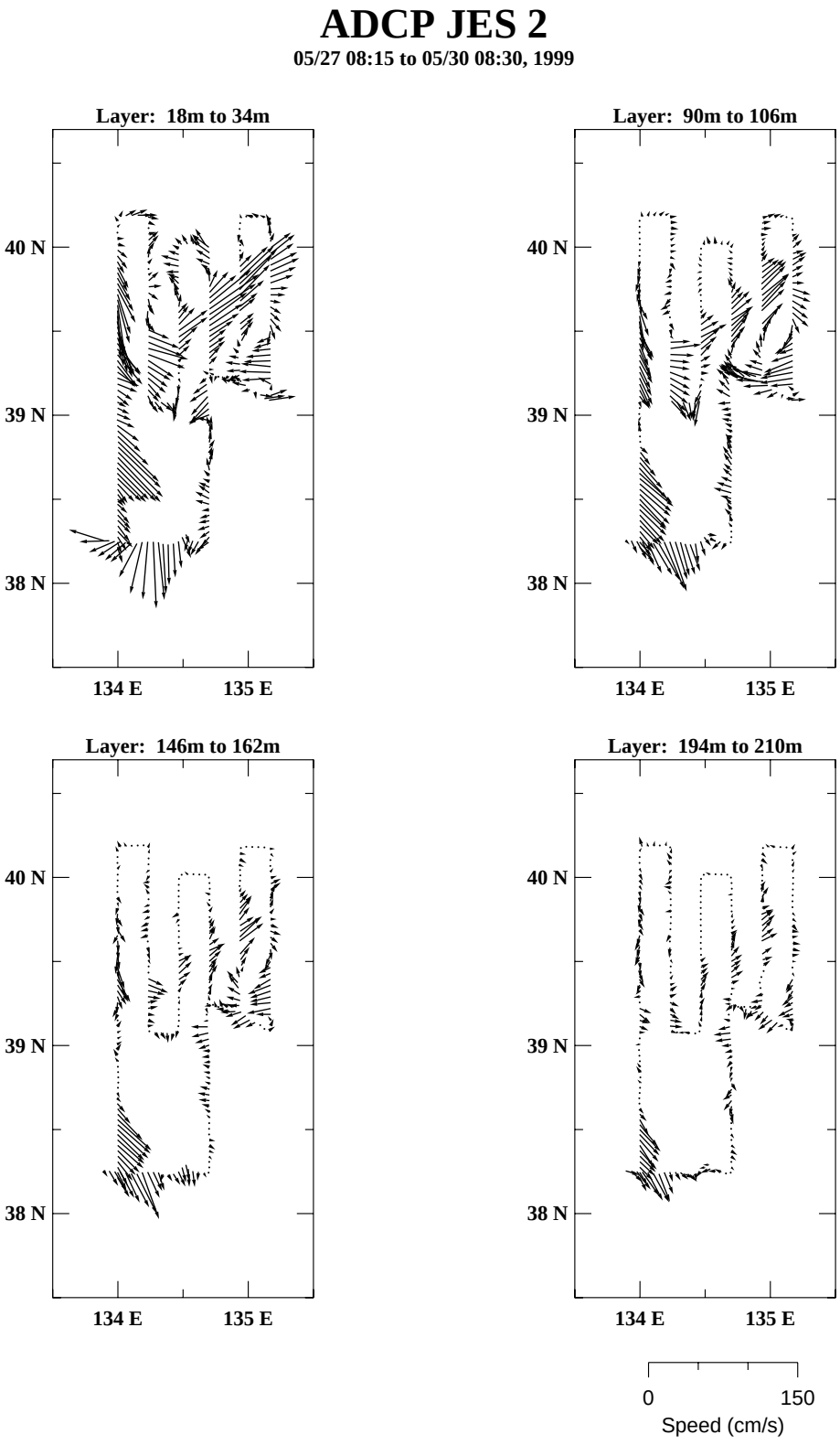

Figure 15. Upper ocean velocities for survey 2, plotted as in Figure 6.

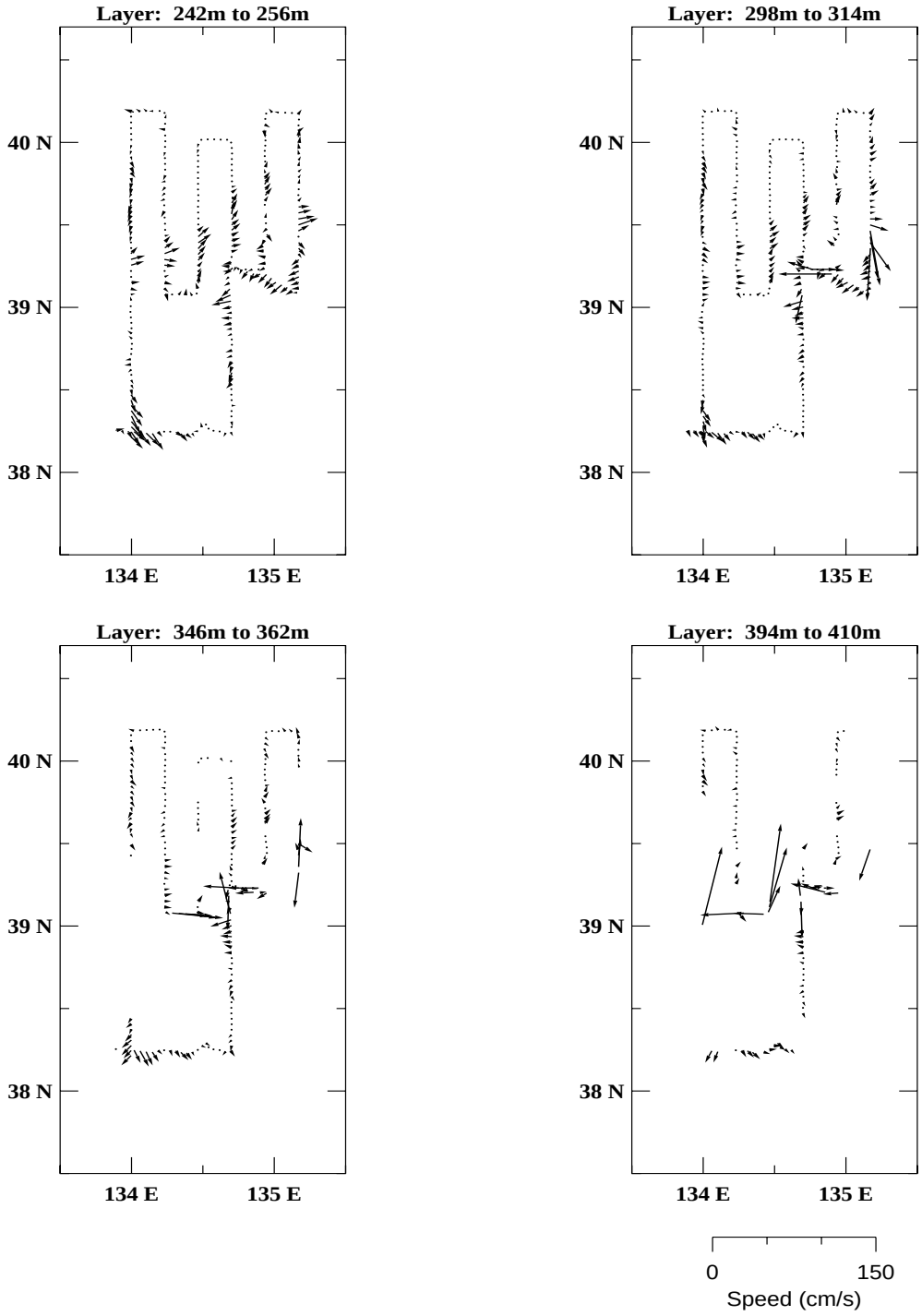

Figure 15, cont.

JES2: Survey 3, Western S−N Section

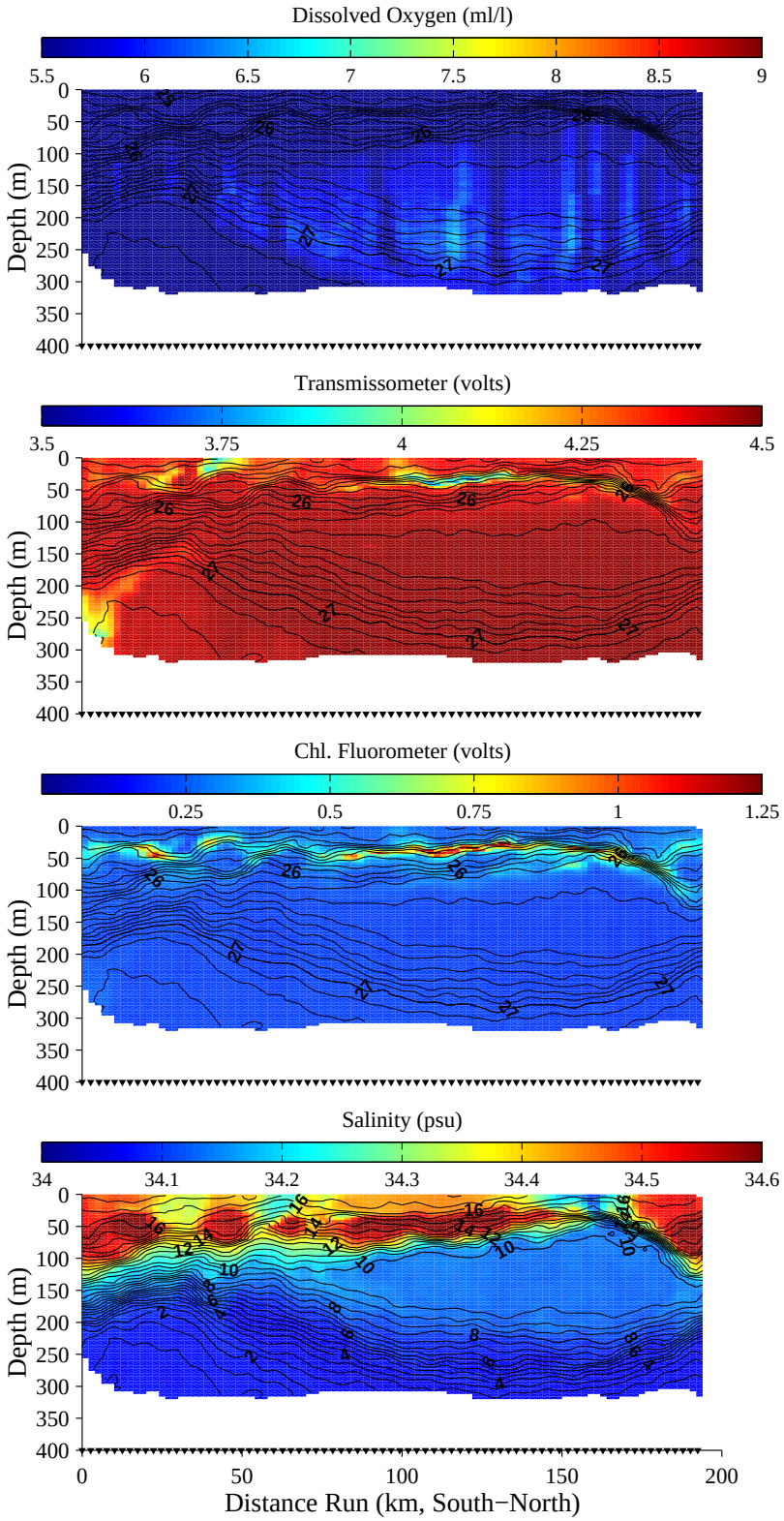

Figure 16a. Meridional section (survey 3) through a meander current (see also Figures 1 and 3), plotted as in Figure 4. The gaps in the eastern meridional section (b) and in the central zonal section (d) separate regions that were sampled several days apart.

JES2: Survey 3, Eastern S−N Section

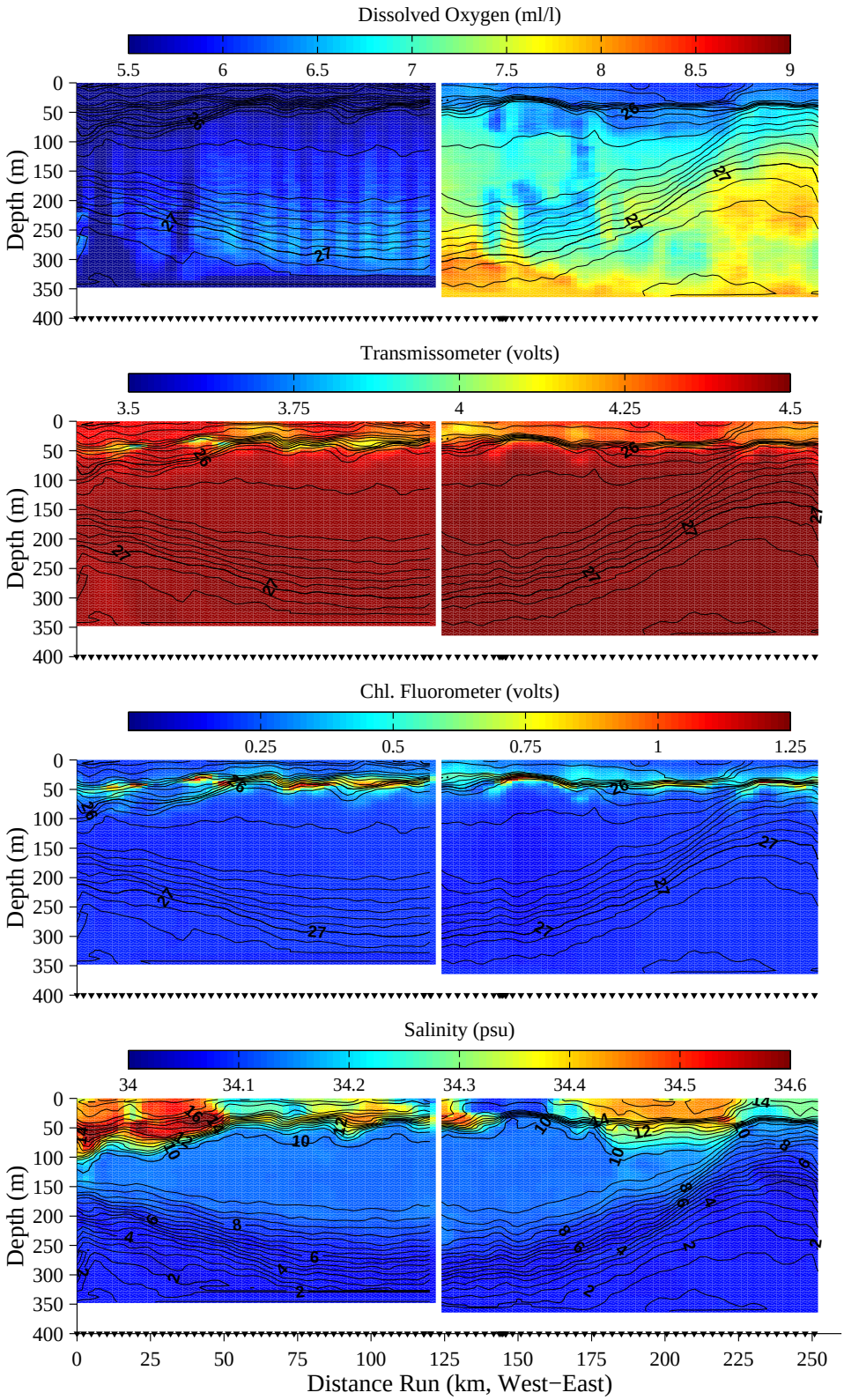

Figure 16b. Meridional section (survey 3) through a meander current, plotted as in Figure 4. The gaps separate regions that were sampled several days apart.

JES2: Survey 3, South W−E Section

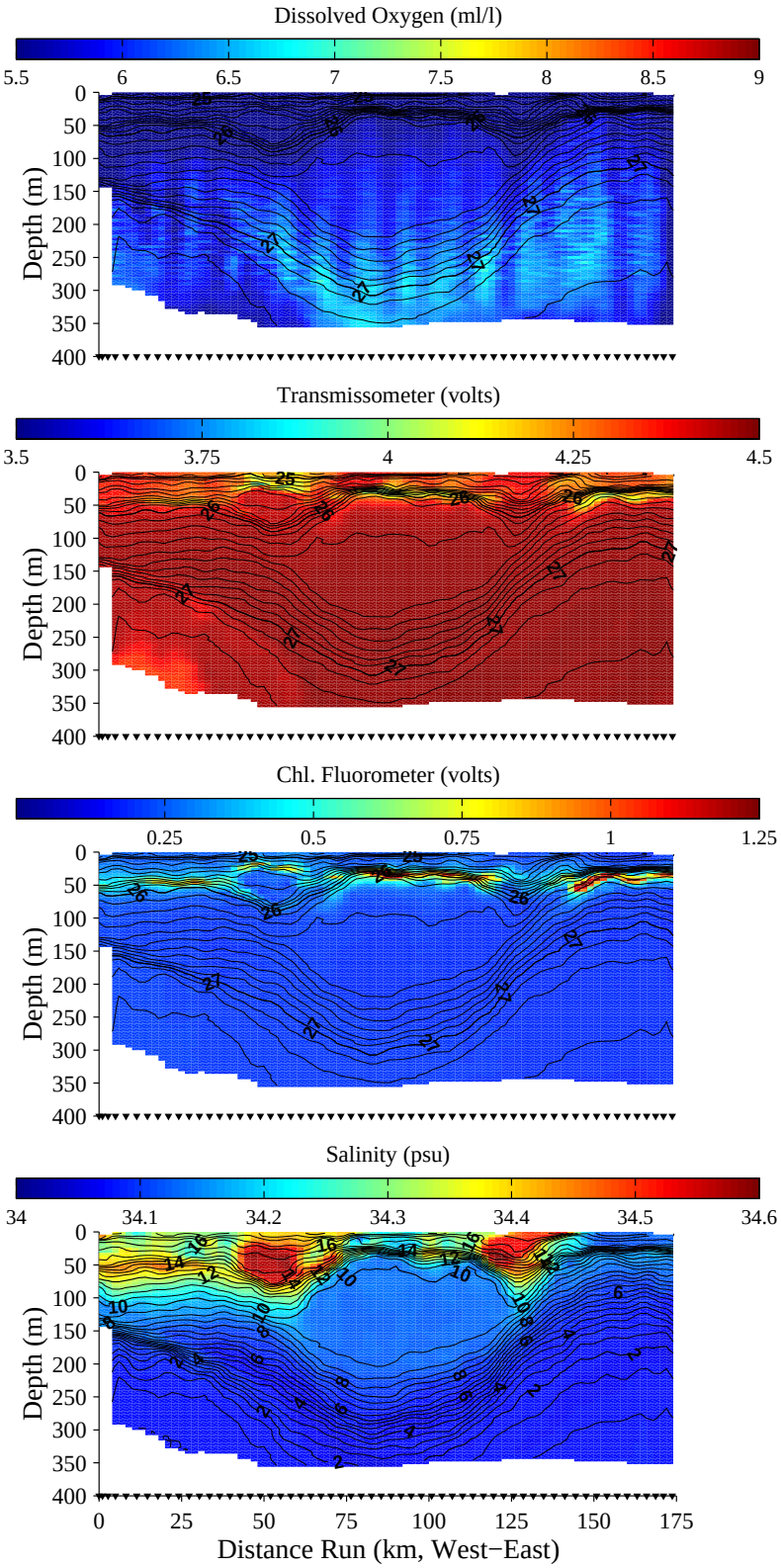

Figure 16c. Zonal section (survey 3) through a meander current, plotted as in Figure 4.

JES2: Survey 3, Central W−E Section

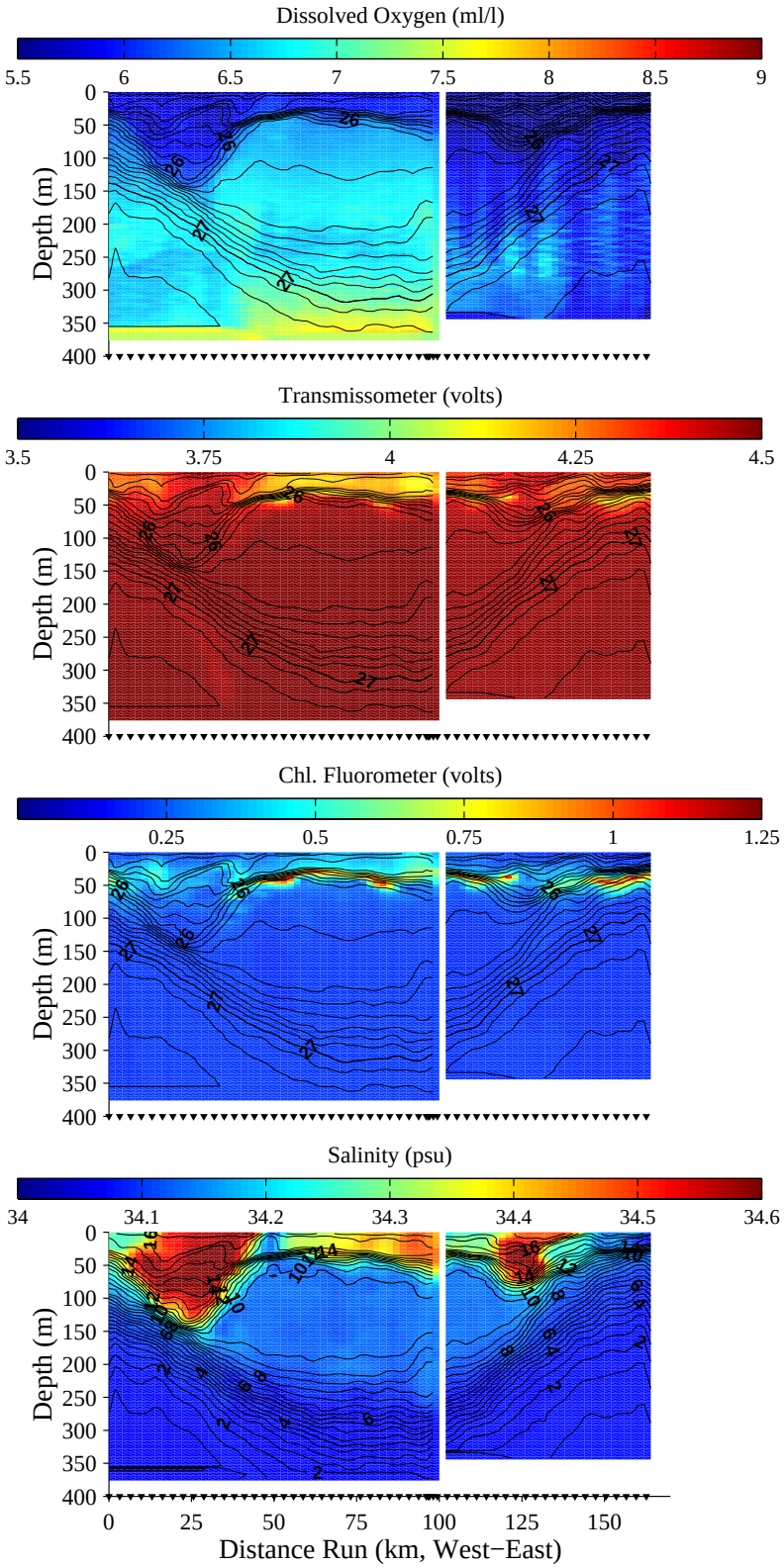

Figure 16d . Zonal section (survey 3) through a meander current, plotted as in Figure 4. The gaps separate regions that were sampled several days apart.

JES2: Survey 3, Northern W−E Section

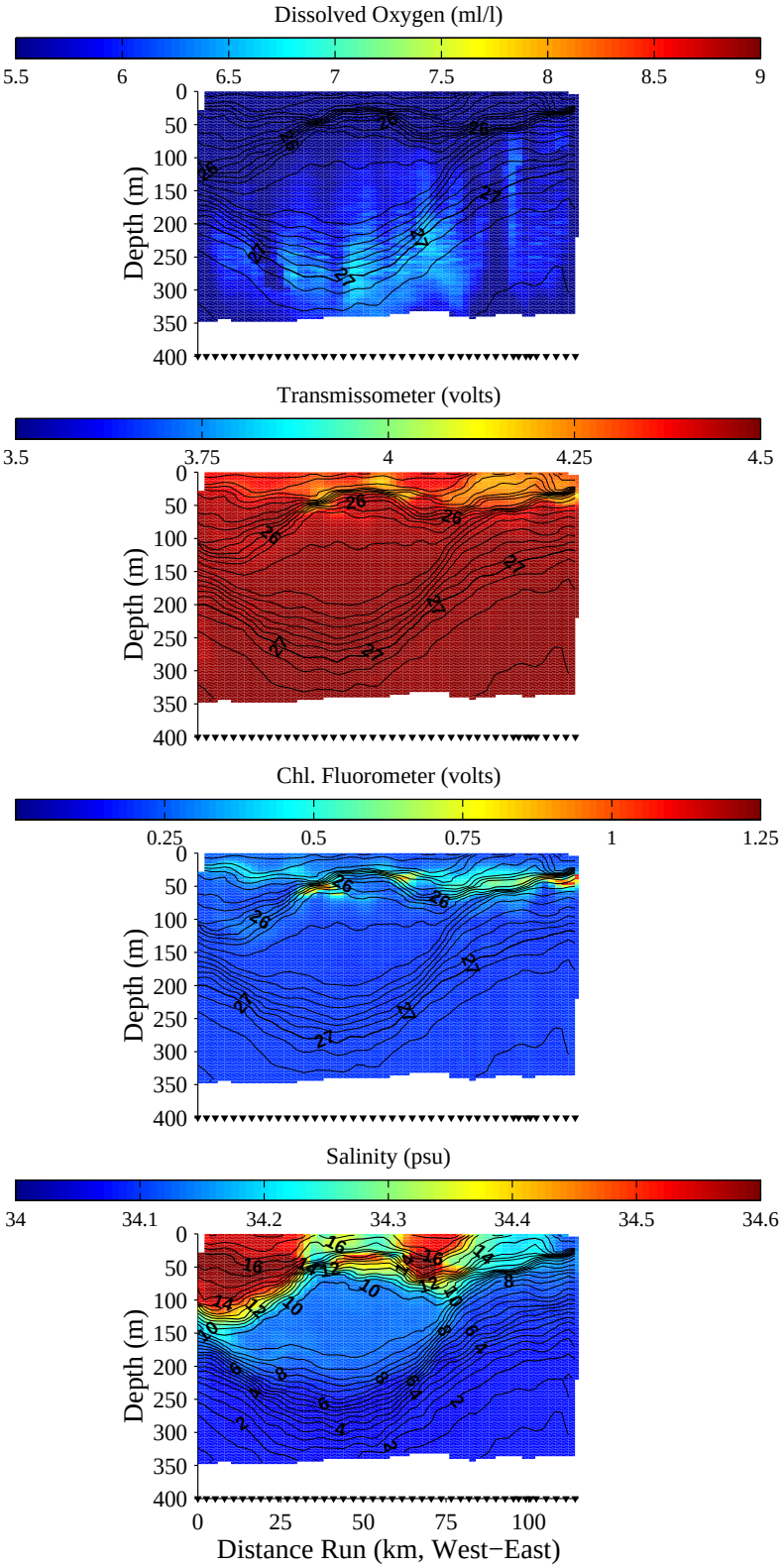

Figure 16e. Zonal section (survey 3) through a meander current, plotted as in Figure 4.

JES2: Cross−Shelf Section 36° 10 N

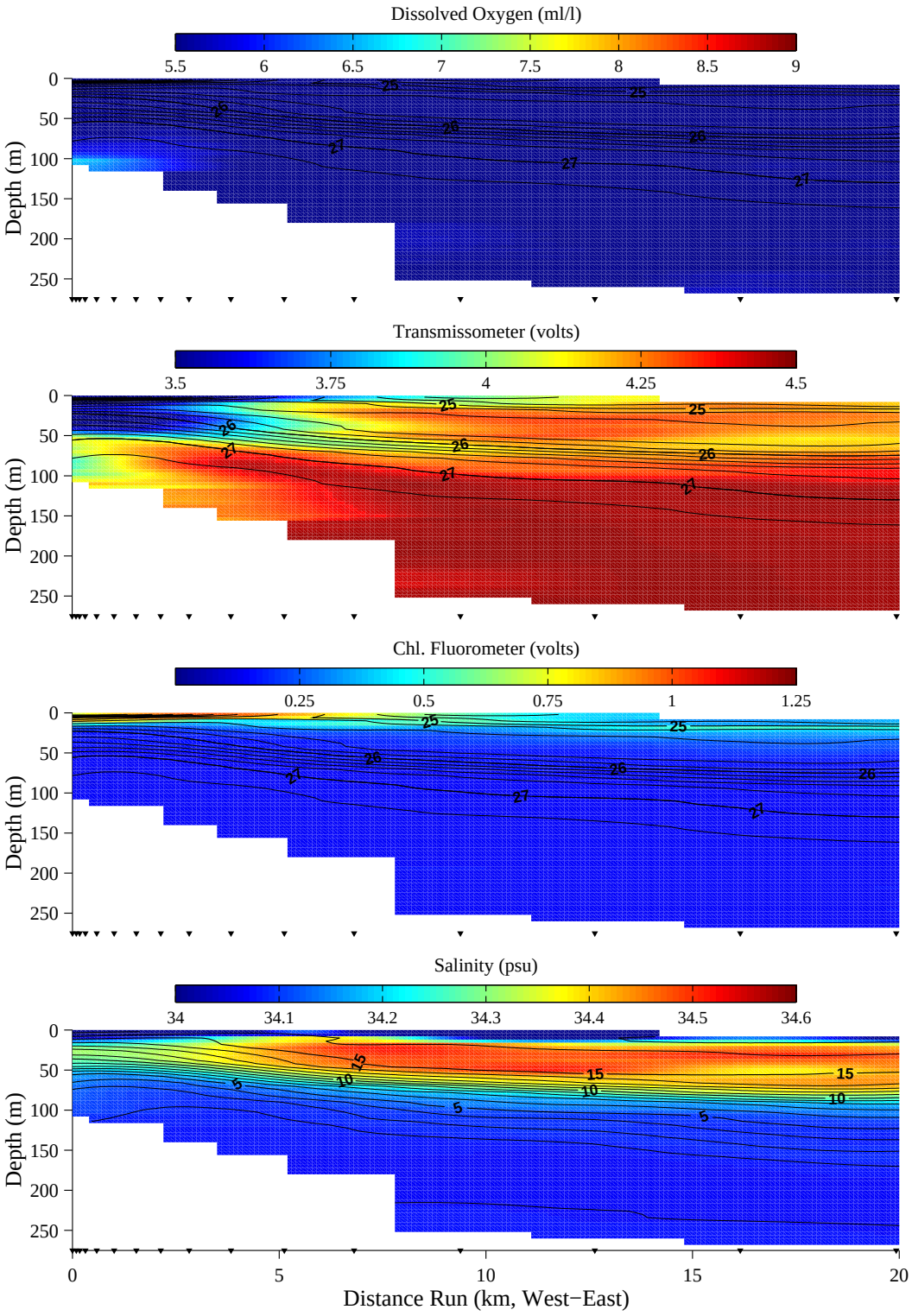

Figure 17. Zonal section across the Korean shelf at 36˚10'N, plotted as in Figure 4. Note the change in horizontal scale from that of previous figures. At the western end of the section (left side), water depth is approximately 100 m. Water depth at the eastern end is approximately 1000 m.

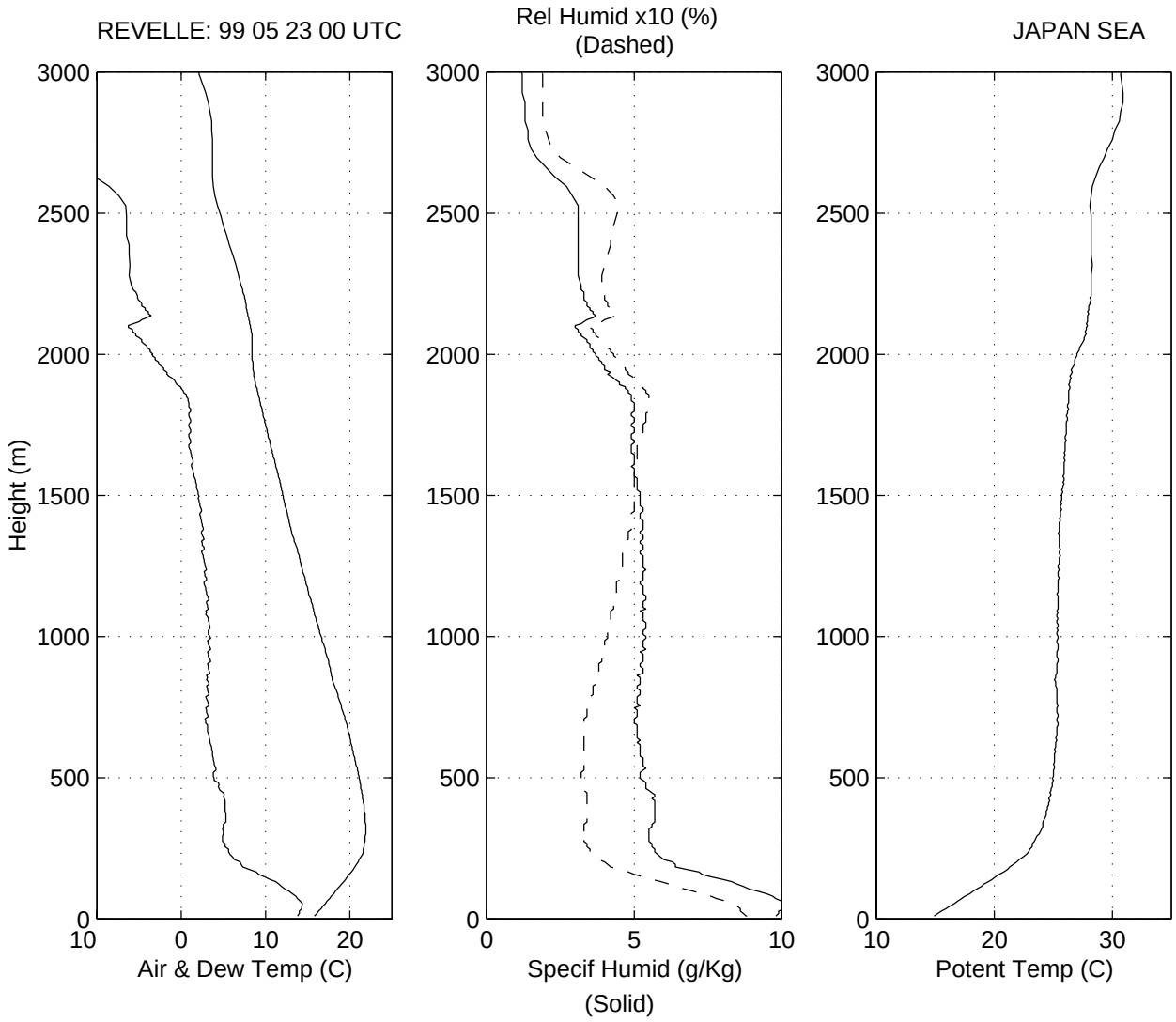

Figure 18. Thermometric profile for sounding on 23 May at 0000 UTC.

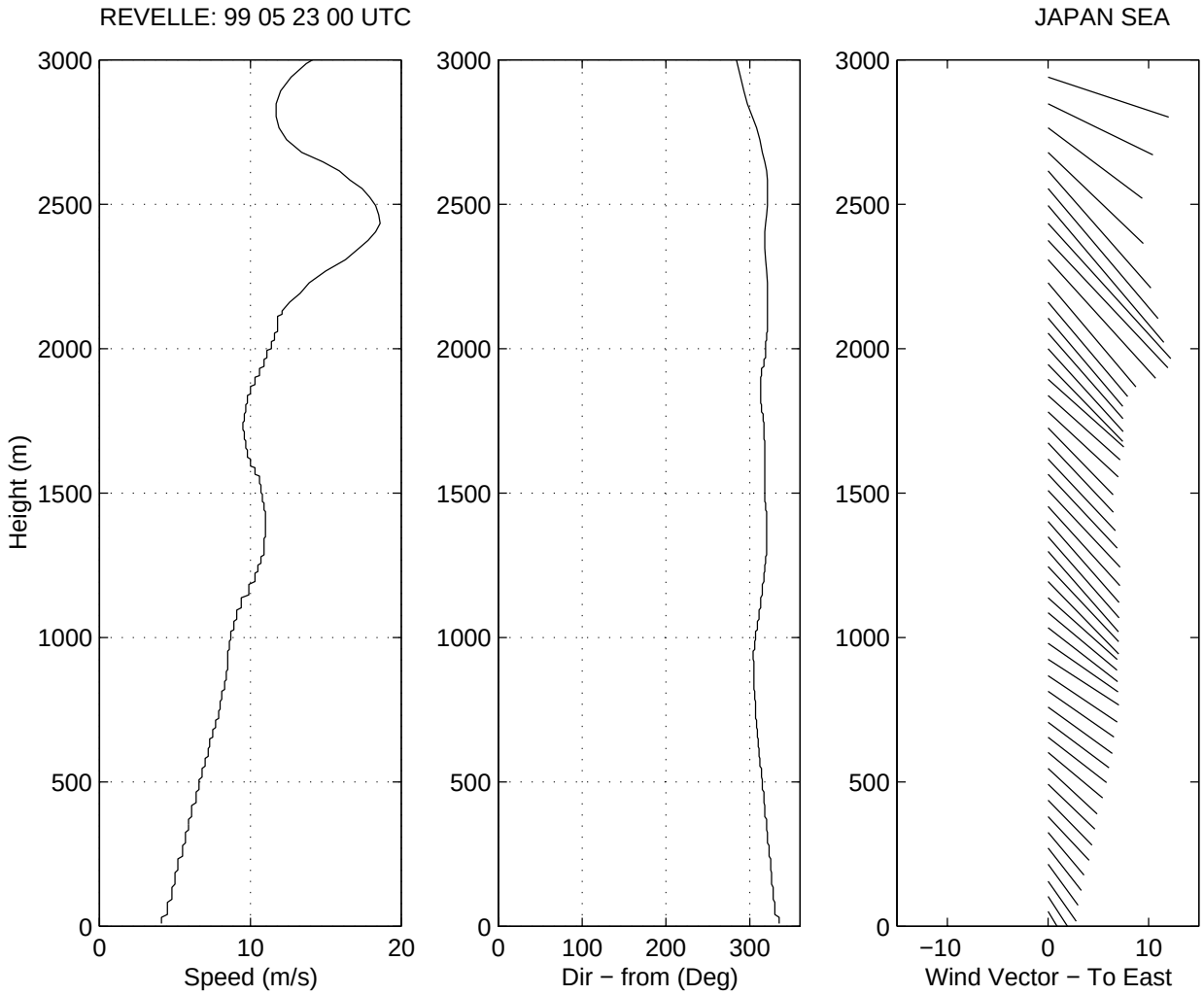

Figure 19. Wind profile for sounding on 23 May at 0000 UTC.

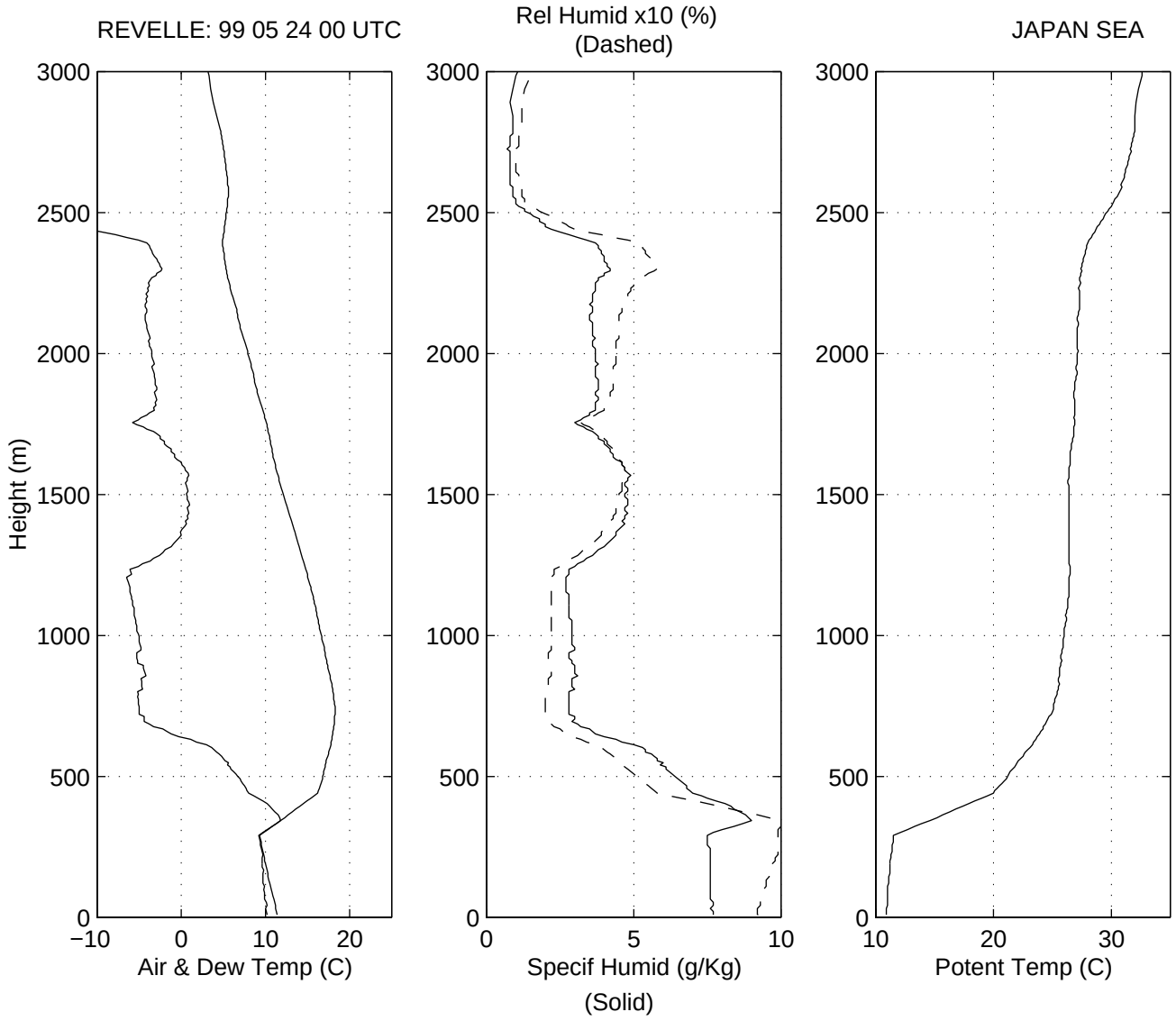

Figure 20. Thermometric profile for sounding on 24 May at 0000 UTC.

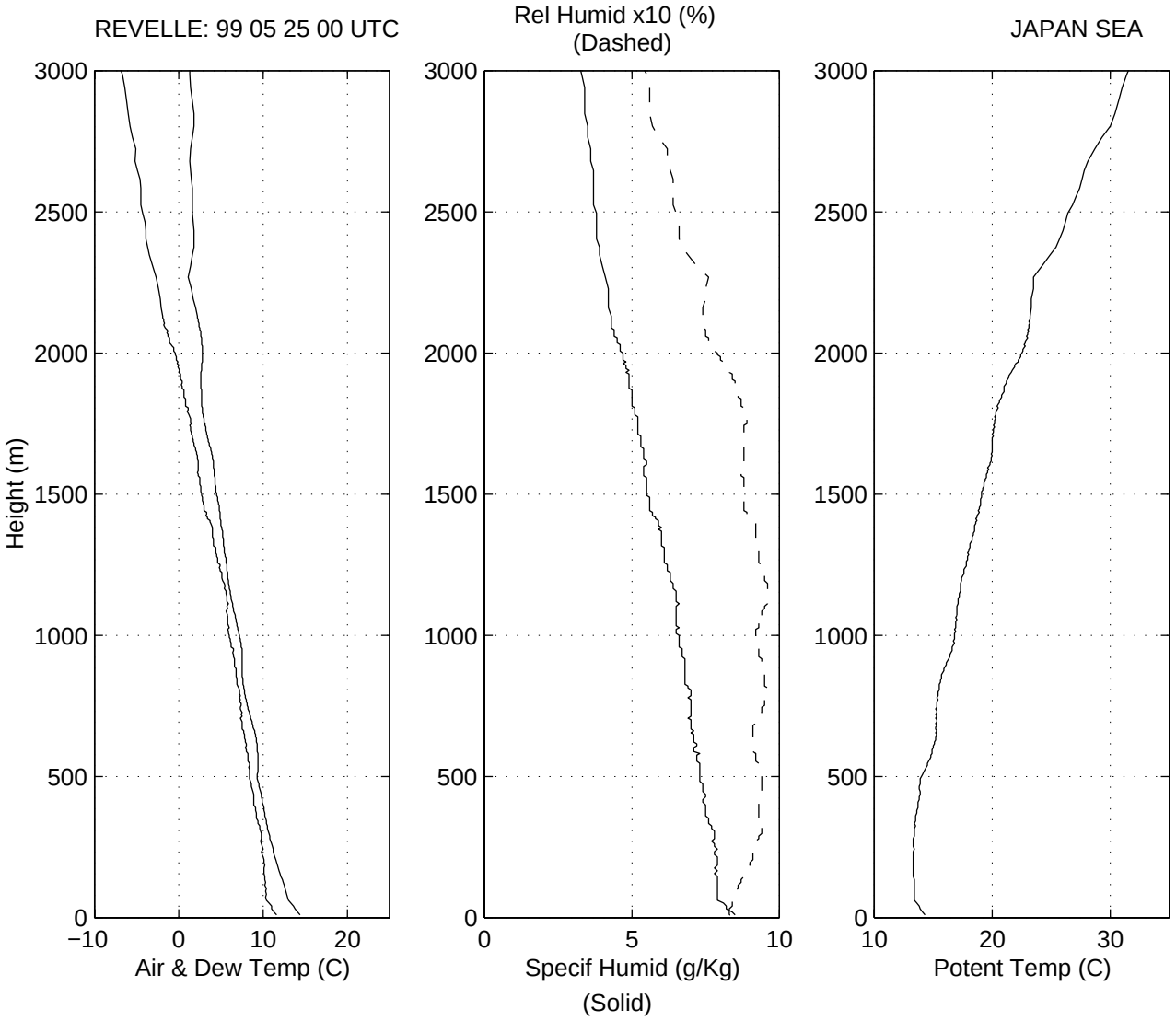

Figure 21. Thermometric profile for sounding on 25 May at 0000 UTC.

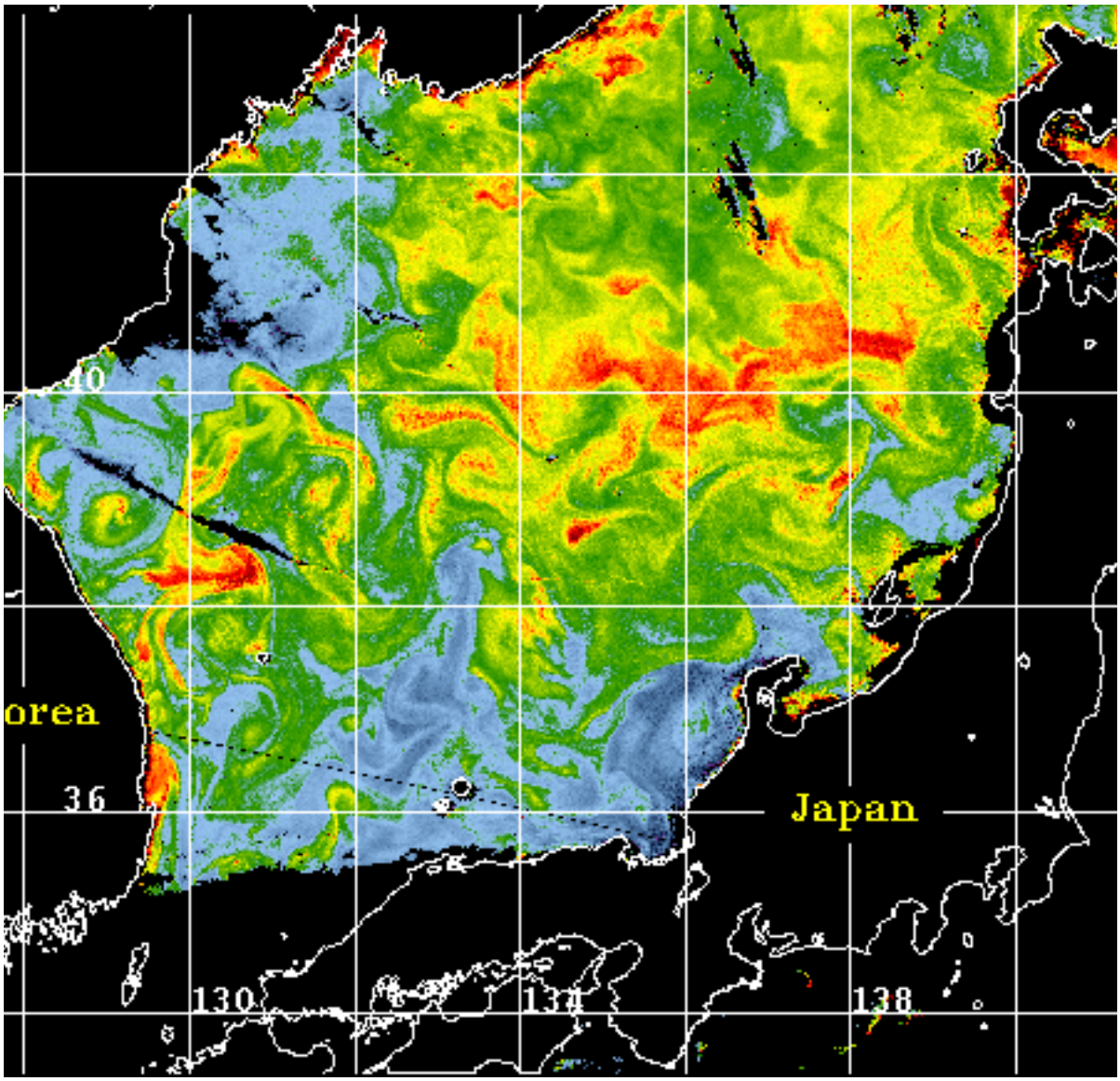

Figure 22. SeaWiFS Chlorophyll image from 21 May 1999. Note high values along eastern region of the subpolar front (40°N).

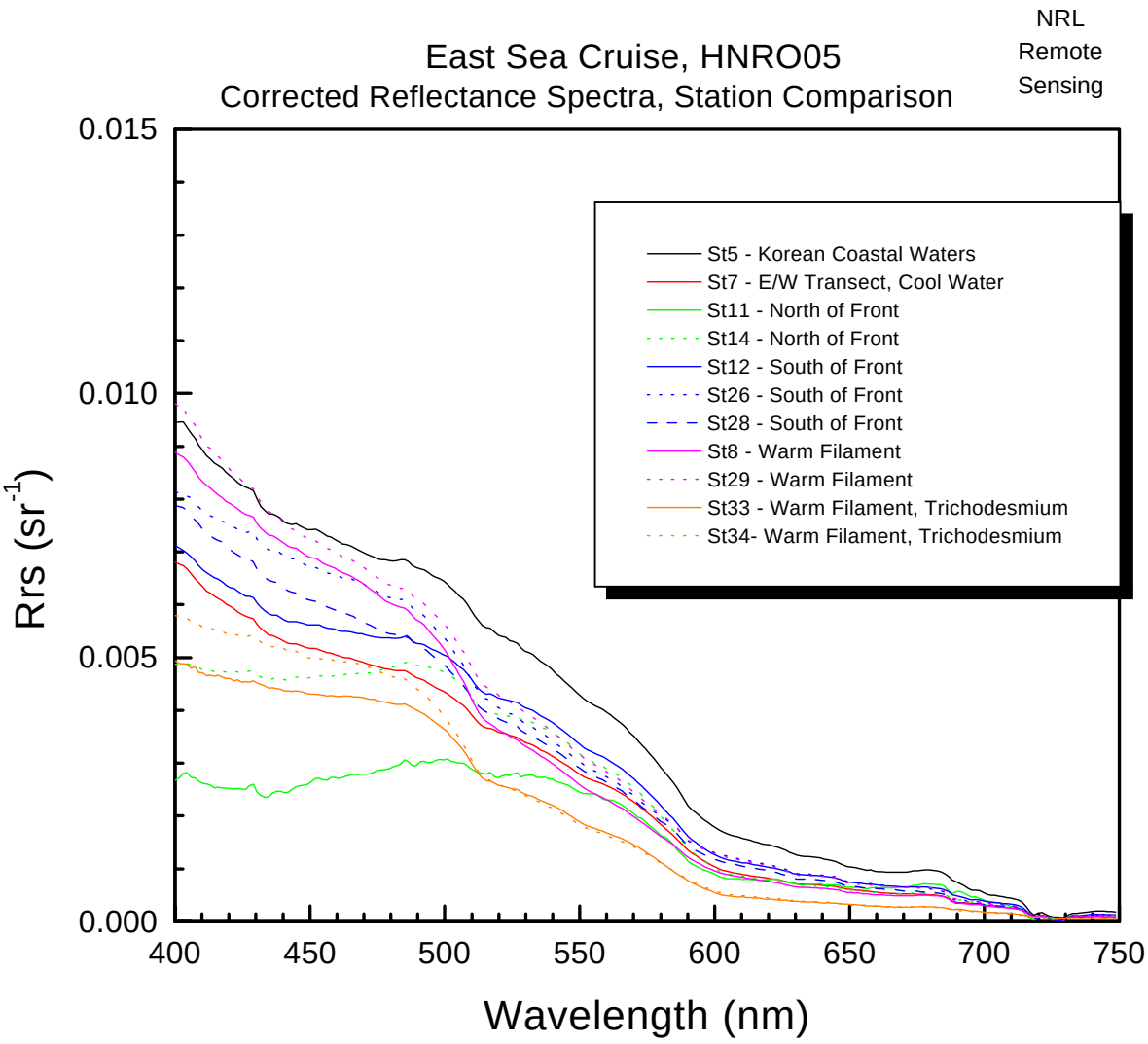

Figure 23. *In situ* remote sensing reflectance (R_{rs}) spectra collected with shipboard field spectroradiometer. Selected stations representing a variety of water types.

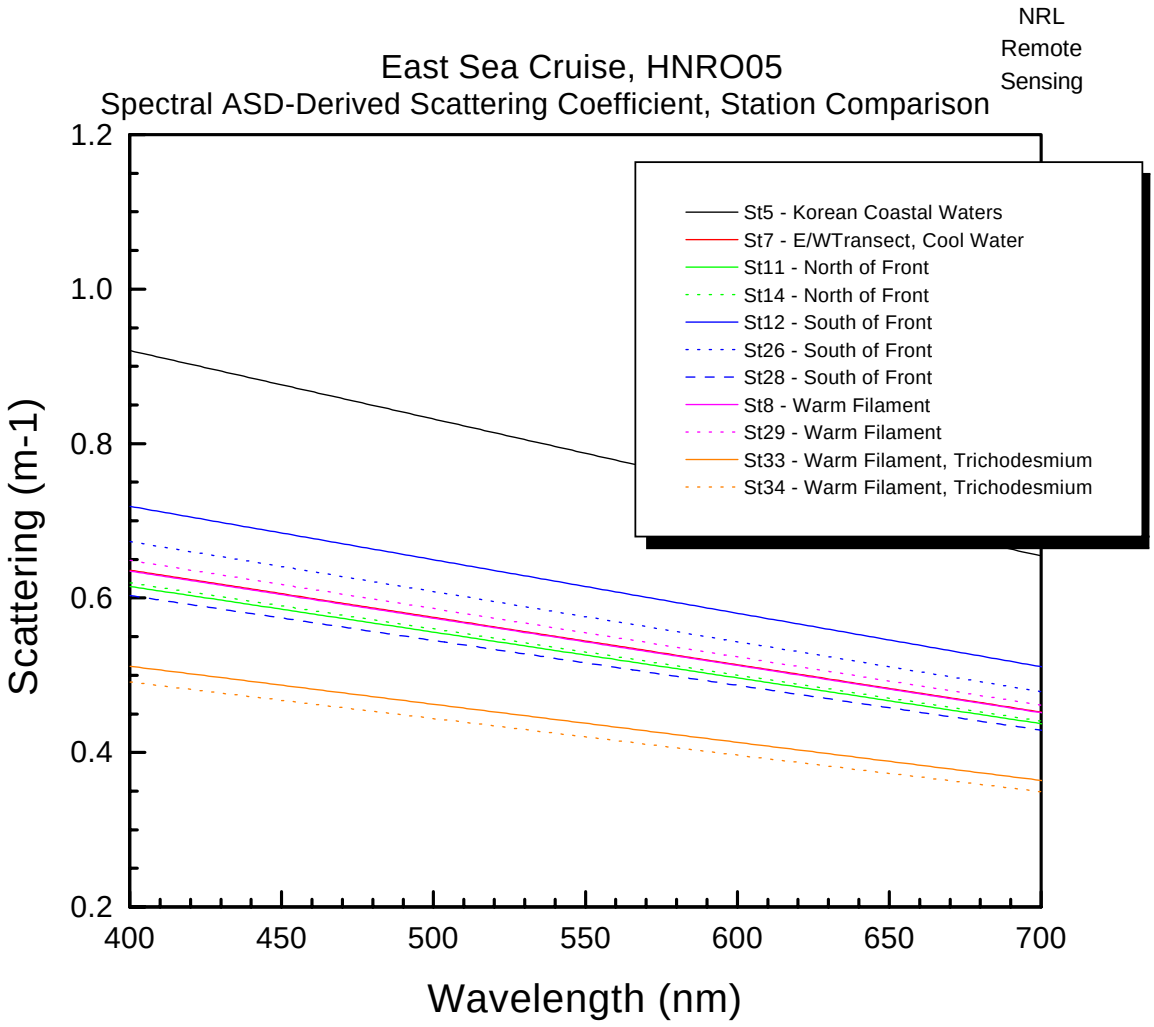

Figure 24. Spectral scattering coefficients, derived from R_{rs} data. Same stations as in Figure 23.

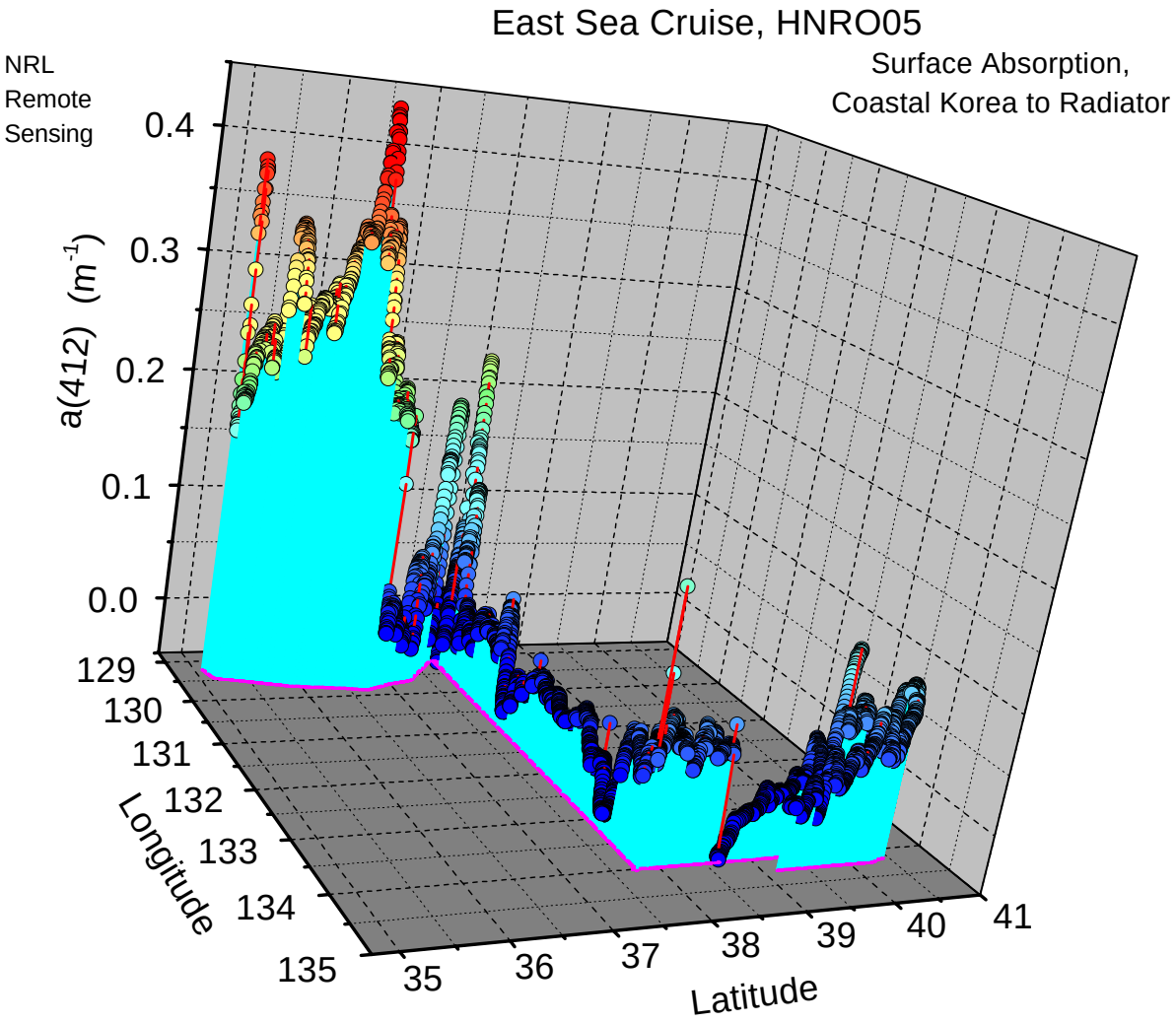

Figure 25. Surface absorption coefficient at 412 nm (a412), obtained from flow-through AC9 along-track measurements during the section extending eastward from the Korean coast along 37˚45'N (Figure 3). Note high coastal values relative to those offshore. Values are uncorrected.

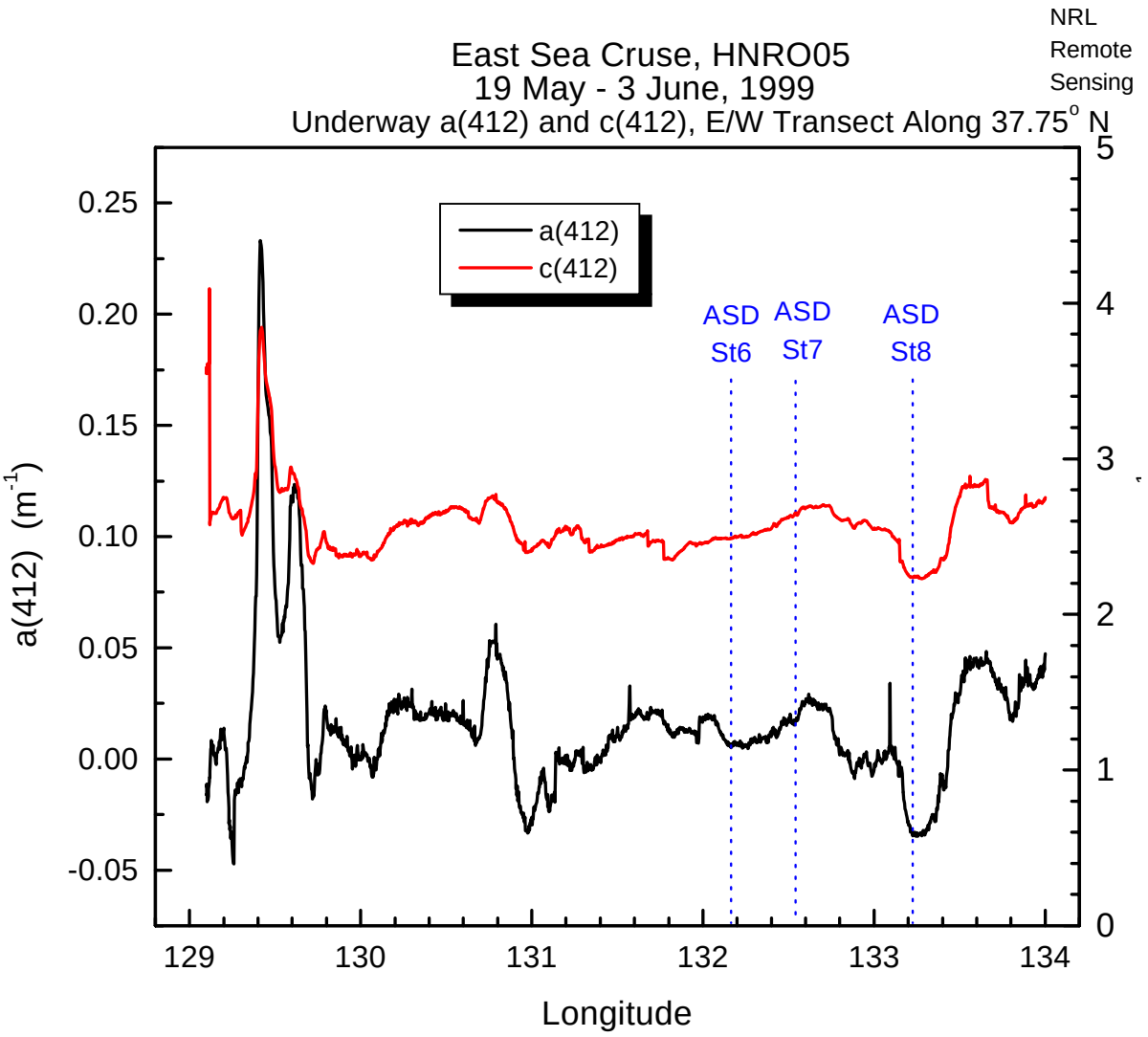

Figure 26. Surface absorption coefficient (a412) and attenuation coefficient (c412) at 412 nm, obtained from flow-through AC9 measurements along 37˚45'°N (east/west section). Values are uncorrected.

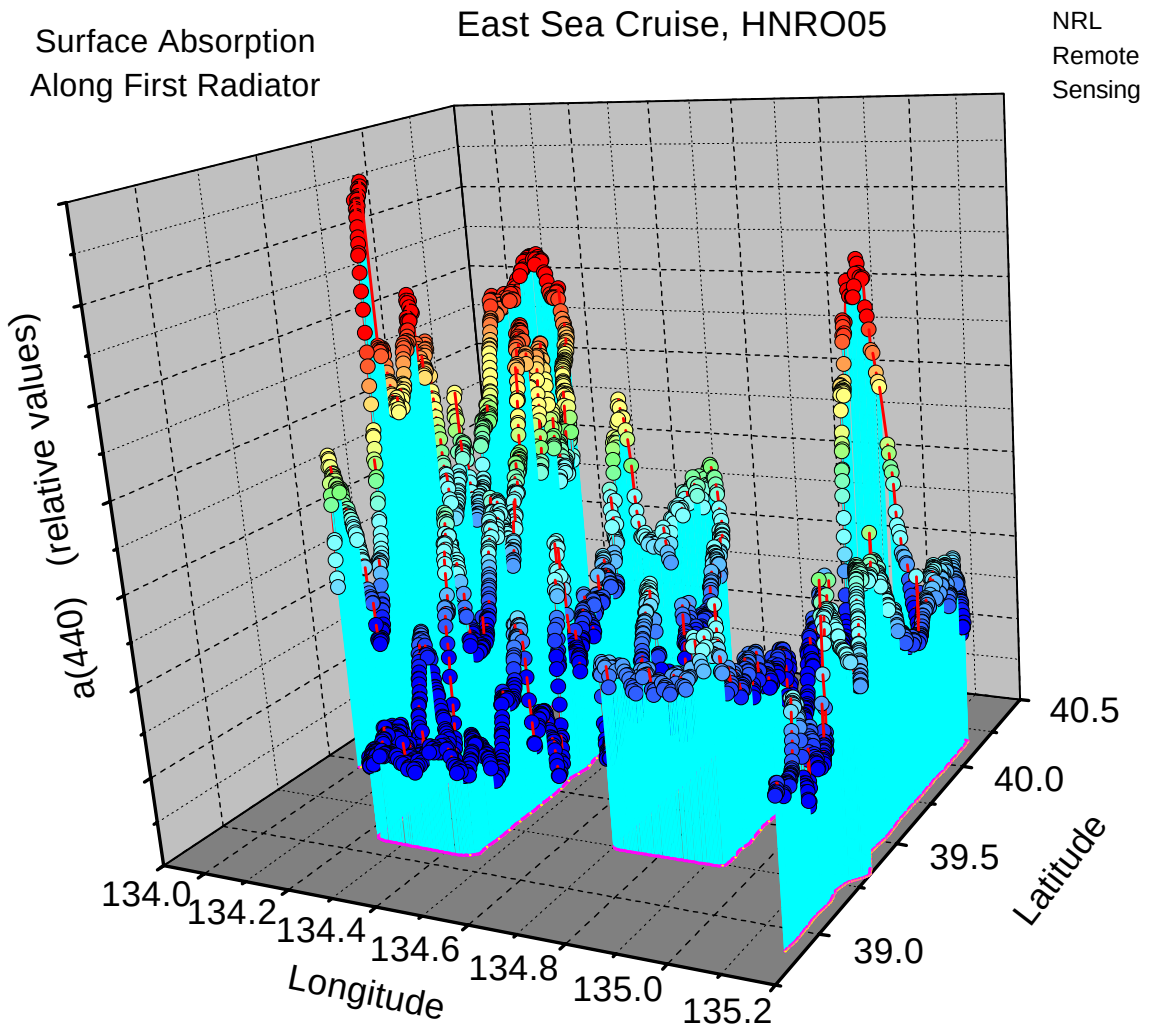

Figure 27. Surface absorption coefficient at 440 nm (a440), obtained from flow-through AC9 measurements along survey 1 at the subpolar front. Note the higher values along sections 1 and 3, north of the front. Values are uncorrected.

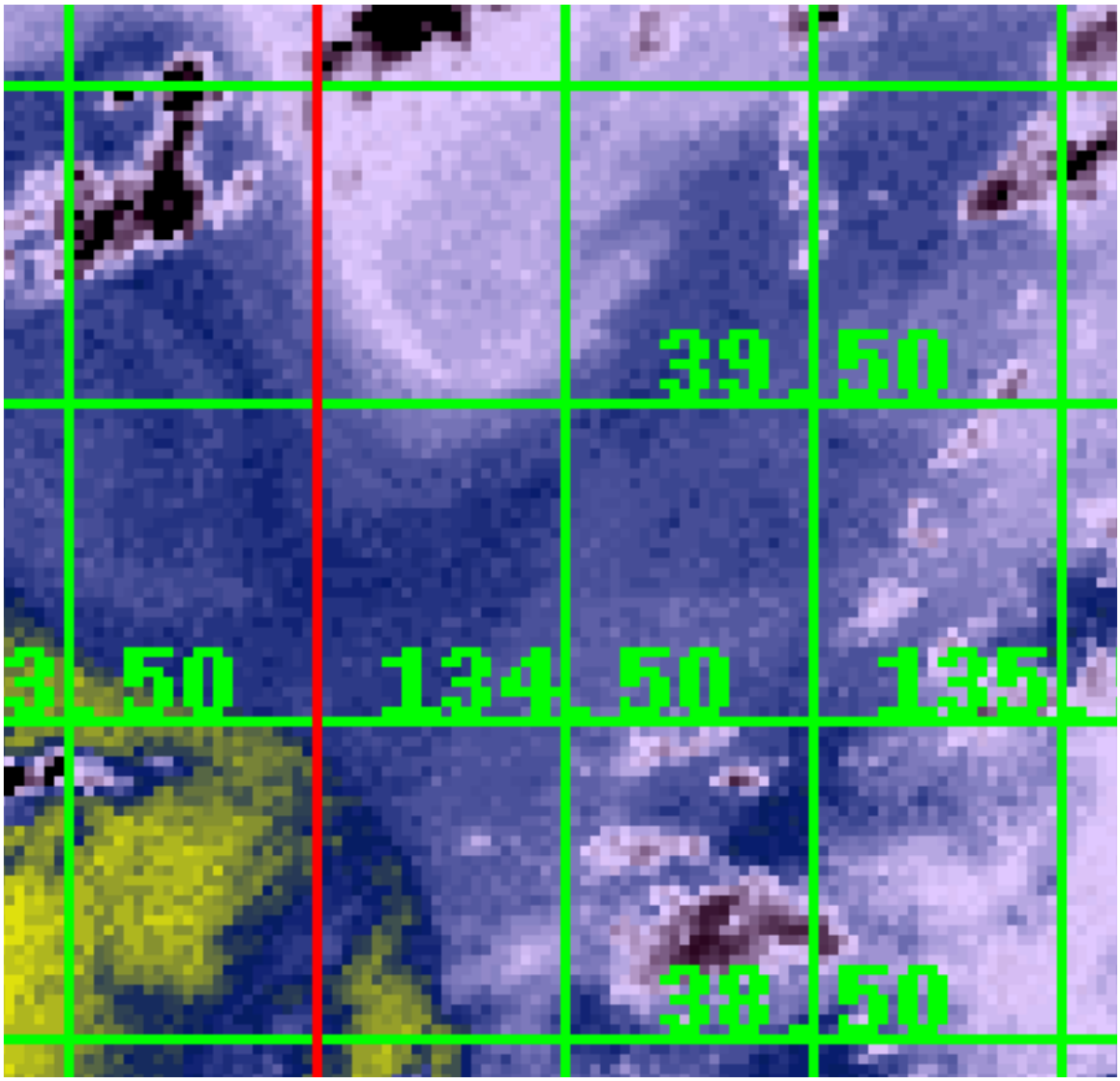

Figure 28. AVHRR SST image from 26 May 1999 showing a zoomed subsection near the subpolar front. The red line along 134°E represents the location of the cross-front hydrographic section (Figures 7–13). Note the wide range of temperature values along the section, approximately 11.5˚C at the northern end and 17.5˚C at the southern end.

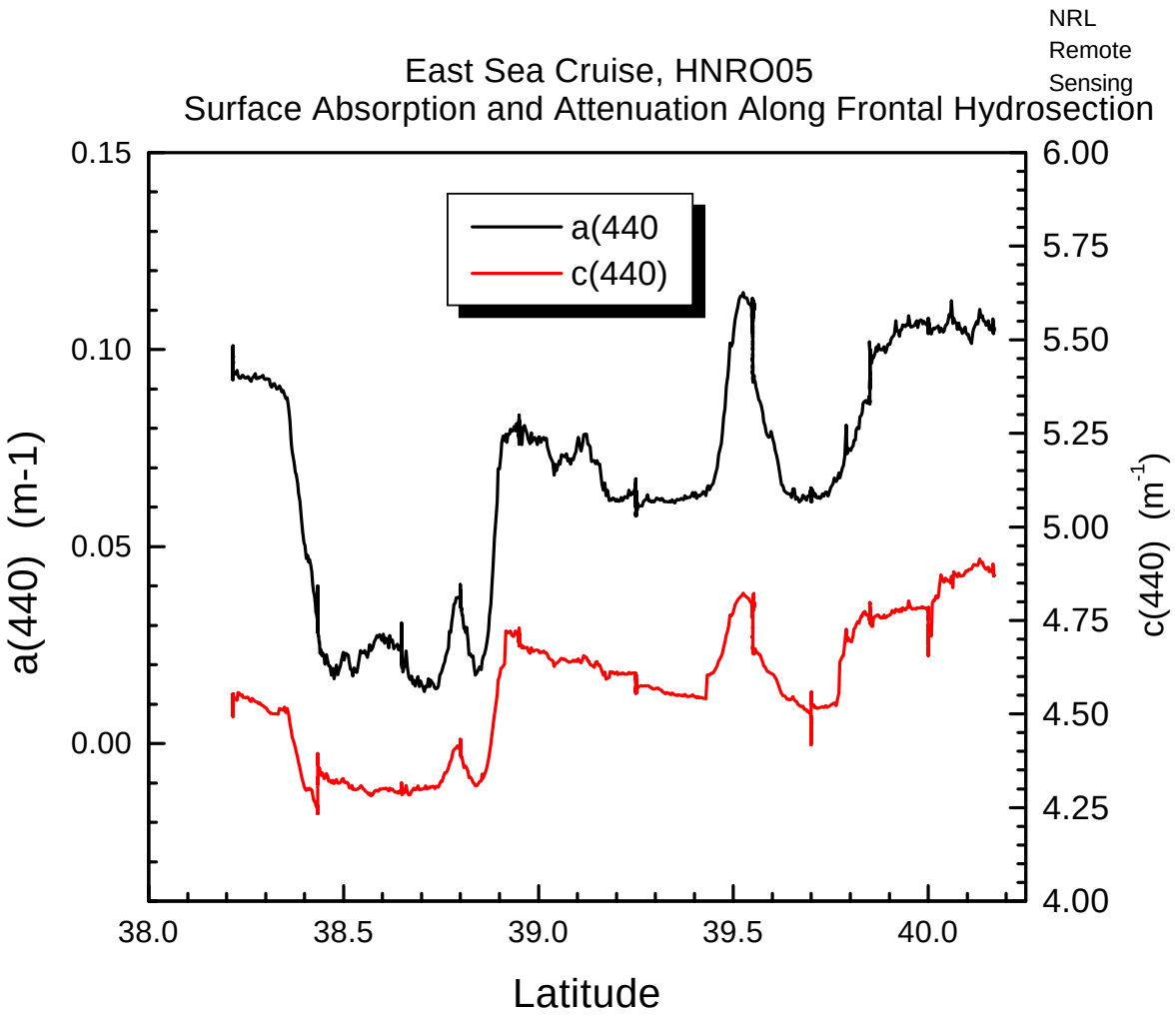

Figure 29. Surface absorption coefficient (a440) and attenuation coefficient (c440) at 440 nm, obtained from flow-through AC9 measurements along the cross-front hydrographic section (red line in Figure 28). Values are uncorrected. Large changes in magnitude correlate with crossings of the SST features in Figure 28.

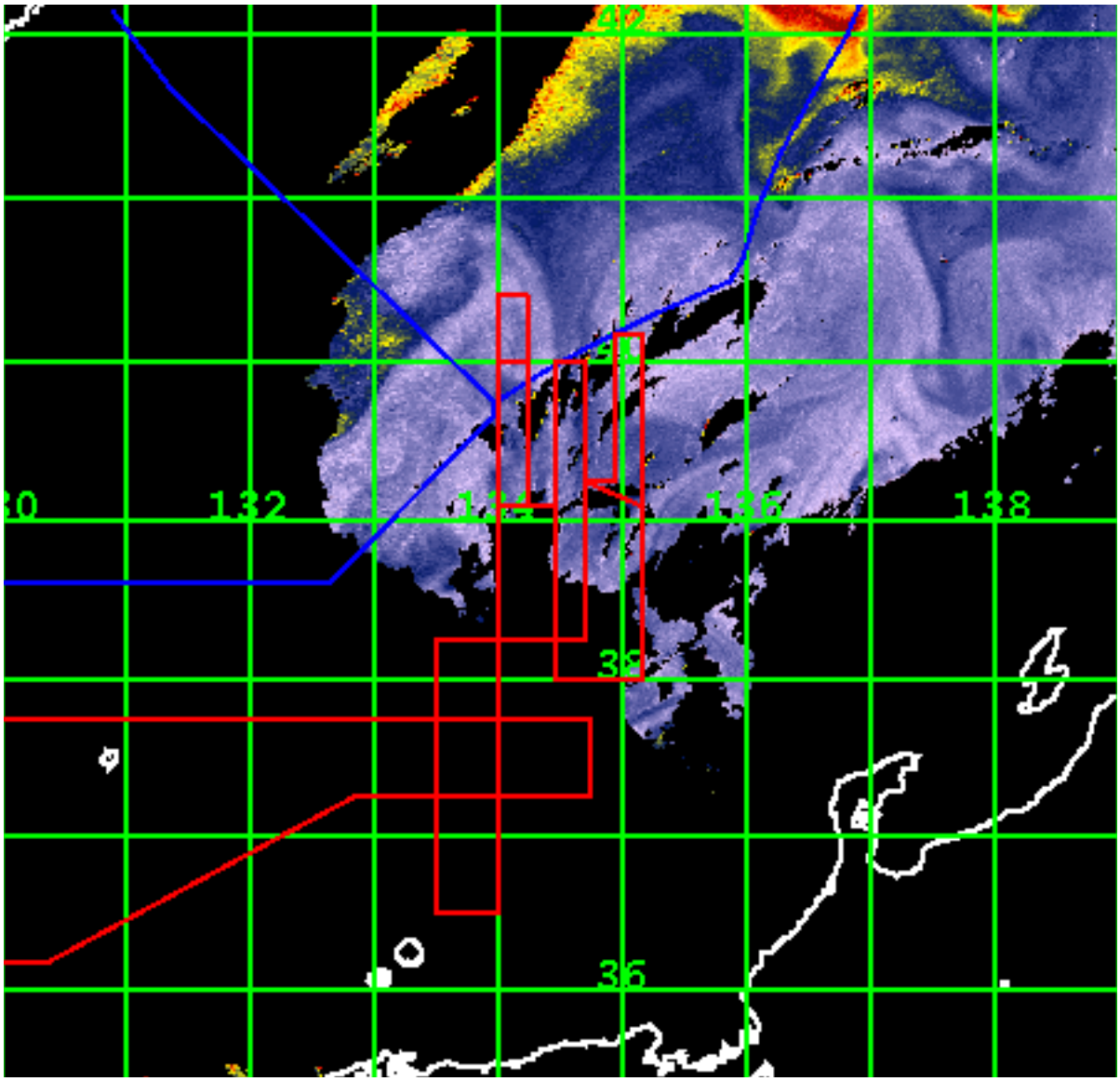

Figure 30. SeaWiFS chlorophyll image from 31 May 1999. The highest chlorophyll values are located along sections 1 and 3, north of the subpolar front, corresponding to the areas of high a(440) values in Figure 27.

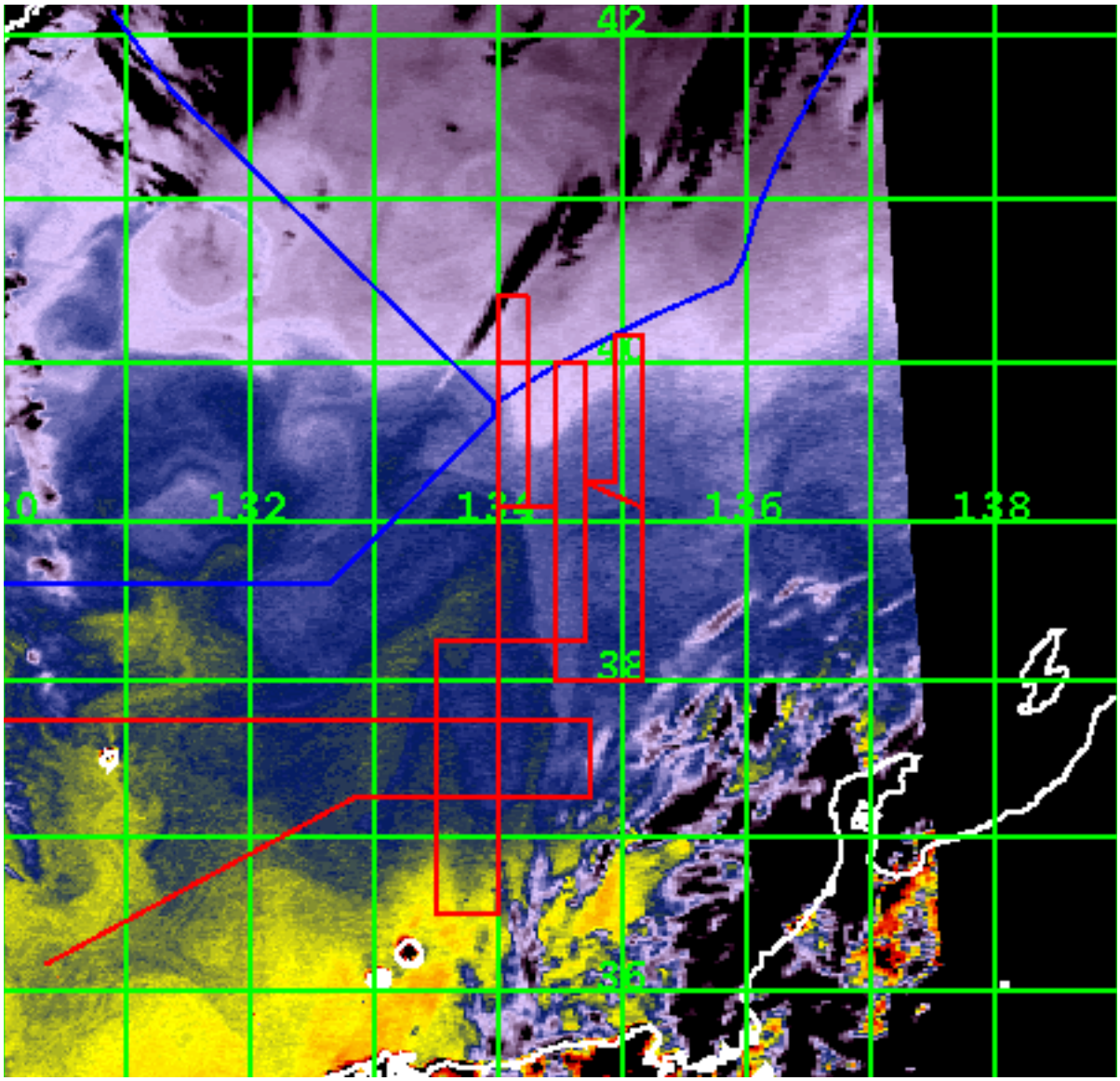

Figure 31. AVHRR SST image from 31 May 1999. Image was collected within 4 hours of the SeaWiFS image in Figure 30. The SST pattern is spatially homogeneous in the northern portion of the survey, in the area where the chlorophyll was spatial variable.

APPENDIX: Science Party List

Name	Institution	Title
Dr. Craig M. Lee	UW/APL	Chief Scientist
Mr. Basil Edward Arthur	NRL	Scientist
Mr. Frank Bahr	WHOI	Research Associate
Dr. Kyung-II Chang	KORDI	Principal research scientist
Mr. Jerome P. Dean	WHOI	Oceanographer Emeritus
Dr. Clive E. Dorman	SDSU/SIO	Professor
Mr. Paul D. Fucile	WHOI	Research Engineer
Mr. Allan G. Gordon	WHOI	Senior Eng. Assistant
Dr. Richard W. Gould	NRL	Oceanographer
Mr. Tae Pyung Han	Univ. of Kwangju	Graduate Student
Mr. Young-Suk Jang	KORDI	Mooring Specialist
Dr. Burton H. Jones	USC	Research Professor
Mr. Ho-Kyung Jun	KORDI	Senior Engineer
Mr. Jong Ki Kim	Univ. of Kwangju	Graduate Student
Mr. Craig D. Marquette	WHOI	Engineer
Dr. Myung-Gil Park	Univ. of Kwangju	Postdoctoral Scientist
Mr. Tae Sung Park	Univ. of Kwangju	Undergraduate
Dr. Alexander Petrov	FERHRI	Scientist
Mr. Eugene Pillard	SIO	Resident Technician
Mr. Matthew A. Ragan	USC	Graduate Student
Dr. Lev Ryzhkov	ROSHYDROMET	Scientist
Dr. Moon-Bo Shim	NORI	Senior Hydrographer
Mr. Marc Silver	SIO	Computer Engineer
Mr. Zhihong Zheng	USC	Research Associate

Abbreviations: APL, Applied Physics Laboratory; FEHRI, Far Eastern Hydrometeorological Research Institute; KORDI, Korean Ocean Research and Development Institute; NORI, National Oceanographic Research Institute; NRL, Navel Research Laboratory; ROSHYDROMET, Russian Federal Service for Hydrometeorological and Environmental Monitoring; SDSU, San Diego State University; SIO, Scripps Institution of Oceanography; USC, University of Southern California; UW, University of Washington; WHOI, Woods Hole Oceanographic Institution.